Structural studies on a novel O_2-protecting mechanism found in [NiFe]-hydrogenase from *Citrobacter* sp. S-77

Citrobacter sp. S-77 株由来[NiFe]ヒドロゲナーゼに見出された
新規酸素防御機構の構造化学的研究

Department of Life Science

University of Hyogo

Leading Program in Doctoral Education

Laboratory of Protein Crystallography

SH15P0001

Hiroaki Matsuura

Table of Contents

論 文 内 容 の 要 旨

論文題目　Structural studies on a novel O_2-protecting mechanism found in [NiFe]-hydrogenase from *Citrobacter* sp. S-77

「*Citrobacter* sp. S-77 株由来[NiFe]ヒドロゲナーゼに見出された新規酸素防御機構の構造化学的研究」

論文提出者　　松　浦　滉　明

[NiFe]ヒドロゲナーゼは主に嫌気性微生物が利用する水素分子の合成・分解を触媒する金属酵素であり，非常に高い触媒活性を有することが特徴である．近年，地球温暖化をはじめとする環境問題への対応や新規のエネルギー源としての使用を視野に入れた水素の利用が注目されており，ヒドロゲナーゼを活用した高効率な水素利用デバイスの開発が期待されている．しかし，本酵素は酸素に非常に敏感であり，低濃度の酸素存在下でも失活するため，デバイス等への応用には酸素に対する安定性が課題であると考えられてきた．

Citrobacter sp. S-77 株由来の Hyb 型[NiFe]ヒドロゲナーゼ（S77HYB）は酸素存在下でも安定であり，かつ高い触媒活性を有することが知られていたが，その酸素防御機構は未解明であった．本研究では S77HYB の空気酸化型，水素還元型，化合物強制酸化型の 3 種の X 線結晶構造解析を行い，それぞれ 1.57，1.84，2. 05 Å で構造決定することに成功した．その結果，活性中心に隣接する鉄硫黄クラスターが近傍のアスパラギン酸残基および水分子と協奏的に構造変化することを見出した．また，電子常磁性共鳴(EPR)法および分子動力学（MD）シミュレーションの結果から，この協奏的な構造変化が酸化還元によって可逆的に起こることを明らかにした．さらに，クロノアンペロメトリー（電気化学）測定や，*Ralstonia eutropha* 株を用いた発現系を S77HYB 活性に依存した独立栄養培養することで，S77HYB が酸素存在下で触媒活性を維持することを確認した．

Summary

Hydrogenase catalyzes reversible conversion of molecular hydrogen to protons and electrons. The highly tuned effective catalysis has been received much attention due to the potential usefulness for applications in H_2-based technologies. However, most of hydrogenases loss their catalytic activities under presence of O_2. In order to make use of the enzyme, O_2-stability is of key importance.

Hyb-type [NiFe]-hydrogenase isolated from *Citrobacter* sp. S-77 (S77HYB) is a highly O_2-stable hydrogenase and has high catalytic activities comparing to the hitherto-identified O_2-tolerant hydrogenases. O_2-tolerant hydrogenase has a special Fe-S cluster, namely [4Fe-3S]-6Cys near the catalytic site, however, S77HYB have a standard [4Fe-4S]-4Cys, which is conserved among O_2-sensitive standard [NiFe]-hydrogenases.

To reveal molecular basis of the O_2-stability of S77HYB, X-ray crystallographic, spectroscopic and theoretical analysis were carried out. Crystal structure of S77HYB was determined at 1.57, 1.92, 2.05Å for air-oxidized, H_2-reduced, and $K_3[Fe(CN)_6]$-oxidized states, respectively. The active site in both oxidized and reduced conditions were similar to those obtained for other hydrogenases. On the other hand, the proximal [4Fe-4S]-4Cys cluster was distorted as found in O_2-sensitive hydrogenases. Although the deformation of the proximal [4Fe-4S]-4Cys cluster had been considered as a result of oxidative damage, spectroscopic and theoretical analysis on S77HYB indicated that the deformation of the proximal cluster in S77HYB was rather stabilized by the negative charge of COO- of the adjacent aspartate and coordinated OH^-. Furthermore, the redox-dependent conformational change in S77HYB is completely reversible concerting with the relocation of water molecules in the highly conserved water-network system in [NiFe]-hydrogenases. These results implied that S77HYB have O_2-reduction mechanism as found in O_2-tolerant hydrogenases.

O_2-reduction ability of S77HYB was monitored by electrochemical measurement. H_2-oxidation activity of S77HYB was monitored, in presence of O_2, by chronoamperometric measurement. Furthermore, O_2-tolerant activity of S77HYB was confirmed using molecular biology technique. S77HYB was heterologously expressed in *Ralstonia eutropha* HF1036 strain (hydrogenase-null mutant of *R. eutropha*). The constructed strain was grown under lithoautotrophic condition in presence of 1– 20% O_2. Both results clearly displayed the O_2-tolerant activity of S77HYB.

In conclusion, the surrounding negative charges from COO^- of aspartate and coordinated OH^- with the relocatable water molecules stabilized the redox-dependent reversible conformational change of the [4Fe-4S]-4Cys cluster. Hence, S77HYB can reduce invaded O_2 and protect the active site even with the [4Fe-4S]-4Cys cluster, instead of [4Fe-3S]-6Cys cluster in O_2-tolerant hydrogenases.

PREFACE

Enzymes are protein molecules which have catalytic activities for various chemical reactions. They are well-tuned in the process of evolution of life and effectively catalyze the chemical reactions normally at ambient temperature and pressure. The core catalytic process is carried out at the active center, likely with model compounds, or inorganic or organic catalysts. The non-biological catalysts are usually used at extreme conditions (*e.g.* at high temperature or high pressure), while enzyme cannot be used at such conditions due to their less stability. In addition to the catalytic active center, enzymes often have an additional system which promotes the catalytic reaction, *e.g.* channels for substrates and products, and electron transfer pathways. Therefore, enzymes can exhibit highly effective catalytic activity without energy loss comparing to the non-biological catalysts.

Hydrogenase is a metalloenzyme which reversibly catalyzes hydrogen oxidation or proton reduction. H_2 can be an energy resource for the next generation, therefore, hydrogenase has received much attention due to its potential usefulness in the H_2 economy. However, though the catalytic reaction is really simple, the reaction mechanism by hydrogenase has not been fully understood. Moreover, most of hydrogenases are easily inactivated by trace amount of O_2, hence, this weak point should be figured out for industrial applications.

Although it is beneficial to develop bio-inspired catalyst by mimicking the catalytic part of enzymes in nature, biotechnological applications of enzymes are also challenging. In past several decades, technologies on genetic modification has been dramatically improved. However, applications of enzymes are quite limited due to poor understandings of the structural basis of the enzymatic reactions. In

particular, investigation on the structural dynamics is an urgent issue for utilization of enzymes.

Even after the increase of oxygen concentrations of the earth, hydrogenase has still found mainly in anaerobic microorganisms. In ancient organisms, hydrogenase was utilized in energy metabolism. One of hydrogenases is phylogenetically related to NADH: quinone oxidoreductase (Complex I), though the Complex I cannot use H_2 as a substrate.

As mentioned above, hydrogenase catalyzes the simple reaction, namely H_2 oxidation or H^+ reduction, however, the reaction mechanism has still been unclear. Moreover, O_2-tolerance has still not been fully understood.

In this study, ambiguous definition of "O_2-tolerance" is reviewed. Furthermore, O_2-stability of hydrogenase is also discussed. Susceptibility to O_2 is a major obstacle for applications of the enzyme.

Chapter 1 provides a general introduction on hydrogenase research in earlier studies. Characteristics of the target hydrogenase in this study, Hyb-type [NiFe]-hydrogenase from *Citrobacter* sp. S-77 (S77HYB), is also described in this chapter. In chapter 2, detailed methodology in this study is described. Chapter 3 presents the results obtained in this study, and the results will be further discussed. Finally, conclusions of this study will be presented in Chapter 4 and several ideas on further investigations of hydrogenases are suggested in the final Chapter 5.

H_2 has been of great interest due to the potential as an energy source for the next generations. Needless to say, hydrogenase must have a key importance to realize H_2 economy. I hope this work will be of some help to facilitate further

investigations on hydrogenases or development of bio-inspired artificial catalysts.

ABBREVIATIONS

Please note that the abbreviated terms (*e.g.* names of organisms, enzymes, chemical reagents) listed below are used in this dissertation without any notice.

Aa: *Aquifex aeolicus*

AaMBH: Membrane-bound O_2-tolerant hydrogenase from *Aquifex aeolicus*

AOXI: Air-oxidized

Av: *Allochromatium vinosum* (formerly *Chromatium vinosum*)

AvISP: ISP-type hydrogenase from *Allochromatium vinosum*

BV: Benzyl viologen (1,1'-dibenzyl-4,4'-bipyridinium dichloride)

CBB: Coomassie brilliant blue

CW-EPR: Continuous wave EPR (Electron paramagnetic resonance)

Db: *Desulfomicrobium baculatum*

Db[NiFeSe]: [NiFeSe]-hydrogenase from *Desulfomicrobium baculatum* (Group 1a)

Dd: *Desulfovibrio desulfuricans*

DdSTD: Standard [NiFe]-hydrogenase from *Desulfovibrio desulfuricans*

DEAE: Diethyl-aminoethyl

Df: *Desulfovibrio fructosovorans*

DfSTD: Standard [NiFe]-hydrogenase from *Desulfovibrio fructosovorans*

Dg: *Desulfovibrio gigas*

DgSTD: Standard [NiFe]-hydrogenase from *Desulfovibrio gigas*

DIALS: Diffraction integration for advanced light sources (a X-ray data processing software developed by the collaborative teams at Diamond Light Source, CCP4, and Lawrence Berkeley National Laboratory)

DvH: *Desulfovibrio vulgaris* Hildenborough

DvH[NiFeSe]: [NiFeSe]-hydrogenase from *Desulfovibrio vulgaris* Hildenborough

DvMF: *Desulfovibrio vulgaris* Miyazaki F

DvMFSTD (DvMSTD): Standard type hydrogenase (Group 1b) from DvMF

Ec: *Escherichia coli*

EcHYB: Hyb-type [NiFe]-hydrogenase from *Escherichia coli*

EcMBH: Membrane-bound O_2-tolerant [NiFe]-hydrogenase from *Escherichia coli*

EPR: Electron paramagnetic resonance

FOXI: Ferricyanide($K_3[Fe(CN)_6]$)-oxidized

FRH: F_{420}-reducing [NiFe]-hydrogenase

FT-IR: Fourier transform infrared

GC: Gas chromatography; also referred to as Glassy carbon

GCE: Glassy carbon electrode

H_2ase: Hydrogenase

HRED: Hydrogen-reduced

Ht: *Hydrogenophilus thermoluteolus* TH-1

HtSH: Soluble [NiFe]-hydrogenase from *Hydrogenophilus thermoluteolus* TH-1

HYB: Hyb-type [NiFe]-hydrogenase belongs to Group 1c

ISP: ISP-type [NiFe]-hydrogenase belongs to Group 1e

Mb: *Methanosarcina barkeri*

MbFRH: F_{420}-reducing [NiFe]-hydrogenase from *Methanosarcina barkeri*

MBH: Membrane-bound [NiFe]-hydrogenase belongs to Group 1d (O_2-tolerant)

MOPS: 3-Morpholinopropanesulfonic acid

MV: Methyl viologen (1,1'-dimethyl-4-4'-bipyridinium dichloride)

NAD^+: Oxidized form of nicotinamide adenine dinucleotide

NADH: Reduced form of nicotinamide adenine dinucleotide

PDB: Protein Data Bank

Pf: *Pyrococcus furiosus*

Re: *Ralstonia eutropha* (currently named *Cupriavidus necator*)

ReAH: Actinobacteria-type [NiFe]-hydrognease from *Ralstonia eutropha*

ReMBH: Membrane-bound O_2-tolerant [NiFe]-hydrogenase from *Ralstonia eutropha*

ReRH: Reguratory [NiFe]-hydrognease from *Ralstonia eutropha*

ReSH: Soluble [NiFe]-hydrogenase from *Ralstonia eutropha*

RH: Regulatory hydrogenase

Se: *Salmonella enterica*

SH: Soluble hydrogenase (*e.g.* NAD^+-reducing hydrogenase)

SHE: Standard hydrogen electrode

SSE: Silver/silver chloride electrode

STD: Standard hydrogenase belongs to Group 1b [NiFe]-hydrogenase

TPF: 1,3,5-triphenylformazan

TTC: 2,3,5-Triphenyl tetrazolium chloride

U: Unit (defined as 1 μmol H_2 oxidation activity per seconds)

U/mg: Unit per milligram

XDS: X-ray detector software (an X-ray data processing sofware developed by Wolfgang Kabsch)

$[4Fe\text{-}4S]_{Prox}$: [4Fe-4S] cluster in the proximal site

$[4Fe\text{-}3S]_{Prox}$: [4Fe-3S] cluster in the proximal site (in O_2-tolerant Group 1d [NiFe]-hydrogenase)

$[3Fe\text{-}4S]_{Med}$: [3Fe-4S] cluster in the medial site

$[4Fe\text{-}4S]_{Dist}$: [4Fe-4S] cluster in the distal site

LIST OF PUBLICATION

Noor Dina Muhd Noor†, Hiroaki Matsuura†, Koji Nishikawa†, Hulin Tai†, Shun Hirota, Jaehyun Kim, Jiyoung Kang, Masaru Tateno, Ki-Seok Yoon, Seiji Ogo, Shintaro Kubota, Yasuhito Shomura and Yoshiki Higuchi

Redox-dependent conformational changes of a proximal [4Fe-4S] cluster in Hyb-type [NiFe]-hydrogenase to protect the active site from O_2

Chemical communications, 54 (2019) 12385-12388

†These authors are equally contributed to this study.

Chapter 1 INTRODUCTION

In this chapter, an overview of earlier investigations relating to this study is described. At the beginning, general introduction of hydrogenase is provided. Following to the beginning section, classification of hydrogenase is shortly described. Next is an overview of earlier structural studies including crystallographic and spectroscopic analyses on hydrogenases. Furthermore, the main focus of this work, O_2-stability or O_2-tolerance of hydrogenases are also described. At the end of this chapter, aim of this study is summarized.

1-1. General introduction

1-1-1. Hydrogenase

Hydrogenase had firstly been identified in 1931 as a H_2 conversion enzyme (Stephenson & Stickland, 1931a,b; Stephenson & Stickland, 1932). Hydrogenase catalyzes H_2 oxidation or H^+ reduction at the active site which is composed from some metals (Eq. 1). To date, it is known that H_2 is heterolytically split into H^- and H^+ (Krasna & Rittenberg, 1954; Rittenberg & Krasna, 1955) during H_2 activation. This catalytic reaction seems to be the simplest reaction in nature, however, the detailed molecular mechanism of the reaction by hydrogenase has still been under debate in spite of the numerous efforts (Evans *et al.*, 2015; Carr *et al.*, 2016; Kawahara-Nakagawa *et al.*, 2019). Accordingly, hydrogenase-inspired model compounds have not still been reached the level of the catalytic efficiency of hydrogenases.

$$H_2 \rightleftharpoons H^- + H^+ \rightleftharpoons 2H^+ + 2e^- \qquad \text{(Eq. 1)}$$

Hydrogenase also catalyzes H/D exchange and para/ortho conversion reactions (Eq. 2 & 3). These reactions are catalyzed without any electron transfer unlike H_2 oxidation or H^+ reduction, thus the reactions are regarded as fundamental catalysis for hydrogenases (Yagi *et al.*, 2013). The reaction itself has been known well, however, detailed mechanism or physiological significance has still been unknown. From the physical viewpoint, it is known that the interconversion of ortho-para state is very slow reaction in an isolated state, while the interconversion is promoted in a physisorption state via interaction with surfaces of not only magnetic but also diamagnetic materials (Fukutani *et al.*, 2013). Recently a Raman spectroscopic study on H/D exchange reaction of [NiFe]-hydrogenase from *Desulfovibrio vulgaris* Miyazaki F (DvMF) strain was reported (Kawahara-Nakagawa *et al.*, 2019) to investigate kinetics of hydrogenases.

$$H_2 + D_2O \rightleftharpoons HD + HDO \rightleftharpoons D_2 + H_2O \qquad \text{(Eq. 2)}$$

$$\text{ortho-}H_2 \rightleftharpoons \text{para-}H_2 \qquad \text{(Eq. 3)}$$

Hydrogenases are widespread among various microorganisms including bacteria, archaea and even eukarya (Kessler *et al.*, 1973). The fact indicates that hydrogen conversion is an important physiological process in microorganisms.

1-1-2. Hydrogen in biology

Many microorganisms utilize hydrogen conversion in anaerobic metabolism. Not only in anaerobic organisms, aerobic organisms also utilize hydrogen, especially with the form of H^+.

H^+ has key importance in organisms for generating energy. Chemiosmotic

hypothesis (Mitchell *et al.*, 1967; Mitchell *et al.*, 2011) suggests that H^+ gradient through the membrane produces the energy for ATP synthesis. Even in organisms utilizing O_2, H^+ gradient is generated for living by several membrane proteins. Some acetogens have only an energy-converting, ion-translocation hydrogenase, called Ech, as a potential respiratory enzyme. In such bacteria, the hydrogenase translocates H^+ and generated H^+ gradient is utilized for ATP synthesis. This hydrogenase-dependent chemiosmotic mechanism for energy conservation may be the simplest respiration system and is considered as an ancient metabolic pathway (Schoelmerich & Müller, 2019). Furthermore, a kind of hydrogenase has quite high sequence similarity to Complex I (NADH:quinone oxidoreductase), hence, hydrogenase may have a function in an ancient respiration mechanism (Burgdorf *et al.*, 2005; Shomura *et al.*, 2017).

As described above, since hydrogen has a fundamental role in energy production, the related enzyme, hydrogenase, has been highly conserved and involved in various organisms in the present day.

1-1-3. Potential usefulness of hydrogenase for H_2 economy

Modern industry heavily depends on large use of fossil fuels. Severe environmental problems involving global warming are caused by the urbanization and the industrialization. To put a brake on such problems, development of clean energy technologies for the next generation is highly desired.

H_2 is a promising candidate which could replace the fossil fuels (Armstrong, 2013). H_2 combustion only generates water, without CO_2 or any other greenhouse gas. Furthermore, H_2 can be stored unlike the electricity. Although currently

available renewable energies (*e.g.* wind power or geothermal power) is not suitable for stable supply because they highly depend on the climate or natural environment. While H_2 can be possibly available as a stable supplying system in everywhere if the effective catalyst is once developed.

Currently, industrial H_2 production depends on a side-product from combustion of fossil fuels. In other way, H_2 can be produced by electrolysis of with platinum electrode. The electrolysis requires electric energy most probably derives from the fossil fuels; it is obviously not "green." Hence, effective catalysts for H_2 production is required (Winter & Brodd, 2004).

Hydrogenase has been received much attention due to their potential usefulness as an efficient bio-catalyst. Despite of a lot of efforts to develop bio-inspired catalytic compounds which mimics the catalytic complex of hydrogenases, no one has still reached to the catalytic efficiency as in hydrogenases (Tard *et al*., 2009; Schilter *et a*l., 2016). Effective catalysis in enzymes is performed not only by the catalytic site, but also the other part of the enzymes, which has an important role for regulation, stabilization or facilitation of the enzyme activities as well.

Recently, several attempt to directly apply hydrogenases to devices has been reported (Plumeré *et al*., 2014; Matsumoto *et al.*, 2014; Adam *et al*., 2016; Szczensny *et al.*, 2018). Mutagenesis studies to improve stability or catalytic turnover have also been carried out (Koo & Swartz, 2018; Zhang *et al.*, 2018). Even in the biotechnological applications, structural details such as the molecular mechanism of the catalysis or enzyme stability are highly required for rational design of the enzymes for the applications.

1-2. Classification of hydrogenase

1-2-1. Overview of the classification of hydrogenase

Hydrogenases fall into three general groups depending on the metal content in the active site, namely [NiFe]-, [FeFe]- and [Fe]-hydrogenases (Fig. 1) (Vignais & Colbeau, 2004; Lubitz *et al.*, 2014). All groups of hydrogenases catalyze reversible H_2 oxidation, however, the activity or the catalytic bias are different depending on the enzymes. Frankly speaking, H_2 oxidation activity is dominant in [NiFe]-hydrogenases, while H^+ reduction activity is dominant in [FeFe]-hydrogenases, although there is an exception. [Fe]-hydrogenase has a unique catalytic activity. it catalyzes one of the reaction steps in the methanogenic energy conversion pathway from CO_2 with H_2 to methane, using tetrahydromethanopterin (H_4MPT).

Other classification schemes have also been reported (*e.g.* according to the phylogeny or redox partners) (Wu & Mandrand, 1993; Vignais & Billoud, 2007). Most recently, Greening and co-worker suggested novel classification scheme along their genomic and metagenomic analysis (Greening *et al.*, 2016; Sødergaard *et al.*, 2016). According to their classification scheme, [NiFe]-hydrogenase has 4 general groups (1–4) with several subgroups (in total 29 categories). [FeFe]-hydrogenase is classified into 3 general groups (A–C) with some subgroups in group A and C (totally 6 categories), and [Fe]-hydrogenase has only one general group (no subgroups). Both [NiFe]-hydrogenases and [FeFe]-hydrogenases are widespread in various phyla in bacteria and archea, also even in eukarya (Kessler, 1973), while [Fe]-hydrogenase has been found only in excusive methanogens.

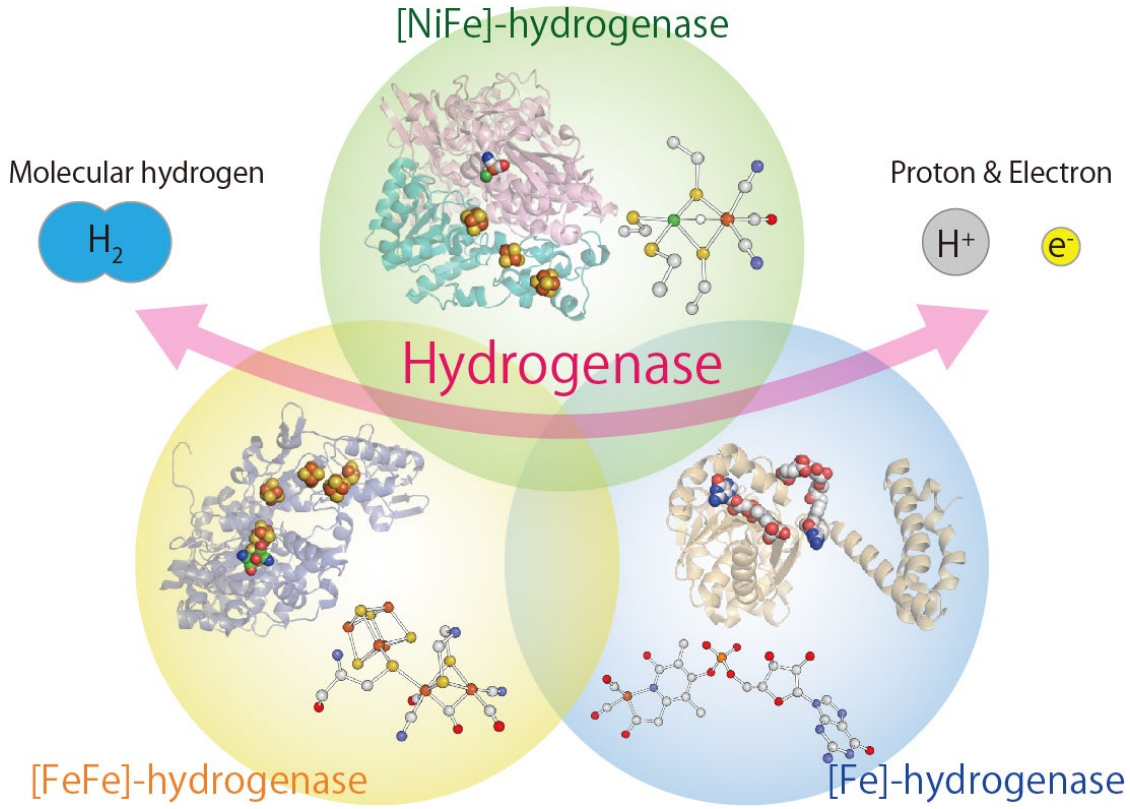

Figure 1. Three general types of hydrogenases.
Hydrogenases are mainly classified into three groups by the metal content in the active site. The catalytic core subunits (hydrogenase unit) for each hydrogenase are illustrated in cartoon representation, and the active site configurations are drawn by ball-and-stick fashion. All three types of hydrogenases catalyze H_2 conversion reaction, however, the catalytic bias depends on the enzyme.

1-2-2. [NiFe]-hydrogenases

[NiFe]-hydrogenase is the well-studied and well-characterized type of hydrogenase. As described above, [NiFe]-hydrogenase has 4 general groups with several subgroups in each group, respectively (in total, 29 categories). Earlier studies are mostly on Group 1 [NiFe]-hydrogenases (see also Table S3). Proposed functions and information on structure determination of the Group 1 [NiFe]-hydrogenases are summarized in Table 1. Other categories and their functions are available from information pages of HydDB (https://services.birc.au.dk/hyddb/;

Søndergaard *et al.*, 2016). In the Group 1 [NiFe]-hydrogenase, crystal structures from 6 of 11 categories have so far been determined, most of them have determined the structure of the hydrogenase unit (without additional physiological electron acceptor).

Table 1. Classification of Group 1 [NiFe]-hydrogenases and their proposed functions according to the metagenomic analysis by Greening and co-worker.

Group	Proposed function	Structure and reference
1a Ancestral	Hydrogenotrophic respiration using sulfate, metal, or organohalide compounds as terminal electron acceptors. Enzyme transfers H_2-liberated electrons through cytochrome *c*$_3$ to terminal reductase.	Db[NiFeSe] (Garcin *et al.*, 1999) DvH[NiFeSe] (Marques *et al.*, 2010)
1b Prototypical	Hydrogenotrophic respiration using sulfate, fumarte, nitrate, metals, and azo compounds as terminal electron acceptors. Enzyme transfers H_2-liberated electrons through cytochromes to terminal reductase.	DgSTD (Volbeda *et al.*, 1995) DvMFSTD (Higuchi *et al.*, 1997) DfSTD (Rousset *et al.*, 1998) DdSTD (Matias *et al.*, 2001)
1c Hyb-type	Hydrogenotrophic respiration using fumarate, sulfate, or metals as terminal electron acceptors. Route of electron transfer unresolved. Can also fermentatively evolve H_2 under hypoxia.	EcHYB (Beaton *et al.*, 2018) S77HYB (this study)
1d O_2-tolerant	Hydrogenotrophic respiration using O_2 or fumarate as terminal electron acceptors. Enzyme transfers H_2-liberated electrons through cyt *b* and quinone to terminal reductase.	ReMBH (Fritsch *et al.*, 2011) HmMBH (Shomura *et al.*, 2011) EcMBH (Volbeda *et al.*, 2012)
1e Isp-type	Hydrogenotrophic respiration using sulfur as terminal electron acceptor. Route of electron transfer unresolved. Complex can also evolve H_2 using sulfur-derived electrons possibly through reversed electron flow or electron-bifurcation.	AvISP (Ogata *et al.*, 2010)
1f O_2-protecting	Unresolved role. Some enzymes mediate hydrogenotrophic respiration using O_2 as a	*N.D.*

	terminal electron acceptor. Enzyme also linked to protection from reactive oxygen species, protection of nitrogenase protection, and recycling of nitrogenase-derived H_2.	
1g Crenarchaeota-type	Hydrogenotrophic respiration using sulfur as terminal electron acceptor. Route of electron transfer unresolved.	*N.D.*
1h Actinobacteria-type	Hydrogenotrophic respiration using O_2 as terminal electron acceptor. Enzyme scavenges electrons from atmospheric H_2 to fuel respiratory chain during carbon-starvation. Route of electron transfer unresolved.	ReAH (Schäfer *et al.*, 2016)
1i Coriobacteria-type	Unconfirmed role. Likely to mediate hydrogenotrophic respiration using unresolved electron acceptor. Enzyme may transfer H_2-liberated electrons through cyt *b* and quinone to unresolved terminal reductase.	*N.D.*
1j Archaeoglobi-type	Hydrogenotrophic respiration using sulfate, iron, or nitrate as terminal electron acceptors. Enzyme transfers H_2-liberated electrons through cyt *b* and quinone to terminal reductase.	*N.D.*
1k Methanophenazine-reducing	Hydrogenotrophic respiration using heterodisulfide as a terminal electron acceptor. Enzyme transfers H_2-liberated electrons through cyt *b* and methanophenazine to heterodisulfide reductase.	*N.D.*

N.D.: Not determined. Proposed functions and previously reported structures are described in HydDB. Some information about the structure and reference are modified or updated by the author.

Although hydrogenase-coding gene organizations are quite different among the groups, the catalytic core subunit, namely hydrogenase unit, is highly conserved. The hydrogenase unit consists of the large subunit and the small subunit (Fig. 2). The Ni-Fe active site is deeply buried in the large subunit. The small subunit harbors three Fe-S clusters which are responsible for the electron transfer during catalysis.

Although gas channels and H^+ pathways are considered to be important factors for the effective catalysis of hydrogenases, they have not still been fully elucidated (Teixeria *et al.*, 2008; Ogata *et al.*, 2015; Kalms *et al.*, 2016).

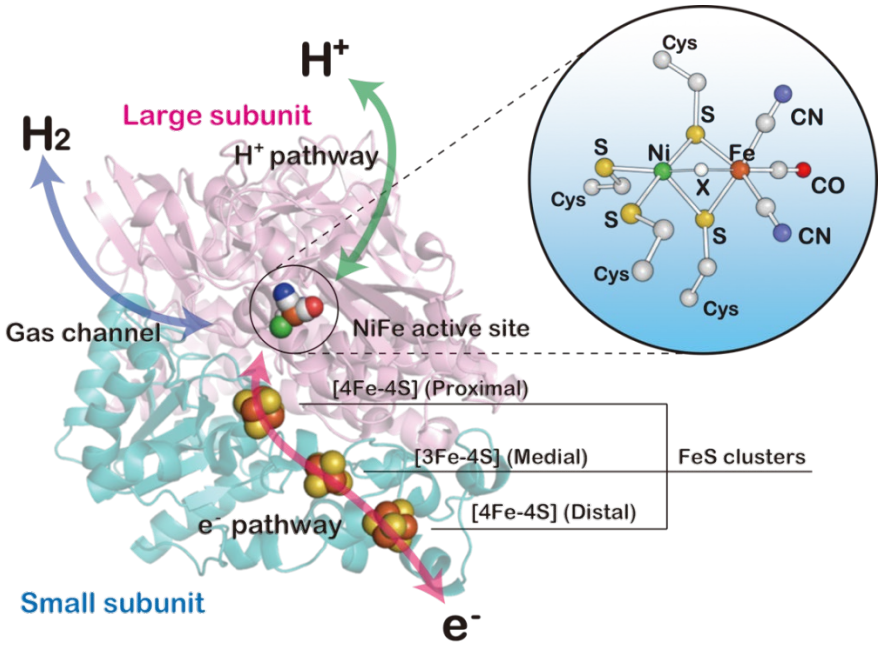

Figure 2. Crystal structure of the hydrogenase unit of a standard [NiFe]-hydrogenase from *Desulfovibrio vulgaris* Miyazaki F (DvMF).

Crystal structure of DvMF (PDB deposition code: 4U9H) is illustrated with several functionally important structures. The large subunit is depicted as cartoon colored light pink, and the small subunit is illustrated as cartoon colored cyan. NiFe active site and FeS clusters are indicated by spheres (white: C, blue: N, red: O, yellow: S, orange: Fe, and green: Ni).

As overall categories, crystal structures of hydrogenases from only several limited groups have been determined, while those from other categories have still been unclear (Table 2, detailed in Table S3–4).

Table 2. Structurally characterized hydrogenases in earlier studies.

Group	Strain	PDB ID	Reference
1b	Dg	1FRV	Volbeda *et al.*, 1995
1b	DvMF	1H2A	Higuchi *et al.*, 1997
1b	Df	1FRF	Rousset *et al.*, 1998
1a	Db	1CC1	Garcin *et al.*, 1999
1b	Dd	1E3D	Matias *et al.*, 2001
1a	DvH	2WPN	Marques *et al.*, 2010
1e	Av	3MYR	Ogata *et al.*, 2010
1d	Re	3RGW	Fritsch *et al.*, 2011
1d	Hm	3AYX	Shomura *et al.*, 2011
1d	Ec	3UQY	Volbeda *et al.*, 2012
1d	Se	4C3O	Bowman *et al.*, 2014
1h	Re	5AA5	Schäfer *et al.*, 2016
3d	Ht	5XFA	Shomura *et al.*, 2017
4d	Pf	6CFW	Yu *et al.*, 2018
1c	Ec	6EHQ	Beaton *et al.*, 2018
1c	S77	5XVB	this study (Noor *et al.*, 2018)
3a	Mb	6QGR	Ilina *et al.*, 2019

For PDB ID in each hydrogenase, only a representative ID is listed. In the reference column, only the first report is listed. Further structural studies are not described here. See also Table S4 for detailed information.

Standard [NiFe]-hydrogenase in Group 1b

Numerous studies on [NiFe]-hydrogenases have been mostly on the enzymes in Group 1b. The enzyme in this group is generally called "standard" hydrogenase. The standard hydrogenase is sensitive to O_2, therefore, easily inactivated in the presence of even trace amount of O_2. Crystal structure from 4 kinds of *Desulfovibrio* species have been determined (Volbeda *et al.*, 1995; Higuchi *et al.*, 1997; Rousset *et al.*, 1998; Matias *et al.*, 2001). In addition, numerous spectroscopic analysis by EPR or FT-IR revealed the structural details on the active site or the catalytic cycle (described in Section 1-3).

O_2-tolerant membrane-bound [NiFe]-hydrogenase in Group 1d

The enzymes in Group 1d are called "O_2-tolerant" hydrogenase. O_2-tolrant hydrogenase can maintain their catalytic activity even in the presence of ambient O_2. Characteristic feature of the hydrogenase in this group is [4Fe-3S]-6Cys cluster at the proximal position. Earlier studies suggested that this special FeS cluster contributes to the O_2-tolerance of the enzyme by complete reduction of O_2 to harmless water (Goris *et al*., 2011). To date, X-ray crystallography (Fritsch *et al*., 2011; Shomura *et al*., 2011; Volbeda *et al*, 2012; Bowman *et al*., 2014), EPR (Saggu *et al*., 2009; Roessler *et al.*, 2012) , FT-IR(Saggu *et al*., 2009), Mössbauer spectroscopy (Pandelia *et al*., 2013), and theoretical studies (Kim *et al*., 2018) have been carried out to identify the key structural features for O_2-tolerance.

Hyb-type [NiFe]-hydrogenase in Group 1c and S77HYB

O_2-tolerance has been considered as one of the important features for the industrial applications of hydrogenases. In addition, the stability in the presence of O_2 is also an important factor. *Citrobacter* sp. S-77 strain was identified from a tepid spring in Aso-Kuju National Park (Eguchi *et al.*, 2012). From this *Citrobacter* strain, Hyb-type [NiFe]-hydrogenase (HYB) which has high O_2-stability was isolated (S77HYB); this is the target hydrogenase in this study. It should be noted that HYB from *Escherichia coli* (EcHYB) was previously reported as an O_2-sensitive hydrogenase (Lukey *et al.*, 2010; Beaton *et al*., 2018).

Immediately before the report of structural analysis on S77HYB (this study; partly described in Noor *et al.*, 2018), crystal structure of EcHYB was reported

(Beaton *et al*., 2018). However, the result suggested that EcHYB is rather O_2-sensitive, not O_2-tolerant.

Table 3. Structural characterization of EcHYB in earlier studies.

PDB ID	state	Resolution[Å]	Reference
6EHQ	as-isolated	2.2	Beaton *et al*., 2018
6EHS	DTT-reduced	1.5	
6EN9	H_2-reduced	1.5	
6GAM	E14Q (as-isolated)	1.4	Evans *et al*., 2018
6GAN	E14Q (fully reduced)	1.6	

One of the remarkable features of the S77HYB is, as described above, high O_2-stability. Even Group 1d O_2-tolerant MBHs lose their catalytic activity after incubation under O_2-containing atmosphere for several hours. In contrast, S77HYB can still maintain 77% of the original activity after 96 hours incubation under 100% O_2 (Eguchi *et al*., 2012). It has been largely believed that O_2-tolerance (or O_2-stability) derives from the structural differences at the proximal FeS cluster, namely [4Fe-3S]-6Cys. Although S77HYB possesses standard [4Fe-4S] cluster (as found in Group 1b O_2-sensitive [NiFe]-hydrogenase, *e.g.* DvMFSTD) instead of [4Fe-3S] cluster, S77HYB exhibited O_2-tolerant catalytic activity (Noor *et al*., 2016).

1-3. Catalytic Mechanism of [NiFe]-hydrogenases

Molecular mechanism of [NiFe]-hydrogenase for H_2 oxidation and H_2 generation has still been unclear, however several catalytic intermediates of the [NiFe]-hydrogenase have been found by spectroscopic methods (Lubitz *et al.*, 2014; Tai *et al.*, 2018). Fig. 3 illustrates the catalytic mechanism and identified catalytic cycle of [NiFe]-hydrogenases. As described in the last section, [NiFe]-hydrogenases

have different subunits as an electron pathway components, therefore, some of the catalytic intermediates are not found in different groups of hydrogenases. Note that here, in Fig. 3, only general catalytic intermediates found in the standard (Group 1b) [NiFe]-hydrogenases are shown. There are additional several intermediates have been identified and characterized by spectroscopic analyses (*e.g.* Ni-SX, Ni-AL, Ni-SL; Osuka *et al.*, 2013; Tai *et al.*, 2017; Tai *et al.*, 2018), however, not depicted in Fig. 3. The catalytic intermediates were well characterized by the *g* values in EPR spectroscopy, and CO and CN frequencies in FT-IR as summarized in Tables S5-S11.

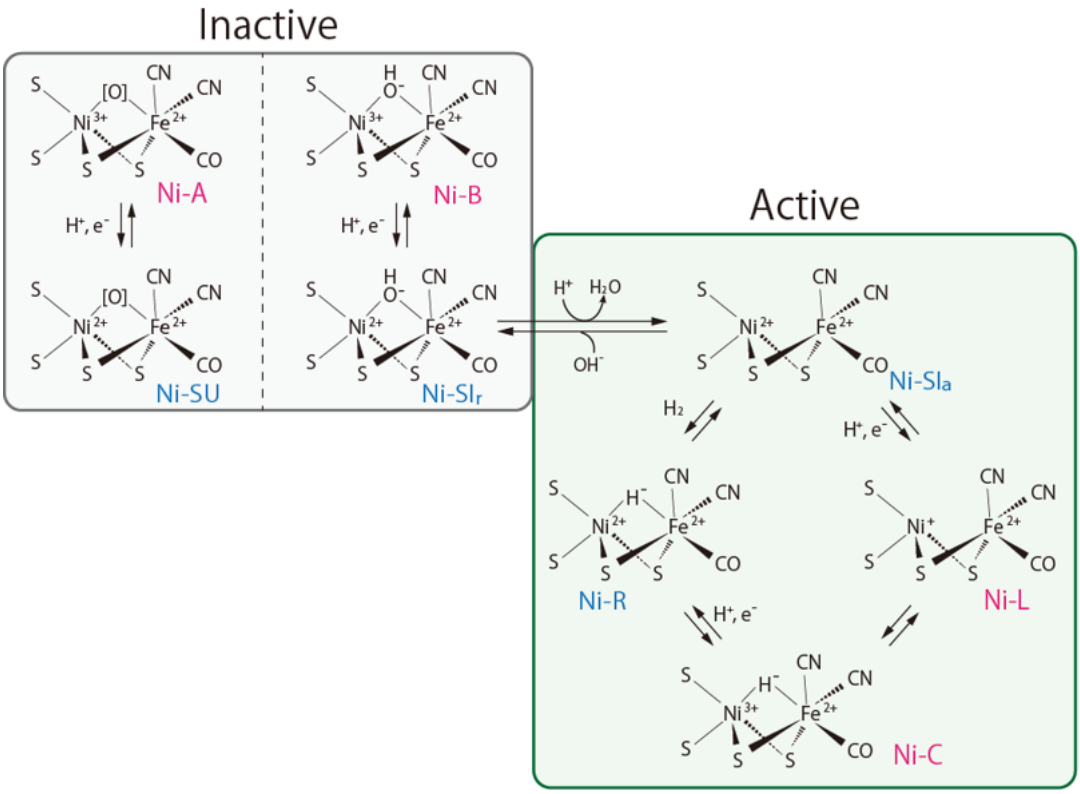

Figure 3. Catalytic cycle and intermediates of [NiFe]-hydrogenases.
Catalytic cycle and catalytic intermediates of standard [NiFe]-hydrogenase is illustrated. The structure of the Ni-Fe active site and the valence of Ni and Fe are depicted according to the earlier studies. Some derivative intermediates by light irradiation, CO-bound state, or poorly understood oxidized state (*e.g.* Ni-AL, Ni-SL, Ni-CO, Ni-SX) are not shown in this figure.

1-4. O_2-tolerant mechanism of [NiFe]-hydrogenases

Hydrogenases are utilized mostly for energy generation under anaerobic atmosphere. Consequently, most of [NiFe]-hydrogenases are sensitive to O_2. To date, several O_2-tolerant [NiFe]-hydrogenase, which can maintain the catalytic activity in the presence of ambient O_2, have been identified and characterized by crystallography, spectroscopy and theoretical analyses. Several terms relating to O_2-tolerance or O_2-stability of [NiFe]-hydrogenases are used in earlier studies, however, there is no consistent definition. To discuss clearly, several terms relating to the O_2-tolerance or O_2-stability of hydrogenases used in earlier studies are summarized in Table 4.

Table 4. Definition of the terms relating to the O_2-tolerance or O_2-stability of hydrogenases used in the earlier studies.

Term	Definition (usage)
O_2-tolerant	The enzyme can maintain the catalytic activity in presence of O_2. Generally only the enzyme which can tolerate under 20% O_2 is called O_2-tolerant. (*e.g.* HmMBH, HtSH, ReRH)
O_2-resistant	The enzyme can be easily reactivated although the enzyme is easily inactivated by even small amount of O_2. (*e.g.* DvMFSTD)
O_2-stable	The enzyme can maintain most of its original activities even after inactivation by O_2. Usually this term is confused and misused for O_2-tolerant and O_2-resistant hydrogenases. (*e.g.* S77HYB)
O_2-sensitive	The enzyme is easily inactivated by O_2. Used for the antonym of "O_2-tolerant" (*e.g.* DvMFSTD, AvISP). The enzymes which irreversibly inactivated by O_2 also called O_2-sensitive (*e.g.* [FeFe]-hydrogenase or [Fe]-hydrogenase)
O_2-insensitive	The enzyme does not interact with O_2. (*e.g.* ReAH)

O_2-tolerance is one of important properties for biotechnological applications of hydrogenases such as industrial H_2 production. In earlier studies, Group 1d O_2-tolerant membrane-bound [NiFe]-hydrogenases (MBH) from

Hydrogenovibrio marinus (Hm), *Ralstonia eutropha* (Re), and *Escherichia coli* (Ec) are well-studied and characterized (Cracknell *et al*, 2009; Lukey *et al*, 2010). Several characterizations revealed that O_2-tolerant MBHs form no or less unready oxidized state, Ni-A (Fig. S2; Lukey *et al*., 2010; Pandelia *et al*., 2011).

The reversible structural movement of $[4Fe\text{-}3S]_{Prox}$ found in MBH from *H. marinus* (HmMBH) (Group 1d) is illustrated in Fig. 4. Group 1d O_2-tolerant MBHs from *R. eutropha* or *E. coli* (ReMBH and EcMBH, respectively) also have same [4Fe-3S]-6Cys type FeS cluster at the proximal site, however, they show slightly different structural change (Volbeda *et al*., 2012; Frielingsdorf *et al*., 2014).

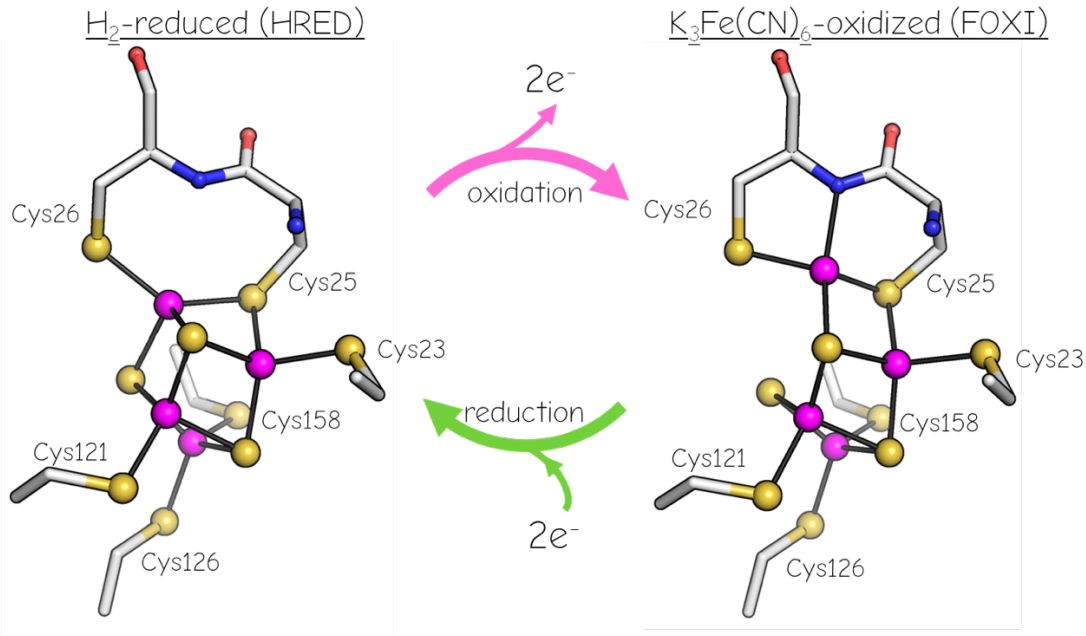

Figure 4. Structural change of the $[4Fe\text{-}3S]_{Prox}$ in HmMBH.
The special $[4Fe\text{-}3S]_{Prox}$ found in Group 1d O_2-tolerant [NiFe]-hydrogenases changes the structure upon oxidation or reduction. Adjacent amide N stabilizes oxidized Fe atoms in $[4Fe\text{-}3S]_{Prox}$ and the structural change is completely reversible. The $[4Fe\text{-}3S]_{Prox}$ provides two electrons, while conventional $[4Fe\text{-}4S]_{Prox}$ can provide only one electron.

Although the slight structural differences were found among Group 1d O_2-tolerant MBHs with $[4Fe\text{-}3S]_{Prox}$, the most important point is the electron donation property of the $[4Fe\text{-}3S]_{Prox}$. Either type of structural change in [4Fe-3S]-6Cys have three redox states, thus, they can provide two electrons for O_2-detoxification without severe oxidative damage. While conventional $[4Fe\text{-}4S]_{Prox}$ stabilizes two redox states, thus the $[4Fe\text{-}4S]_{Prox}$ can provide only one electron.

Furthermore, the [4Fe-3S]-6Cys cluster has another merit to detoxify molecular oxygen. For effective O_2 reduction, the redox potential of Fe–S cluster is important to smoothly transfer electrons. [4Fe-3S]-6Cys cluster has a higher redox potential comparing to the conventional [4Fe-4S]-4Cys cluster found in standard O_2-sensitive hydrogenases. This is known as a "high-potential" and "low-potential" Fe-S cluster as discussed in the earlier studies (Armstrong *et al.*, 2016).

O_2-tolerance without [4Fe-3S]-6Cys cluster

Recently several hydrogenases which do not have $[4Fe\text{-}3S]_{Prox}$ were identified as O_2-tolerant hydrogenase. S77HYB is one of the examples of them (Eguchi *et al.*, 2012; Noor *et al.*, 2016). Most of those enzymes have canonical [4Fe-4S]-4Cys cluster at the proximal position. This $[4Fe\text{-}4S]_{Prox}$ normally has two oxidation states ($[4Fe\text{-}4S]^{+}$ and $[4Fe\text{-}4S]^{2+}$), and can produce only one electron to the active site when the enzyme is oxidized. The standard $[4Fe\text{-}4S]_{Prox}$ has low redox potential, thus the electron transfer to molecular oxygen is not effective comparing to "high-potential" Fe–S cluster ([4Fe-3S]-6Cys). Due to the insufficient structural information on such enzymes, molecular mechanisms of O_2-tolerance in those

hydrogenases have still been unknown.

In the recent study on O_2-tolerant ReMBH, O_2-tolerant catalytic activity was confirmed only with the large subunit (Hartmann *et al.*, 2018). The result implies that ReMBH is rather "O_2-insensitive" hydrogenase, even it is classified into Group 1d "O_2-tolerant" hydrogenase. However, the O_2-tolerant activity of ReMBH was measured for H/D exchange catalysis, therefore, it does not require any electron transfers. The results obtained by Hartmann and co-workers should be discussed in further investigations.

Furthermore, structural analysis on EcMBH revealed that the quaternary structure of the hydrogenase have an important role for O_2-tolerance. Hitherto-determined crystal structures of Group 1d O_2-tolerant hydrogenases have dimer of heterodimer configuration. This configuration enables electron transfer via distal FeS clusters, therefore the intermolecular electron transfer also contributes to the O_2-tolerance of the hydrogenase (Wulff *et al.*, 2016).

Moreover, several hydrogenases have blocking mechanism against O_2 invasion. [NiFeSe]-hydrogenase (Group 1a [NiFe]-hydrogenase) protects the active site from O_2 by selenocysteine residues coordinating to Ni in the active site (Marques *et al*., 2017). Gas channel has also been considered as an important structural feature for O_2-tolerance because narrower channel enables to block the access of O_2 into the active site (Dementin *et al*, 2009).

In addition, SH (Group 3d soluble [NiFe]-hydrogenase) from *H. thermoluteolus* TH-1 (HtSH) or from *R. eutropha* (ReSH) are reported as O_2-tolerant [NiFe]-hydrogenases even with $[4Fe–4S]_{Prox}$. However, the enzymes have several FeS

clusters (more than three FeS clusters) which can be contributed to produce electrons for O_2-reduction. Additionally, structural analysis of HtSH revealed that the oxidized HtSH has unidentified coordination (Fig. 5) which can protect the Ni–Fe active site from further oxidative damage (Shomura *et al.*, 2017). This structural change should correspond to the protecting mechanism against further oxidative damage found in the standard [NiFe]-hydrogenases in Group 1b (*e.g.* DvMFSTD), most probably HtSH is more robust comparing to DvMFSTD.

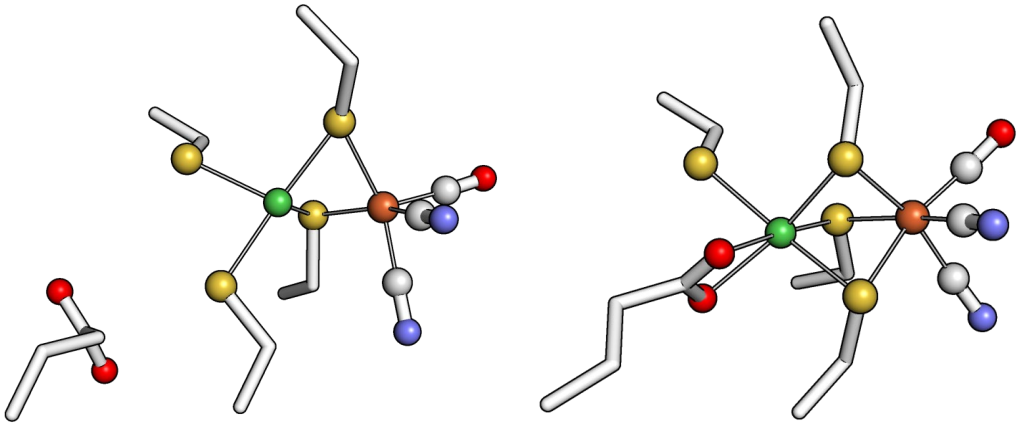

Figure 5. Structural change at the Ni–Fe active site found in HtSH.
Crystal structure of the Ni–Fe active site in (A) HRED and (B) AOXI state. In AOXI state, Glu was involved in Ni coordination and S atom of coordinated Cys bridged at the third bridging position. This is an exceptional active site configuration comparing to other hitherto-determined [NiFe]-hydrogenases.

Taken together, current understandings on O_2-tolerance or O_2-stability of hydrogenases should be updated for further applications of the enzyme.

1-5. Aim of this study

As described above, the efficient catalysis by hydrogenases has been received much attention due to their potential usefulness to the biotechnological

applications to realize H_2 economy. Above all, O_2-tolerance or O_2-stability are of key importance for the applicational use of the enzyme.

S77HYB has high catalytic activities with exceptionally high stability against O_2. Although the O_2-tolerant MBHs have only H_2 oxidation activity, S77HYB can catalyze more potent H_2 oxidation activity and H^+ reduction (H_2 generation) activity as well. Therefore, S77HYB exhibits promising catalytic features for industrial use. However, the structural details of the enzyme had been unraveled.

The first aim of this study is to elucidate the molecular mechanism of extremely high O_2-stability of S77HYB. Group 1c [NiFe]-hydrogenase has been known as an O_2-sensitive hydrogenase (*e.g.* EcHYB (Lukey *et al*., 2010)), however, S77HYB exhibits the catalytic activities in the presence of O_2. During this study, fortunately, crystal structures of EcHYB at several conditions were determined and reported by Beaton and co-workers (Beaton *et al*., 2018). In this study, the structures of S77HYB and EcHYB are carefully compared. The structural differences among various hydrogenases were also investigated in this study in order to elucidate the molecular mechanism of O_2-stability of hydrogenases.

Another aim of this study is to revisit the O_2-tolerance or O_2-stability of [NiFe]-hydrogenases. Definitions of the term relating to O_2-stability of hydrogenases are still ambiguous, and sometimes confusing. In this study, O_2-tolerance and O_2-stability of [NiFe]-hydrogenases are reviewed.

Chapter 2. MATERIALS AND METHODS

2-1. Bacterial culture of *Citrobacter* sp. S-77

Citrobacter sp. S-77 strain is a facultative anaerobic bacterium, but can grow well under both aerobic and anaerobic atmospheres. In this study S-77 strain was cultured under aerobic atmosphere as described in the literature (Eguchi *et al*., 2012; Noor *et al*, 2016a, b).

Bacterial stock was prepared by mixing precultured cells with 50% *v/v* glycerol at 1:1 ratio and stored at -80°C until use.

1 mL of the glycerol stock was transferred to 200 mL of culture media (the composition of the culture media described in Table 5 and Table S1). S-77 strain was precultured for 48 hours at 30°C without shake in 250 mL glass bottle tightly capped with septum rubber in order to avoid further O_2 dissolving during the cultivation.

Table 5. Composition of the media for the bacterial culture of *Citrobacter* sp. S-77.

Reagent	Liquid media (g/L)
Yeast extract	3.0
Polypeptone	3.0
$(NH_3)_2SO_4$	3.0
$Mg_2SO_4 \cdot 7H_2O$	0.5
K_2HPO_4	2.0
KH_2PO_4	1.0
$Na_2S_2O_3 \cdot 5H_2O$	2.0
Ammonium ferric citrate	0.2
$CaCl_2$	0.1

pH is in the range of 6.8–7.0 without any control. The medium composition is same in both preculture and main culture.

Precultured bacteria were then inoculated into 16 L of the media (compositions are same as used in the preculture) and incubated at 30°C for 64–67 hours without shake. Bacterial cells were harvested at late-exponential phase by

centrifugation at 12,000 × *g* for 10 minutes at 4°C. Collected cell precipitations were then washed with 10 mM MOPS-KOH pH 7.0 and centrifuged again at 12,000 × *g* for 15 min at 4°C. Finally obtained cells were frozen in liquid nitrogen and stored at -80°C until purification.

2-2. Purification of S77HYB

All the purification procedures described below were carried out at room temperature under anaerobic condition using the anaerobic glove box (Type B, Coy Laboratory Products, USA) unless otherwise noted. Detailed procedures were also described in the literatures (Eguchi *et al*., 2012; Noor *et al.*, 2016a, b). Buffers used for purification of S77HYB from *C.* S-77 are listed in Table 6 (see also Table S2).

Table 6. Buffer composition used for purification of S77HYB.

Buffer	Compositon
Disruption	10 mM MOPS-KOH pH 7.0, 1 mM DTT
Solubilization	10 mM MOPS-KOH pH 7.0, 1 % *w/v* Triton X-100, 1 mM DTT
1A	10 mM MOPS-KOH pH 7.0, 0.03% *w/v* Triton X-100, 0.5 mM DTT
1B	10 mM MOPS-KOH pH 7.0, 0.03% *w/v* Triton X-100, 1 M NaCl, 0.5 mM DTT
2A	10 mM MOPS-KOH pH 7.0, 0.5 mM DTT
2B	10 mM MOPS-KOH pH 7.0, 1 M NaCl, 0.5 mM DTT
3A’	10 mM MOPS-KOH pH 7.0, 0.4 M Ammonium sulfate, 0.5 mM DTT
3A	10 mM MOPS-KOH pH 7.0, 0.2 M Ammonium sulfate, 0.5 mM DTT
3B	10 mM MOPS-KOH pH 7.0, 0.5 mM DTT
Dialysis	10 mM MOPS-KOH pH 7.0, 0.2 M NaCl

Isolation of the hydrogenase from membrane

All procedures until the solubilization of S77HYB from the membrane were

performed under aerobic condition. Harvested cells (ca. 70 g) were suspended into 400 mL of disruption buffer and stirred well for 1 hour prior to the sonication. Bacterial cells were disrupted by sonication with following parameters (Table 7) using Q700 sonicator (QSONICA, USA). Temperature was strictly monitored and kept below 20°C during sonication in order to avoid aggregation or damage of the protein.

Table 7. Parameters for sonication by QSONICA.

Parameters [unit]	Values
Amplitude	27
Process time [min]	38
Pulse on [sec]	5
Pulse off (interval) [sec]	5

The sonicated lysate was ultracentrifuged at 150,000 × *g* for 1 hr at 4°C using NX-80 ultracentrifuge (Hitachi, Japan). Supernatant was discarded because S77HYB is anchored to the periplasmic membrane by single helix located in the C-terminus of the small subunit HybO. Precipitated membrane fractions were suspended with 200 mL of solubilization buffer without any detergent (10 mM MOPS-KOH pH 7.0, 1 mM DTT). 200 mL of solubilization buffer (10 mM MOPS-KOH pH 7.0, 1 mM DTT with 2% (*v/v*) Triton X-100) was then added to solubilize the hydrogenase from the membrane. Membrane suspended solution was further degassed with vacuum pump over 1 hour in the anaerobic glove box to remove dissolved O_2 in order to avoid aerobic inactivation, aggregation, or degradation of hydrogenase. Degassed membrane suspension was tightly sealed with septum rubber cap and stirred gently at 4°C for overnight. Solubilized hydrogenase was collected by ultracentrifugation at 150,000 × *g* for 1 hr at 4°C.

Trypsin digestion

S77HYB isolated from the membrane contains flexible single helix in C-terminus of HybO (the small subunit). Previous preriminary crystallographic study revealed that the flexible helix affects the crystal packing, quality of the cyrstals, and the yield of the purified enzyme (Noor *et al*., 2016a, b). Therefore, collected supernatant including S77HYB was digested by 15 mg of trypsin in order to remove the flexible loops. Trypsin was anaerobically added into the supernatant after the last ultracentrifuge, then tightly sealed the bottle with the septum rubber cap, and incubated at 37 °C for 1hr.

Anion exchange column chromatography with DEAE Sepharose Fast Flow

Immediately after trypsin digestion of solubilized protein solution, the hydrogenase solution was applied into an anion exchange column, DEAE Sepharose Fast Flow (column volume (CV): 80 mL of resin in XK 26/20 column, GE Healthcare, UK),preequilibrated with the buffer 1A (10 mM MOPS-KOH pH 7.0, 0.03% v/v Triton X-100, 1 mM DTT), and hydrogenase was eluted by linear gradient of buffer 1B (10 mM MOPS-KOH pH 7.0, 0.03% (*v/v*) Triton X-100, 0.5 mM DTT with 1 M NaCl). All the column chromatography described here was carried out using AKTA prime plus (GE Health Care, USA). Activities of hydrogenases in fractionated eluates were checked by Native-PAGE with 8% polyacrylamide gel and active staining by the active staining buffer(10 mM MOPS-KOH pH 7.0, 1 mM Benzyl viologen (BV) and 1 mM Triphenyl tetrazolium chloride (TTC)) with H_2 gas bubbling for 10 min at 30 °C.

Anion exchange column chromatography with HiTrap Q HP

Since collected eluate includes a little amount of NaCl, pooled fraction was firstly diluted with buffer 2A (10 mM MOPS-KOH pH 7.0, 0.5 mM DTT) for approximately two times prior to applying into the column in order to avoid flowing throw the hydrogenases. Diluted hydrogenase solution was then applied to an anion exchange column, HiTrap Q HP (CV: 5 mL, pre-packed column, GE Healthcare, UK), preequilibrated by buffer 2A (10 mM MOPS-KOH pH 7.0, 0.5 mM DTT). Applied hydrogenase solution was then eluted with buffer 2B (10 mM MOPS-KOH pH 7.0, 1 mM DTT with 1 M NaCl). Eluted fraction was checked by Native-PAGE and active staining as described in the previous step.

Hydrophobic interaction column chromatography with HiTrap Phenyl HP

Collected fraction from the last anion exchange column chromatography was diluted with buffer 3A' (10 mM MOPS-KOH pH 7.0, 0.5 mM DTT with 0.4 M ammonium sulfate) prior to applying to an hydrophobic interaction column, HiTrap Phenyl HP (CV: 5 mL, pre-packed column, GE Healthcare, UK). After elution with buffer 3B (10 mM MOPS-KOH pH 7.0, 1 mM DTT), eluate was checked by Native-PAGE with active staining, and SDS-PAGE using 13% acrylamide gel with CBB staining. Finally, collected fractions were concentrated to less than 5 mL using Vivaspin Turbo 15 (Molecular weight cut off (MWCO): 30,000 Da; Sartorius, Göttingen, Germany), then purified S77HYB was anaerobically dialyzed against dialysis buffer (10 mM MOPS-KOH pH 7.0, 0.5 mM DTT with 0.2 M NaCl) using Spectra-Por Float-A-Lyzer G2 (MWCO: 8-10 kDa; Repligen Corp., Massachusetts,

USA) for overnight. Dialysis buffer was exchanged once in an hour and the enzyme solution with the dialysis membrane was gently stirred for overnight at 4 °C.

H_2-oxidation activity measurement using benzyl viologen

H_2 oxidation activities of purified hydrogenases were monitored by change of the absorbance at 600 nm colored by reduced benzyl viologen (BV; 1,1'-dibenzyl-4,4'-bipyridinium dichloride, E=-350 mV vs. SHE). The electrons produced by the catalysis of hydrogenases are transferred to BV via FeS clusters in HybO (small subunit of the hydrogenase) and BV will be reduced and colored blue.

Reaction setup for the activity measurement is summarized in Table 8. 2870 μL of 10 mM MOPS-KOH pH 7.0 with 10 μL of purified hydrogenase solution was filled into 5 mL cuvette and was tightly sealed with septum rubber cap. H_2 gas was introduced into the cuvette with the speed of 50 mL/min for 10 minutes in order to remove dissolved O_2 and reactivate hydrogenases. The cuvette was then transferred to the Peltier temperature control sample holder of UV-vis spectrophotometer V-660(JASCO, Japan) and incubated for 3 minutes. 120 μL of reaction reagent (500 mM benzyl viologen dissolved in 10 mM MOPS-KOH pH 7.0) was injected using gas-tight syringe and time dependent absorbance change at 600 nm was monitored at 30°C.

Table 8. Reaction setup for H_2-oxidation activity measurement using BV.

Reagent	Volume Volume [μL]
10 mM MOPS-KOH pH 7.0	2870
Protein sample	10
500 mM BV	120
Total	3000

Determination of S77HYB concentration

Concentration of purified S77HYB was determined from the absorbance at 400 nm, where the molar extinction coefficient $\varepsilon_{400,ox}$ = 13 $mM^{-1}cm^{-1}$, and protein concentration determination kit, DC protein assay kit purchased from the manufacturer (Bio-rad Laboratories, Inc., USA). Molar extinction coefficient were estimated from the result of amino acid analysis performed by Prof. Dr. Hironobu Hojo at Institute for Protein Research, Osaka University.

2-3. Crystallization of S77HYB and preparation of HRED- and FOXI-S77HYB

2-3-1. Crystallization of air-oxidized S77HYB

Concentration of the purified S77HYB was estimated from the absorbance at 400nm, where oxidized Fe-S clusters have broad peak, using molar extinction coefficient ε = 13 $mM^{-1}cm^{-1}$. Crystals of S77HYB were aerobically obtained by following conditions (Table 9). Brown crystals appeared within 3 days and grown for 2 weeks, then fished and flash cooled by liquid nitrogen until the diffraction experiments.

Table 9. Crystallization conditions for S77HYB.

Method	Sitting-drop vapor diffusion
Temperature (K)	283
Protein concentration (mg/mL)	15
Buffer composition of protein solution	10 mM MOPS pH 7.0, 0.2 M NaCl
Composition of reservoir solution	0.1 M Tris-HCl pH 8.5, 0.2 M NaCl, 19% *w/v* PEG 10,000, 20% *w/v* glycerol
Volume and ration of drop (μL)	0.5:0.5
Volume of reservoir	70

2-3-2. H_2-reduction and $K_3[Fe(CN)_6]$-oxidation of S77HYB crystals

Aerobically obtained crystals were transferred into a glass vial (0.2 mL) with 70 μL of crystallization buffer including 1 mM BV, where the concentration of PEG 10,000 was increased 1 % in order to avoid crystal decay. Gas phase of the glass vial was well degassed and 100% H_2 gas was purged into the vial. After overnight incubation at 10°C, crystals were reduced (H_2-reduced; HRED), then fished and flash cooled inside the anaerobic chamber.

For obtaining ferricyanide-oxidized crystals, H_2-reduced crystals were further soaked into the crystallization buffer with 5 mM ferricyanide (without any artificial electron mediator). Following to the incubation at 10°C for overnight, the crystals were fished, and flash cooled by liquid nitrogen inside the glove box. All the crystals were stored in a dewar filled with liquid nitrogen until the diffraction measurements.

2-4. X-ray diffraction data collection and structural analysis of S77HYB

X-ray diffraction datasets for air-oxidized (AOXI), H_2-reduced (HRED) and $K_3[Fe(CN)_6]$-oxidized (FOXI) S77HYB crystals were obtained at BL44XU beamline in SPring-8 (Hyogo, Japan). Native datasets were collected with the wavelength of λ = 0.90000 Å (Table 10), and anomalous datasets were collected with λ = 1.74 Å.

Diffraction datasets were processed using X-ray Detector Software (*XDS*) program package (Kabsch, 2010) and some data reduction software. Firstly, AOXI-S77HYB structure was determined. Initial phase determination for AOXI-S77HYB was performed by molecular replacement method using the program *Phaser* (McCoy *et al.*, 2007) in *CCP4* suite (Winn *et al.*, 2011) with the coordinate of Group 1d O_2-

Table 10. Experimental parameters for native data collection of S77HYB.

	AOXI	HRED	FOXI
X-ray source	BL44XU	BL44XU	BL44XU
Wavelength[Å]	0.90000	0.90000	0.90000
Temperature [K]	100	100	100
Detector	MX-300 HE (Rayonics)	MX-300 HE (Rayonics)	MX-300 HE (Rayonics)
Crystal-to-detector distance [mm]	160.0	270.0	250.0
Oscillation range [deg]	0.5	1.0	0.5
Total rotation range [deg]	180	180	180
Exposure time per image [s]	0.5	1.0	1.0

tolerant membrane-bound [NiFe]-hydrogenase from *H. marinus* (PDB accession code: 3AYX) as a search model (Shomura et al., 2011). Jelly-body refinement was applied by the program *Refmac5* (Murshudov *et al*., 2011) following to the molecular replacement. Iterative cycles of manual model building and refinement were carried out by *Coot* (Emsley *et al.*, 2004; Emsley *et al*., 2010) and *Refmac5*. Further refinement for occupancies was conducted by command line version of *phenix.refine* program (Adams *et al.*, 2010; Afonine *et al.*, 2012).

Radiation damages for each datasets were calculated by *RADDOSE-3D* (Zeldin *et al*., 2013) to confirm whether the X-ray dose were well below the Garman limit of 20 MGy (Owen *et al*., 2006).

Initial phasing for HRED- and FOXI-S77HYB datasets were performed by the molecular replacement method using the program Phaser with the atomic coordinate of AOXI-S77HYB as a reference structure. Further model building and structural refinement process were similarly carried out as well as AOXI-S77HYB.

2-5. EPR and FTIR spectroscopic studies on S77HYB

Spectroscopic measurements were performed in order to identify correlations between the structural change and O_2-stability of S77HYB. The measurements were mainly conducted by Dr. Hulin Tai (Nara Institute of Science and Technology, NAIST; currently a researcher of Sun Yat-Sen University). Detailed information about materials and methods is described in Supporting Information.

2-6. Theoretical calculation for S77HYB and DvMFSTD.

Theoretical calculations were conducted to investigate the structural change of the $[4Fe\text{-}4S]_{Prox}$ of S77HYB and compare the structural flexibility of the $[4Fe\text{-}4S]_{Prox}$ between S77HYB and DvMFSTD. The calculations were performed by Dr. Jiyoung Kang and Prof. Dr. Masaru Tateno. Detailed methodologies are described in the supplementary material.

Chapter 3. RESULTS AND DISCUSSIONS

3-1. Bacterial culture of *Citrobacter* sp. S-77

70 – 80 g (wet weight) of bacterial cells are routinely obtained from 32 L cultivation of *Citrobacter* sp. S-77 strain (*C*. S-77). Harvested cells were frozen by liquid nitrogen and stored at -80°C until use.

3-2. Purification of S77HYB from *Citrobacter* sp. S-77

Overview of the purification result

Purification of S77HYB from *C.* S-77 was carried out with or without trypsin treatment. Due to the flexible single helix located in C-terminal of HybO (the small subunit of S77HYB), trypsin digestion effectively increased the stability and yield of the enzyme. 3–5 mg of S77HYB were obtained from the purification without trypsin treatment, while approximately 10 mg of S77HYB are routinely obtained from the purification with trypsin treatment. Detailed information is also described in the earlier studies (Noor *et al.*, 2016a, b). Here only a purification result with trypsin treatment is described.

First column chromatography with DEAE Sepharose FF

Solubilized S77HYB solution was digested by 15 mg of trypsin at 37°C for 1 hour. The digested sample solution was applied to an anion-exchange column DEAE Sepharose FF and S77HYB was eluted with linear gradient of NaCl.

Elution curve obtained from the first anion exchange column chromatography is shown in Fig. 6. S77HYB appeared mainly in the second broad peak (fraction number: 13 – 21) of the elution curve. Fractionated eluate was

checked by Native-PAGE and following active staining (Fig. 7), then the fractions containing highly active hydrogenase (fraction number: 13 – 17) were collected and applied to the next column chromatography.

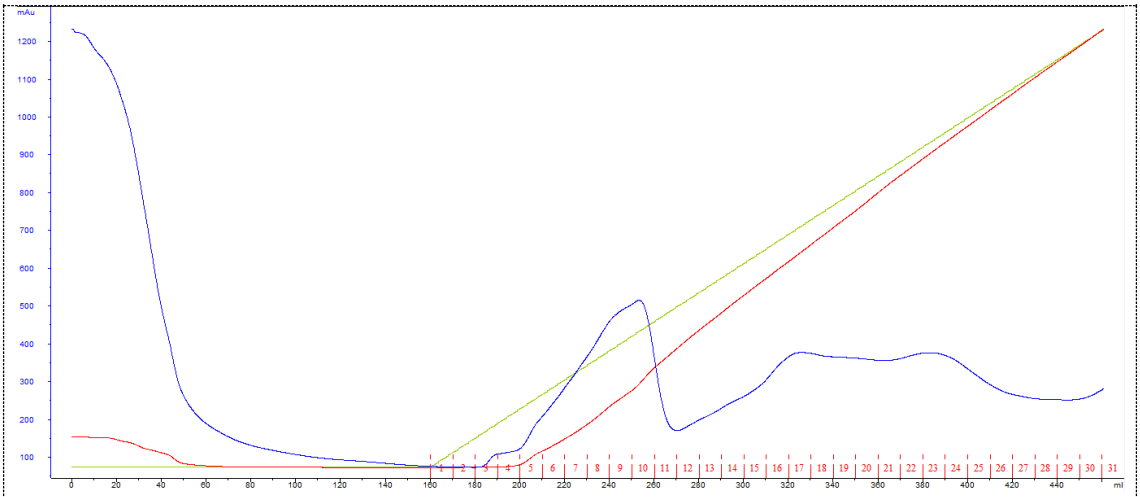

Figure 6. Elution curve from the first anion exchange column chromatography using DEAE Sepharose Fast Flow.

Blue: Absorbance at 280 nm, Red: Conductivity, Lightgreen: Concentration of Buffer 1B. The number depicted with short vertical dashes indicate the fraction number.

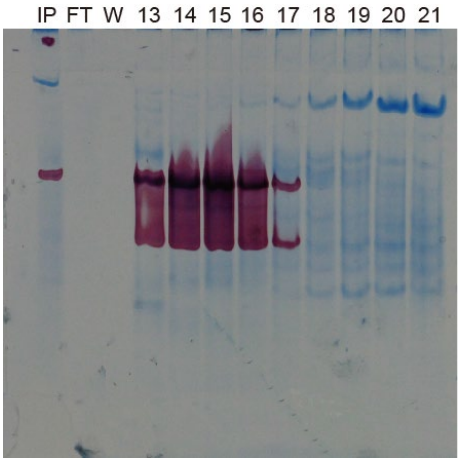

Figure 7. Result of the active staining after the first anion exchange column chromatography DEAE Sepharose Fast Flow.

Input sample (IP), flow through (FT), wash (W) and eluate factions were checked by Native-PAGE and stained by active staining and CBB. The band colored red corresponds to the active hydrogenase.

Second column chromatography with HiTrap Q

Pooled fractions from the last column chromatography was diluted by Buffer 2A (10 mM MOPS-KOH pH 7.0, 1 mM DTT) in order to decrease the concentration of NaCl. The diluted sample was applied to an anion exchange column, HiTrap Q HP, and S77HYB were eluted by NaCl linear gradient. Elution curve and the result of Native-PAGE stained by the active-staining are shown in Figs. 8 and 9. Fractions with highly active hydrogenase (fraction number: 9 – 11) were collected and applied to the next column chromatography.

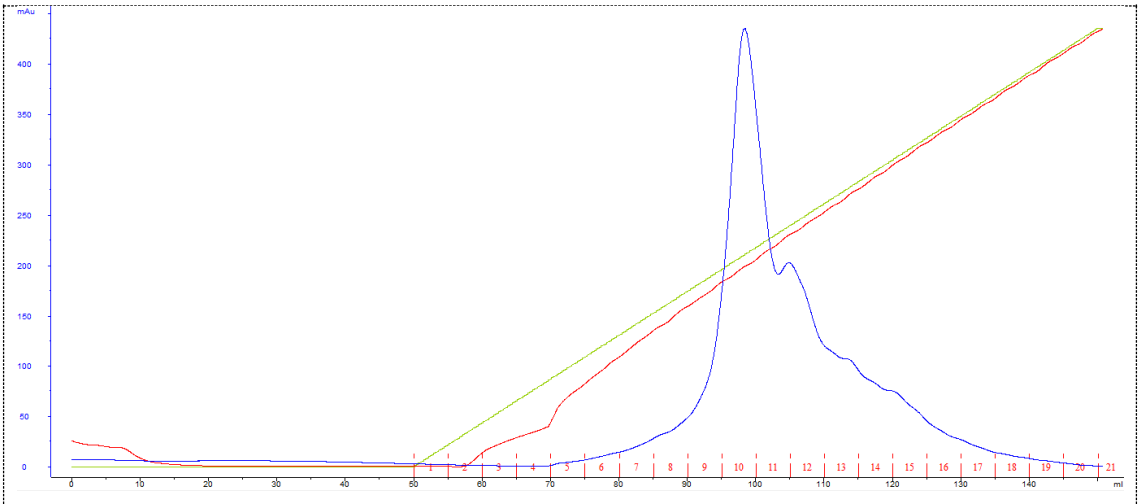

Figure 8. Elution curve from the second anion exchange column chromatography using HiTrap Q HP.

Blue: Absorbance at 280 nm, Red: Conductivity, Lightgreen: Concentration of buffer 2B. The number depicted with short vertical dashes indicate the fraction number.

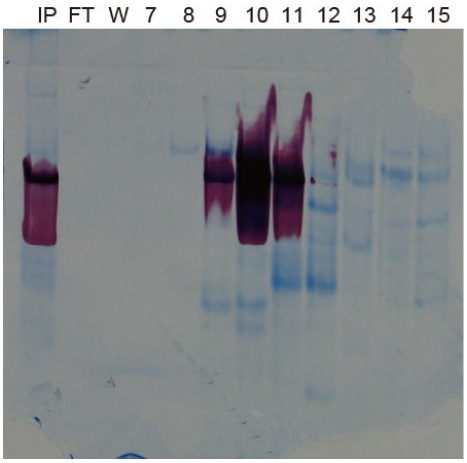

Figure 9. Result of the active staining after the second anion exchange column chromatography with HiTrap Q HP.

Input sample (IP), flow through (FT), wash (W) and eluate faction was checked by Native-PAGE and stained by active staining and CBB. The band colored red corresponds to the active hydrogenase.

Final column chromatography: HiTrap Phenyl HP

Pooled fractions were diluted with Buffer 3A' (10 mM MOPS-KOH pH 7.0, 0.4 M Ammonium sulfate, 1 mM DTT) in order to bind the hydrogenase sample to a hydrophobic interaction column, then applied to HiTrap Phenyl HP. Hydrogenases were eluted by linear gradient of buffer 3B (10 mM MOPS, 1 mM DTT). Elution curve of the hydrophobic interaction column chromatography is shown below (Fig. 10).

Eluates were checked by both Native-PAGE and SDS-PAGE in order to confirm the activity and purity of eluted fractions (Figs. 11 and 12). Active hydrogenase bands were appeared in 7 minutes bubbling with H_2 gas.

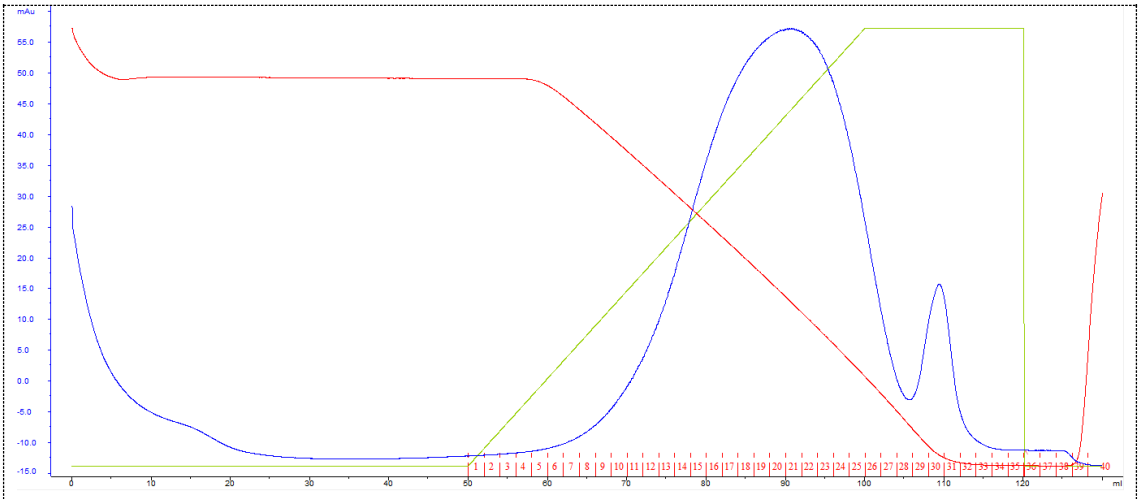

Figure 10. Elution curve from the hydrophobic interaction column chromatography using HiTrap Phenyl HP.

Blue: Absorbance at 280 nm, Red: Conductivity, Lightgreen: Concentration of buffer 3B. The number depicted with short vertical dashes indicate the fraction number.

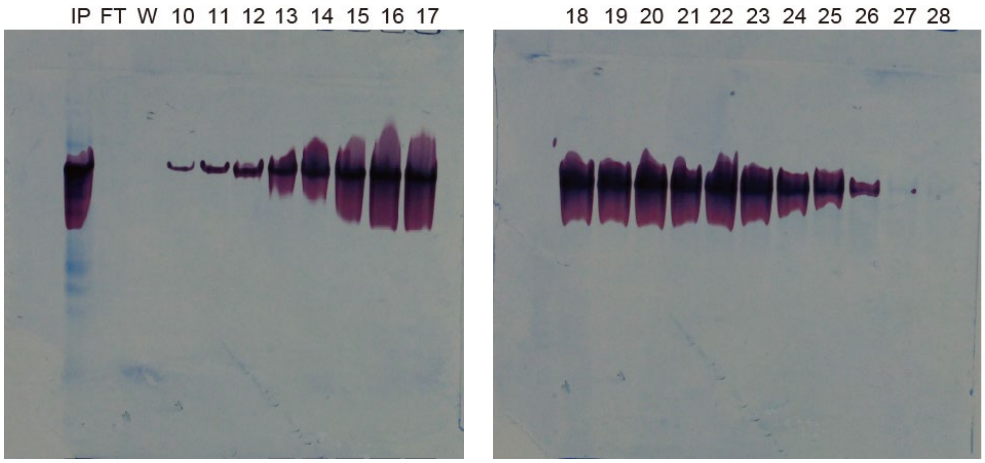

Figure 11. Result of the active staining after the hydrophobic interaction column chromatography with HiTrap Phenyl HP.

Input sample (IP), flow through (FT), wash (W) and eluate faction (fraction number) was checked by Native-PAGE and stained by active staining. The band colored red corresponds to the active hydrogenase.

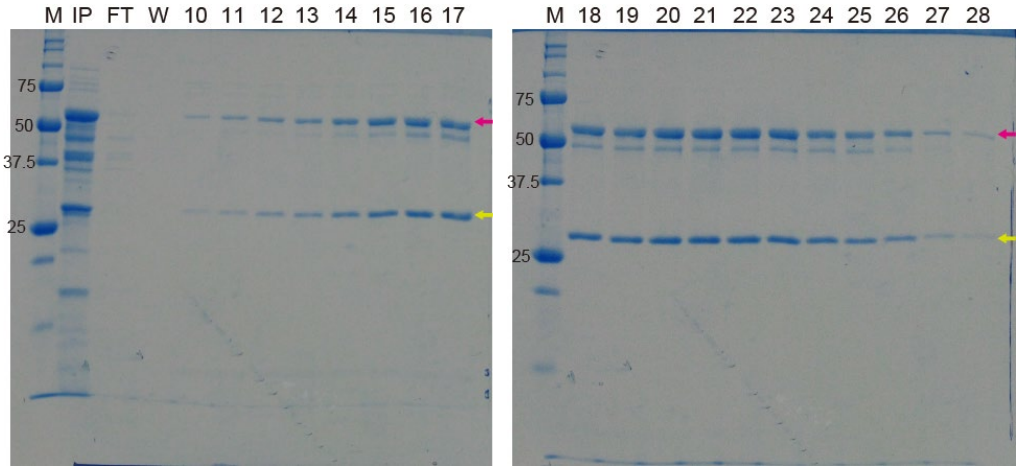

Figure 12. Result of the SDS-PAGE after the hydrophobic interaction column chromatography with HiTrap Phenyl HP.

Input sample (IP), flow through (FT), wash(W) and eluate fraction (fraction number) was checked by SDS-PAGE and stained by CBB. Molecular weight marker were loaded in each polyacrylamide gel. The large subunit has ca. 58.4 kDa and the small subunit has ca. 35.0 kDa indicated by magenta and yellow arrow, respectively.

Active hydrogenase with high purity (fraction number: 13 – 26) was collected and anaerobically dialyzed against dialysis buffer for overnight. Dialyzed hydrogenase sample was concentrated to an appropriate concentration for further experiments (crystallization or spectroscopic measurements). The activity of purified S77HYB was determined by the activity measurement using BV, and the specific activity was estimated from the results. The specific activity of the S77HYB after purification was routinely over 600 U/mg as well as that reported in earlier studies (Eguchi *et al.,* 2012, Noor *et al.*, 2016a, b).

3-3. Crystallization of S77HYB

3-3-1. Crystallization of S77HYB under aerobic conditions

Crystals of S77HYB was aerobically obtained under the similar conditions described in the earlier studies (Noor *et al.*, 2016a, b). Brown crystals of S77HYB

were appeared within 3 days, however, the obtained crystals were grown for two weeks before freezing or any treatments. The crystals were appeared in similar conditions around the crystallization conditions described in the previous report (Table 11). One of the examples of obtained crystals suitable for the diffraction measurements is shown in Fig. 13.

Table 11. Crystallization conditions where S77HYB crystals were obtained in this study.

Method	Sitting-drop vapor diffusion
Temperature (K)	283
Protein concentration (mg/mL)	15–25
Buffer composition of protein solution	10 mM MOPS pH 7.0, 0.2 M NaCl
Composition of reservoir solution	0.1 M Tris-HCl pH 8.5, 0.2 M NaCl, 19-21% *w/v* PEG 10,000, 20% *w/v* glycerol
Volume and ration of drop (μL)	0.5:0.5
Volume of reservoir	70

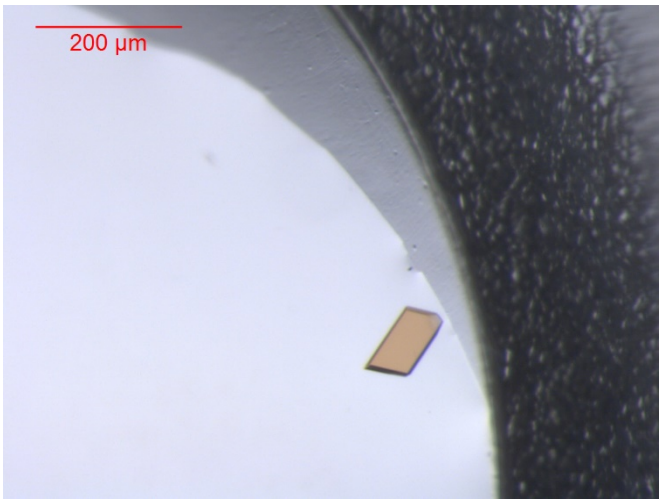

Figure 13. Crystal of S77HYB obtained under aerobic conditions.
A brown crystal was obtained from the crystallization conditions described in the literature (Noor *et al*, 2016a, b). The crystal was obtained at the following reservoir conditions: 0.1 M Tris-HCl pH 8.5, 20% *w/v* PEG 10,000, 0.2 M NaCl and 20% *w/v* glycerol (Protein concentration: 15 mg/mL).

Crystals of S77HYB were mostly appeared at the following reservoir composition: 0.1 M Tris-HCl pH 8.5, 20% *w/v* PEG 10,000, 0.2 M NaCl with 20% *w/v* glycerol at the protein concentration of 15–25 mg/mL. The obtained AOXI-S77HYB crystals were flash cooled in liquid nitrogen (LN_2) and stored in the dewar filled with LN_2 until the diffraction measurements.

3-3-2. H_2-reduction and $K_3[Fe(CN)_6]$-oxidation of S77HYB crystals

Aerobically obtained crystals of S77HYB (AOXI state) was reduced by H_2 to obtained H_2-reduced state (HRED). AOXI-S77HYB crystals were fished from the crystallization drop, then transferred into the crystallization buffer with 1% *w/v* higher concentration of PEG 10,000 to avoid melting. In order to facilitate H_2 reduction in the crystalline state, benzyl viologen (BV) was further added in the crystallization mother liquor (final concentration of 1 mM). Several AOXI-S77HYB crystals were fished and collected in 0.2 mL glass vial with 70 μL of above-mentioned crystallization buffer including BV. The glass vial was tightly closed with septum rubber cap and the vial was purged with pure H_2. The crystal mix solution was then incubated at 283 K for overnight. H_2-reduction of AOXI-S77HYB crystals were confirmed by the blue color of reduced BV ($BV^{+\cdot}$). HRED-S77HYB crystals were fished and flash cooled in LN_2 (inside the anaerobic glove box). The frozen crystals were stored in the dewar filled with LN_2 until use.

In order to distinguish the aerobic and anaerobic oxidation, chemically oxidized crystals of S77HYB were prepared using $K_3[Fe(CN)_6]$. HRED-S77HYB crystals were soaked into 70 μL of the crystallization buffer including 5 mM of

$K_3[Fe(CN)_6]$ (no BV, 1% *w/v* higher concentration of PEG 10,000 from the crystallization condition). The vial was tightly closed with septum rubber cap, and incubated for overnight. $K_3[Fe(CN)_6]$-oxidized (FOXI) crystals were fished and flash cooled with LN_2 as well as HRED crystals.

3-4. X-ray structure analysis on S77HYB

3-4-1. Data processing of diffraction datasets

Native dataset for three states, namely air-oxidized (AOXI), H_2-reduced (HRED) and $K_3[Fe(CN)_6]$-oxidized (FOXI) states were collected at BL44XU, a beamline for biological macromolecular assemblies, in SPring-8 (Hyogo, Japan) with the experimental parameters as described in Section 2-4. All the data were recorded not to exceed the Garman Limit of 20 MGy (Owen *et al*., 2006) in order to avoid severe radiation damage.

To assign the exact position of Fe atoms in the proximal FeS cluster, especially for distorted structure under oxidized conditions, anomalous dispersion dataset for AOXI, HRED and FOXI state were recorded at the same beamline BL44XU at SPring-8 with the X-ray wavelength of 1.74 Å, where the edge wavelength for Fe. Since anomalous signals of S atoms can be observed at this wavelength, anomalous signals of Fe atoms were also confirmed at the wavelength of 0.9 Å used for native data collection.

All diffraction datasets were initially processed by *HKL2000* (Otwinowski & Minor, 1997) , *XDS* (Kabsch, 2010), *DIALS* (Winter *et al.,* 2018) and *iMosflm* (Battye *et al.*, 2011). As a result, all the datasets were processed at the best by *XDS* program package. Statistical values for data reduction by *XDS* are summarized in Table 12.

Table 12. Statistics for data collection of S77HYB crystals.

	AOXI	HRED	FOXI
Crystal parameter			
Space group	$P2_1$	$P2_1$	$P2_1$
Cell parameters			
a, *b*, *c* [Å]	63.94, 118.98, 96.81	65.73, 121.61, 98.88	65.97, 121.83, 99.17
β (°)	100.57	102.65	102.93
Data collection			
Wavelength [Å]	0.90000	0.90000	0.90000
Resolution range	50.00 – 1.57	50.00 – 1.84	50.00 – 2.05
[Å]	(1.58 – 1.57)	(1.89 – 1.84)	(2.10 – 2.05)
Total reflections	737813	497642	363558
Unique reflections	382238	251118	184162
R_{merge}	6.9 (55.8)	5.8 (57.6)	8.3 (52.9)
<I/σ(I)>	7.3 (1.8)	11.3 (1.4)	10.9 (2.4)
Completeness	97.5 (99.3)	96.8 (95.3)	97.5 (96.8)
Redundancy	1.9 (1.9)	1.9 (1.9)	2.0 (2.0)

3-4-2. Phasing and manual model building

Firstly the structure of AOXI-S77HYB was determined. Initial phasing was conducted by molecular replacement method with program *Phaser* using the available crystal structure of [NiFe]-hydorgenase from *H. marinus* (PDB accession code: 3AYX) as a search model. The initial phasing for HRED and FOXI datasets were performed by the molecular replacement with *Phaser* using the atomic coordinate of AOXI-S77HYB as a search model. 100 cycle of jelly-body refinement was conducted immediately after the molecular replacement. Iterative cycles of manual model building and refinement were performed by *Coot* and *Refmac5*. Positional, B-factor refinement was also performed by *Refmac5*. During the model building and refinement, external restraints were generated for the proximal Fe-S cluster and the Ni-Fe active center. Further refinement for occupancies was conducted by *phenix.refine* program. Structures of S77HYB at AOXI, HRED and FOXI state were finally refined to 1.57, 1.84 and 2.05 Å, respectively. The final refinement statistics

were summarized in Table 13.

Table 13. Final refinement statistics of native dataset of S77HYB in AOXI, HRED, and FOXI state.

	AOXI	HRED	FOXI
Resolution range	31.72 – 1.57	38.02 – 1.84	37.86 – 2.05
Total reflections	196578	130761	94895
Rwork/Rfree	0.122/0.166	0.180/0.219	0.166/0.217
Atoms in an asymmetric unit			
Protein	12838	12678	12662
other molecules (without solvent)	84	64	68
Solvent	1142	525	522
Deviation from ideal geometry			
Bond distances	0.008	0.010	0.010
Angle distances	1.302	1.438	1.328
Chiral volumes	0.074	0.099	0.093
Mean isotropic B-factors			
Main chain	17.5	22.2	13.7
Side chain	20.2	23.8	15.4
Ligand	17.4	22.6	12.6
Solvent	30.8	21.6	12.2
Ramachandran plot			
Favored (%)	96.4	96.2	96.3
Allowed (%)	3.5	3.5	3.6

3-4-3. Overall structures of AOXI-, HRED- and FOXI-S77HYB

Overall structures of S77HYB had $\alpha_2\beta_2$ dimer of heterodimer configuration (Fig. 14) which is similar to those obtained for Group 1d O_2-tolerant MBHs from *H. marinus* or *E. coli* (Shomura *et al.*, 2011; Volbeda *et al.*, 2012).

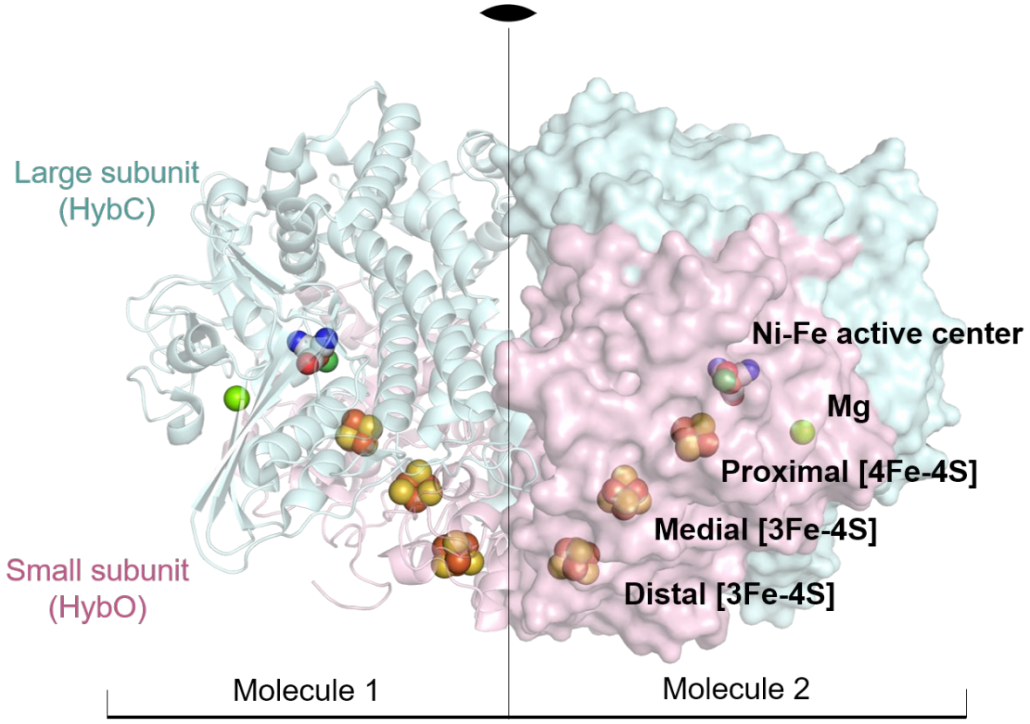

Figure 14. Overall structure of S77HYB in AOXI state.
S77HYB has a dimer of heterodimer configuration as well as Group 1d MBHs (*e.g.* HmMBH).

RMSD values between AOXI structures and HRED or FOXI structures were 0.246 and 0.242 (Table 14). Therefore, oxidation or reduction of S77HYB does not cause any significant change to overall folding (Fig. 15).

Table 14. RMSDs for overall structure among AOXI-, HRED-, and FOXI-S77HYB.

	AOXI	HRED	FOXI
AOXI		0.246	0.242
HRED	0.246		0.110
FOXI	0.242	0.110	

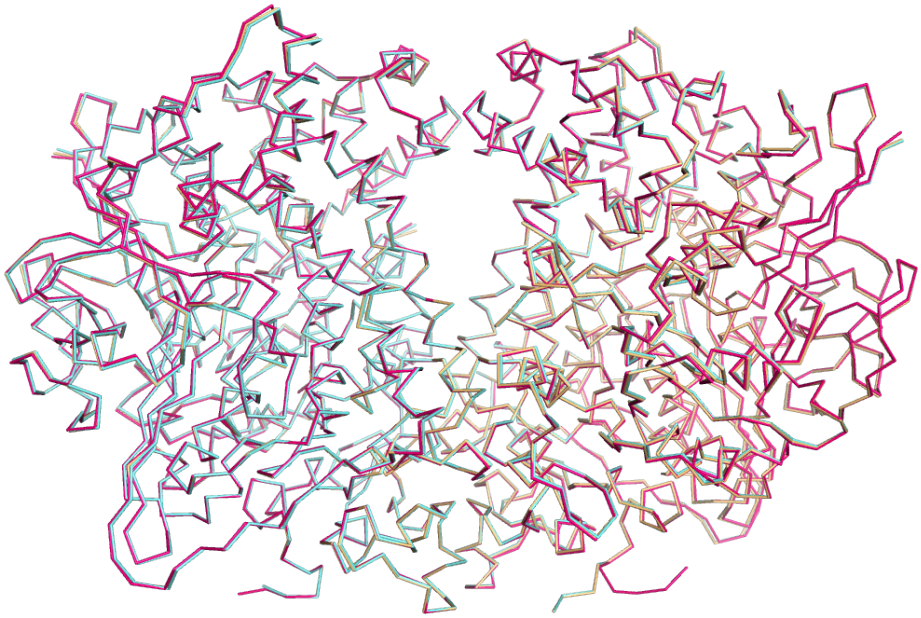

Figure 15. Structural differences among AOXI-, HRED-, and FOXI-S77HYB.
Overall structure of S77HYB in three different states (AOXI, HRED, and FOXI) are illustrated in ribbon representation. AOXI: magenta, HRED: palecyan, FOXI: lightorange. No significant difference was observed for overall folding.

3-4-4. Atomic coordinate at the Ni-Fe active site

The structure of the Ni-Fe active site was varied along surrounding redox environment as reported in earlier studies on [NiFe]-hydrogenases (Lubitz *et al.*, 2014, Nishikawa *et al.*, 2019). The active site configuration of S77HYB in AOXI, HRED, FOXI states are illustrated in Fig. 16. As found in other [NiFe]-hydrogenases, 4 cysteine was coordinated to Ni atom, 2 of them are bridged between Ni and Fe. For Fe atom, 2 CN and 1 CO were coordinated. In AOXI- and FOXI-S77HYB, an oxygen species, most probably hydroxyl ligand, was coordinated in the third bridging position between Ni and Fe. Additional oxygenic modification was observed at Cys546 in both AOXI and FOXI states, while no oxygen modification was found in HRED state.

Redox-dependent structural changes at the Ni-Fe active site of S77HYB were similar to those of well-characterized Group 1 [NiFe]-hydrogenases, namely Group 1b standard [NiFe]-hydrogenases (*e.g.* from *Desulfovibrio* species) or Group 1d O_2-tolerant membrane-bound [NiFe]-hydrogeanses (*e.g.* from *H. marinus*). Therefore, no significant structural difference which can explain the high O_2-stability of S77HYB was observed at the Ni-Fe active site.

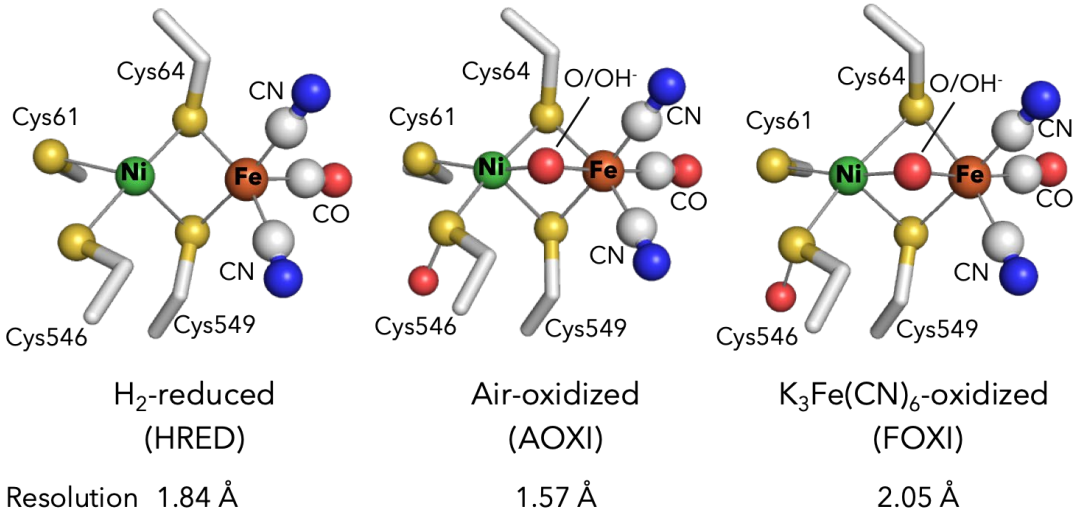

Figure 16. Structure of the Ni-Fe active site of HRED-, AOXI-, and FOXI-S77HYB.
Active site of S77HYB was redox-dependently altered as well as other [NiFe]-hydrogenases in well-characterized Group 1b or Group 1d.

3-4-5. Atomic model of the proximal FeS cluster

Earlier studies revealed that the structure of the proximal FeS cluster has key importance for O_2-tolerance. In Group 1d O_2-tolerant MBHs, the proximal FeS cluster is [4Fe-3S]-6Cys type instead of [4Fe-4S]-4Cys type. Upon oxidation, the $[4Fe\text{-}3S]_{Prox}$ changes its structure concerting with coordinated Cys residues. As a result, $[4Fe\text{-}3S]_{Prox}$ reversibly forms three oxidation states (3+/4+/5+), which is

suggested to enable effective oxygen reduction. On the other hand, the [4Fe-4S]-4Cys type cluster in the standard [NiFe]-hydrognease (*e.g.* from DvMF) does not change the cubane conformation upon oxidation, therefore $[4Fe\text{-}4S]_{Prox}$ has only two oxidation state (1+/2+).

Indeed, significant structural changes were observed in the $[4Fe\text{-}4S]_{Prox}$ of S77HYB upon oxidation (Fig. 17). In HRED-S77HYB, the $[4Fe\text{-}4S]_{Prox}$ formed a canonical cubane form as found in the standard [NiFe]-hydrogenases (*e.g.* from DvMF). However, there were an additional density in 2Fo-Fc maps of AOXI- and FOXI-S77HYB, suggesting that the $[4Fe\text{-}4S]_{Prox}$ was deformed upon oxidation.

In some cases (*e.g.* AvISP), the structure of $[4Fe\text{-}4S]_{Prox}$ was distorted, however, it is considered irreversible structural change (as a result of oxidative damage or radiation damage). During the data collection of oxidized S77HYB, X-ray dose were carefully controlled in order to avoid the structural change due to the radiation damage. Radiation dose estimated by *RADDOSE-3D* program were 0.19, 0.67, 1.00 MGy for AOXI-, HRED- and FOXI-S77HYB, respectively. These values were significantly less than the Garman limit. Furthermore, HRED- and FOXI-S77HYB were obtained from AOXI-S77HYB, suggesting the structural change found in S77HYB is not a result of irreversible oxidative damage, but reversible and have physiological significance.

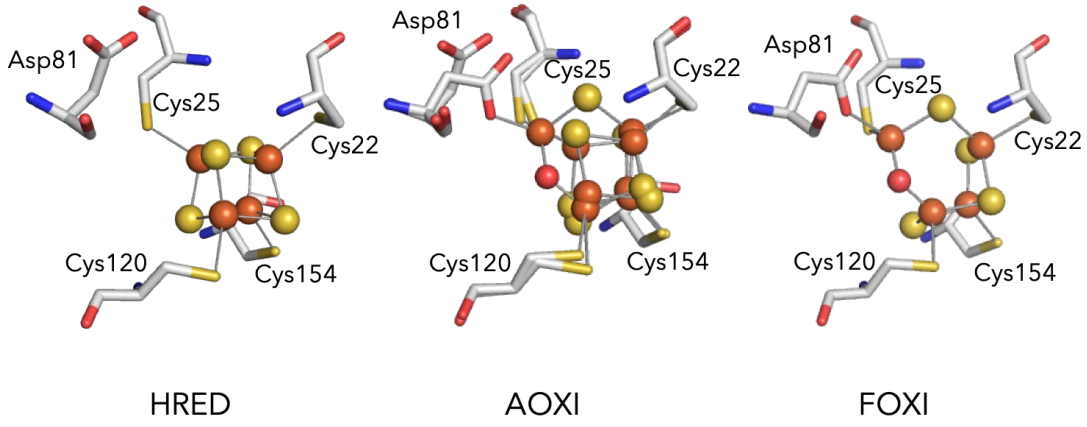

Figure 17. Structural change of the [4Fe-4S]$_{Prox}$ of HRED-, AOXI- and FOXI-S77HYB.
Atomic model of the [4Fe-4S]$_{Prox}$ in HRED-, AOXI-, and FOXI-S77HYB is illustrated. [4Fe-4S]$_{Prox}$ is illustrated with ball-and-stick fashion in the middle of each figure. Coordinated four Cys (residue number: 22, 25, 120, 154) and the adjacent Asp (residue number: 81) are depicted by stick representation.

In order to precisely assign the position of Fe in the [4Fe–4S]$_{Prox}$ in AOXI- and FOXI-S77HYB, anomalous data were collected with the wavelength of the absorption edge for Fe. Furthermore, anomalous signal of Fe was confirmed with the native dataset (wavelength: 0.9000Å). Consequently, the [4Fe–4S]$_{Prox}$ in AOXI- and FOXI-S77HYB was deformed. Fe4 was largely moved towards nearby Asp81, in addition, Asp81 was flipped towards the [4Fe–4S]$_{Prox}$. Other Fe atoms (Fe1 and Fe3) and S atoms in the [4Fe-4S]$_{Prox}$ were also slightly shifted (Fig. S4 and Table S13). 2Fo-Fc map showed a small density between Fe4 and Fe2, and was tentatively assigned to OH^- most probably formed by oxidation of nearby water molecule (Fig. 18–19). Theoretical analysis on this oxygenic species found between Fe4 and Fe2 suggested OH^- was bridged between two Fe atoms (Fig. S6 and Table S16).

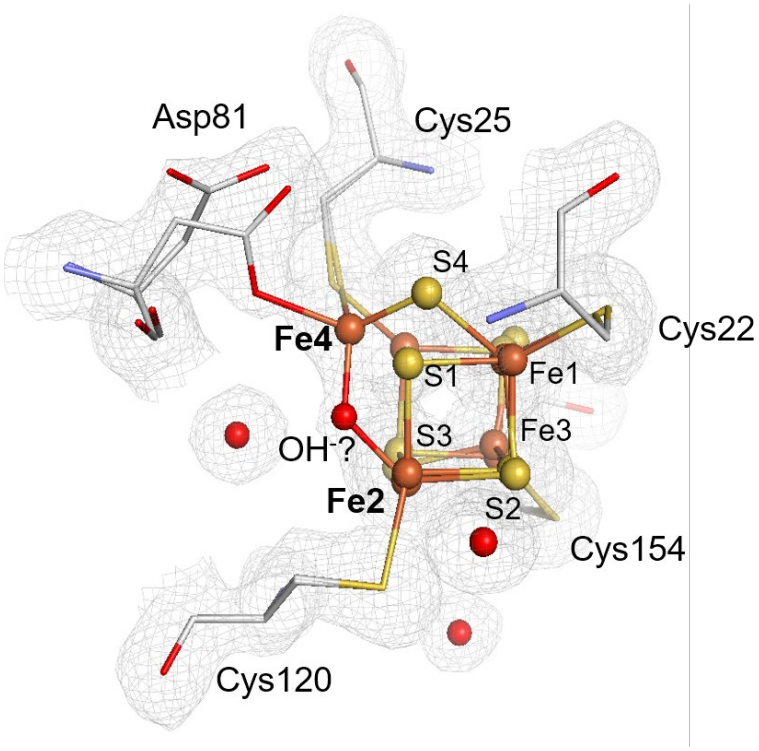

Figure 18. Electron density map around the [4Fe-4S]$_{Prox}$ in AOXI-S77HYB.
[4Fe-4S]$_{Prox}$ of AOXI-S77HYB is illustrated with 2Fo-Fc electron density map contoured at 1.0σ. Oxygenic species bound between Fe4 and Fe2 is tentatively assigned as OH^-, suggested from theoretical analysis.

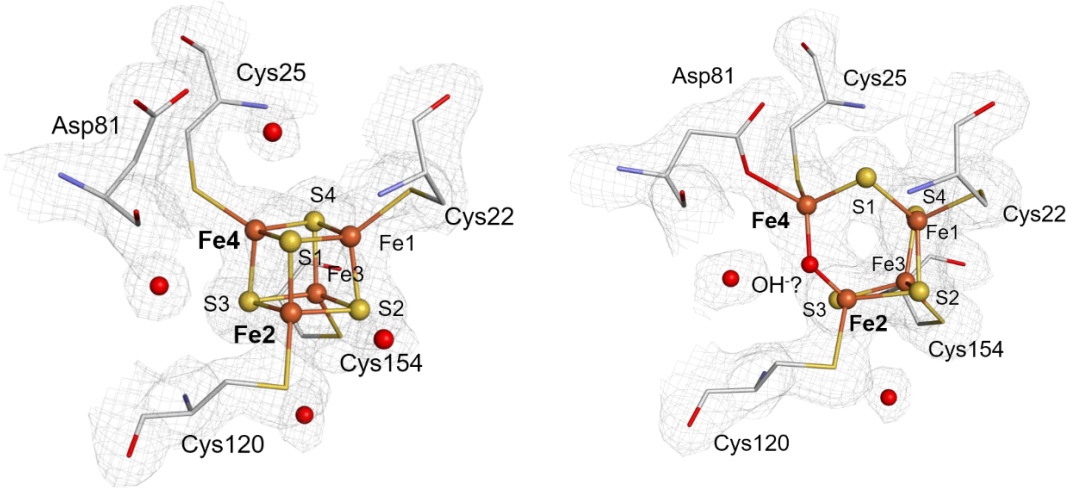

Figure 19. [4Fe-4S]$_{Prox}$ in HRED- and FOXI-S77HYB with electron density map.
[4Fe-4S]$_{Prox}$ of HRED- (left) and FOXI-S77HYB (right) is illustrated with 2Fo-Fc electron density map contoured at 1.0σ.

On the contrary, the [4Fe–4S]$_{Prox}$ in the standard [NiFe]-hydrogenase from DvMFSTD was not deformed even with $K_3[Fe(CN)_6]$-oxidation (unpublished data; data not shown). The medial and the distal FeS clusters were similar to those in other [NiFe]-hydrogenases. These results suggested that the high O_2-stability of S77HYB should be derived from the structural change of the [4Fe–4S]$_{Prox}$.

What is a trigger for structural movement of [4Fe-4S]$_{Prox}$ in S77HYB?

For the structural change of [4Fe–4S]$_{Prox}$ concerting with the movement of the adjacent Asp required relocation of the water molecule (W1) positioned between the side chain of Asp and the [4Fe–4S]$_{Prox}$ (Fig. 20).

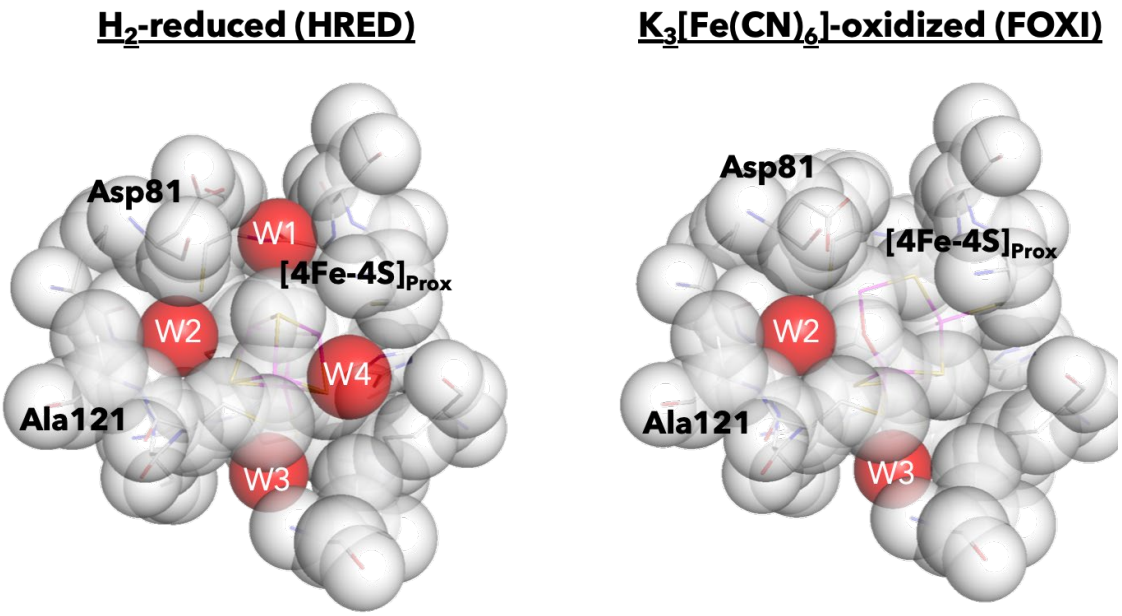

Figure 20. Structural cavity around the [4Fe-4S]$_{Prox}$ in S77HYB.
Structural cavity around the [4Fe–4S]$_{Prox}$ in HRED- and FOXI-S77HYB are illustrated. The water molecule (W1) should be relocated for the flip of adjacent Asp81 upon oxidation.

Upon oxidation, the water molecule (W1) was missing from the original position in HRED-S77HYB, thus the adjacent Asp81 can be flipped towards the [4Fe–4S]$_{Prox}$. While standard [NiFe]-hydrogenase have Glu instead of Asp (*e.g.* DvMFSTD), therefore, the bulky side chain of Glu makes the structural change of [4Fe–4S]$_{Prox}$ difficult in the standard hydrogenase.

3-4-6. Water distribution around the [4Fe–4S]$_{Prox}$

As above described, the relocation of the water molecule (W1) positioned between the nearby Asp/Glu residue and the [4Fe–4S]$_{Prox}$ might have an important role for triggering the structural change of the [4Fe–4S]$_{Prox}$. In order to further investigate the water relocation system, water molecules and hydrogen bonding network around the [4Fe-4S]$_{Prox}$ was compared between S77HYB and DvMFSTD (Fig. 21).

The careful observation of the water molecules and hydrogen bonding network around the [4Fe-4S]$_{Prox}$ revealed that the water relocation depends on the presence of "wall" (consists of Gly18–Thr23; this numbering is based on S77HYB) , which may interrupt water traffic between the vicinity of [4Fe-4S]$_{Prox}$ and water pool. In DvMFSTD (the "wall" consists of His13-Glu16), His13 interrupts the water traffic towards the water pool. However, in S77HYB, this His residue is replaced with Gly, therefore water molecule can be distributed across the wall. This result indicated that the mobility of the water molecules around the [4Fe-4S]$_{Prox}$ may explain the structural flexibility of the [4Fe-4S]$_{Prox}$, resulting in O_2-stability.

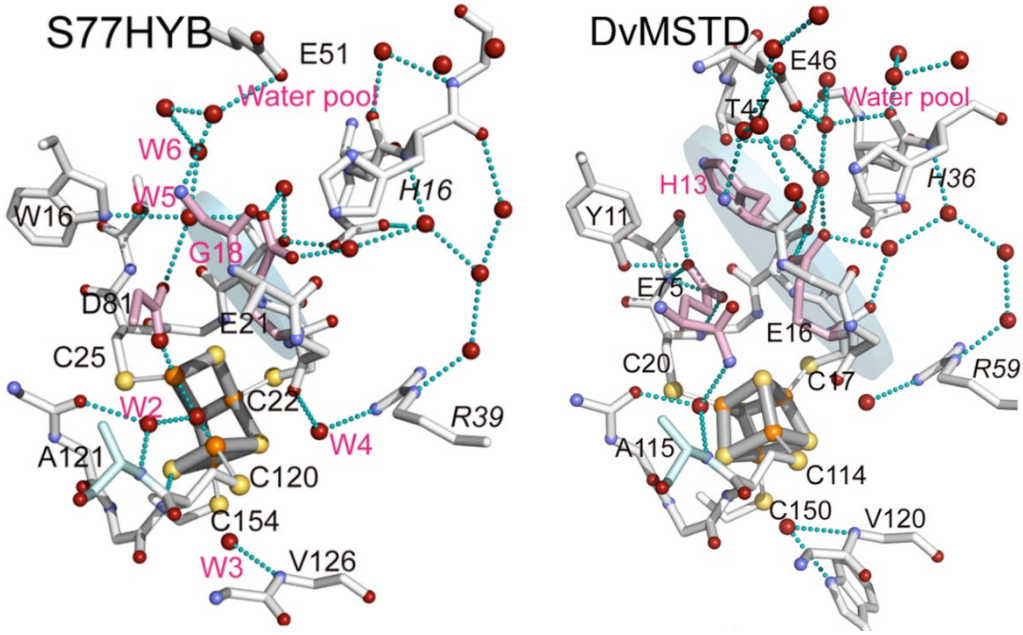

Figure 21. Water molecules and hydrogen bonding network around the [4Fe-4S]$_{Prox}$ in S77HYB and DvMFSTD.

Water molecules and hydrogen bonding network around the [4Fe-4S]$_{Prox}$ for FOXI-S77HYB and AOXI-DvMFSTD are depicted. In DvMFSTD, due to the blocking "wall" (illustrated with a gray disk) with bulky His residue (His13), no water molecule and hydrogen bonding were observed across the area around the [4Fe-4S]$_{Prox}$ and the water pool connecting to the bulk solvent. In S77HYB, since the His residue is replaced by Gly (Gly18), water molecule can distribute across this wall.

The water relocation system around the proximal FeS cluster is also confirmed in other [NiFe]-hydrogenases (Fig. S7). As a result, AvISP (Group 1e) has Ser at the position of Gly18 in S77HYB, therefore it may interrupt reversible structural change of the [4Fe-4S]$_{Prox}$. O_2-tolerant ReMBH (Group 1d) has His at the position similar to standard [NiFe]-hydrogenase (Group 1b). However, oxidized [4Fe-3S]$_{Prox}$ is mostly stabilized by nearby amide N in conserved Cys, and water relocation system may not have key importance unlike in S77HYB. In ReMBH, OH^- derive from water molecule, bound to oxidized [4Fe-3S]$_{Prox}$, accordingly there might be another water escape route in Group 1d O_2-tolerant hydrogenases.

In order to further investigate the water relocation system, water distribution around the [4Fe–4S]$_{Prox}$ in S77HYB and DvMFSTD simulated by molecular dynamics (MD) were compared. Intriguingly, the theoretical analysis revealed that the water distribution was interrupted by bulky His13 in DvMFSTD, while the His residue was replaced by Gly residue in S77HYB, hence, water molecules can distribute not only in the vicinity of the [4Fe–4S]$_{Prox}$ but also water molecules can access to water pool in S77HYB(Fig. 22).

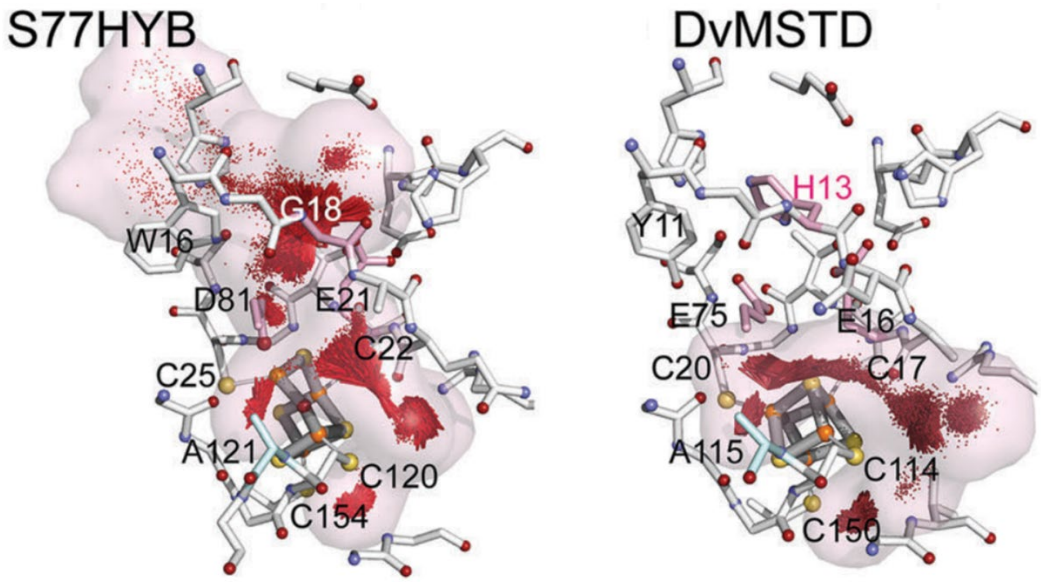

Figure 22. Water molecules distribution around the [4Fe-4S]$_{Prox}$ in S77HYB and DvMFSTD investigated by MD simutaions.

The structures around the [4Fe–4S]$_{Prox}$ in S77HYB and DvMFSTD are illustrated. [4Fe–4S]$_{Prox}$ is represented by bold stick (dark gray), and the others are represented by normal stick. Water molecule distribution is indicated by red points, and the surface of the water molecule distribution is indicated by light pink.

Difference of O_2-susceptibility between S77HYB and EcHYB

Although EcHYB has quite high sequence similarity comparing to S77HYB, O_2-susceptibility is different between these two enzymes. The amino acid sequence

is 95% identical to that of S77HYB, only five residues are different in the small subunit (Fig. 23). The difference in the whole hydrogenase unit is mapped in Fig. S8. As clearly found in these figures, most of the differences are found in far from the NiFe active center or FeS clusters, thus they seems to have no significant impact on the O_2-tolerance or O_2-stability of the hydrogenases. However, a difference is found near the $[4Fe\text{-}4S]_{Prox}$ (Ala121 is replaced by Ser121 in EcHYB).

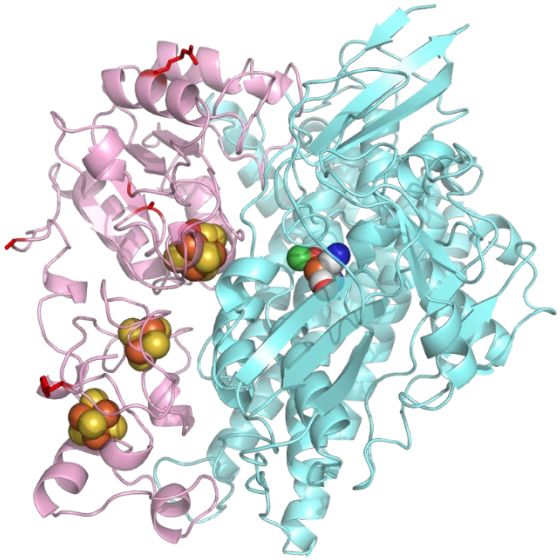

Figure 23. Amino acid difference found in the small subunit of EcHYB and S77HYB. Structure of AOXI S77HYB is depicted as cartoon representation. Ni-Fe active center and three FeS clusters are illustrated as spheres. The point of the five amino acid residues different in EcHYB are colored in red.

The $[4Fe\text{-}4S]_{Prox}$ in oxidized EcHYB formed different structure comparing to that of S77HYB (Fig. 24). Fe4 was only slightly moved toward the adjacent Asp81 in EcHYB. Therefore, the structural flexibility of the $[4Fe\text{-}4S]_{Prox}$ and surrounding environment should be different in EcHYB. Overall structure of EcHYB was very similar to S77HYB (RMSD: 0.242; between AOXI-S77HYB and as-isolated EcHYB),

thus the difference of the structure around the [4Fe-4S]$_{Prox}$ may explain the difference between these enzymes.

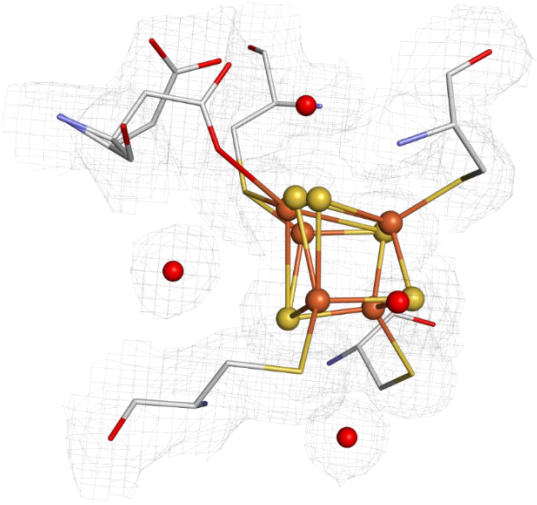

Figure 24. Structure of the [4Fe-4S]$_{Prox}$ of oxidized EcHYB.
Atomic model of the [4Fe-4S]$_{Prox}$ of oxidized EcHYB is illustrated with 2Fo-Fc electron density map contoured at 1.0σ. No additional density was confirmed in the position of OH^- (between Fe4 and Fe2) of oxidized S77HYB.

No significant density was observed at the position of OH^- in oxidized S77HYB, indicating that the structural change of the [4Fe-4S]$_{Prox}$ is completely different between S77HYB and EcHYB. The difference should be derived from the volume of the structural cavity surrounding the [4Fe–4S]$_{Prox}$. The cavity for S77HYB was enough large for the flexible deformation of the [4Fe–4S]$_{Prox}$ and the water relocation, while that for EcHYB seemed to be insufficient due to bulge of Ser121 (Fig. 25). Due to the repulsion against Oγ of Ser121, W2 cannot move, hence the water molecule (W2) might interrupt the deformation of the [4Fe–4S]$_{Prox}$. At this moment, it is unclear that the mobility of W2 is related to the structural change of

[4Fe-4S]$_{Prox}$. If the OH^- derived from water molecule bound between Fe4 and Fe2 as well as in S77HYB, there may repulsion between W2 and Oγ of Ser121. It should be difficult to stabilize the oxidized [4Fe-4S]$_{Prox}$ without OH^-, therefore the structural change of the [4Fe-4S]$_{Prox}$ in EcHYB may seem to be insufficient comparing to S77HYB. Further structural studies on EcHYB are highly desired to investigate the difference of O_2-susceptibility between EcHYB and S77HYB.

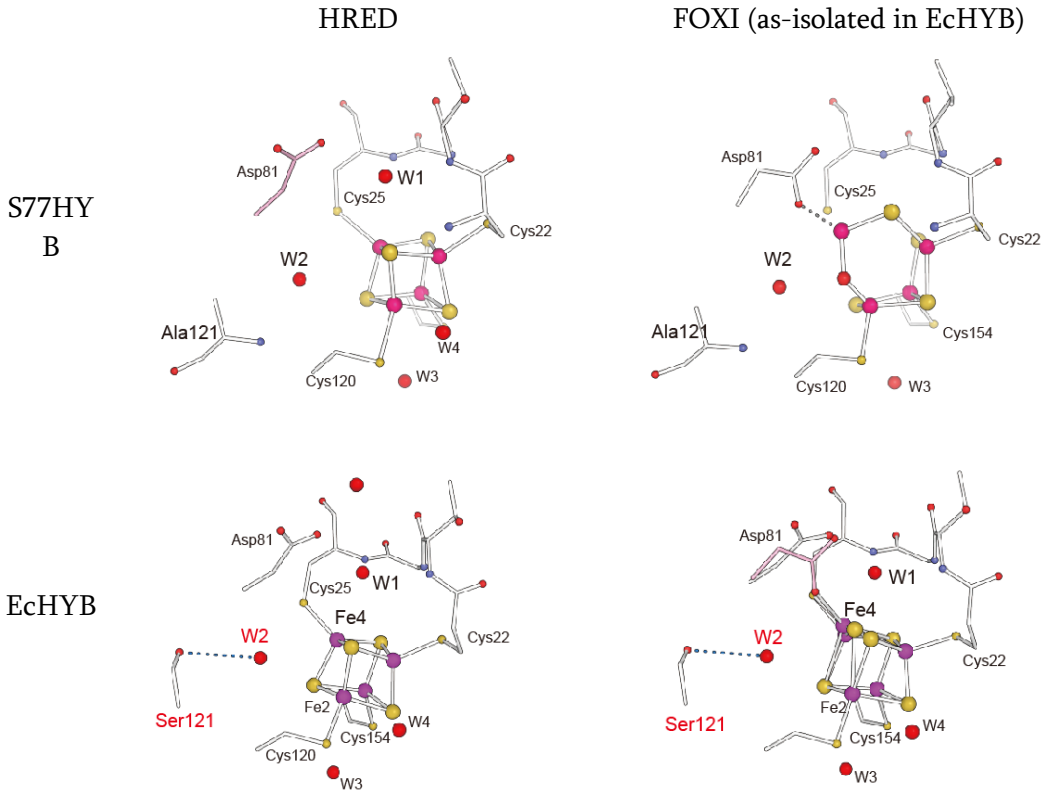

Figure 25. Comparison of the [4Fe-4S]$_{Prox}$ and structural flexibility of the cluster upon oxidation and reduction.

The [4Fe-4S]$_{Prox}$ in HRED and FOXI (as-isolated in EcHYB) state is illustrated by ball-and-stick representation. Ala121 of S77HYB is replaced by Ser121 in EcHYB. This difference might reduce the structural flexibility of the [4Fe-4S]$_{Prox}$ of EcHYB.

3-5. EPR and FT-IR spectroscopic studies on S77HYB

To investigate the catalytic intermediate and detailed structural information,

spectroscopic analysis on S77HYB were carried out. In crystallography, the catalytic intermediate is not well distinguished from the electron density map because the obtained density reflects the mixture of several catalytic intermediates and the structural information is averaged out. Furthermore, it is difficult to detect hydrogens or protons by X-ray crystallography. In contrast, the catalytic intermediates are easily distinguished by spectroscopic measurements (*e.g.* EPR or FT-IR) because the signal from all the catalytic intermediates are normally appeared at different position. The spectroscopic results shown below is mainly recorded by Dr. Hulin Tai.

3-5-1. EPR spectra of S77HYB at 77K

In EPR spectroscopy of [NiFe]-hydrogenase, signal from Ni in the active site is mainly observed (active site Fe is always EPR-silent in [NiFe]-hydrogenase). The valence of Ni alters from Ni^{+} to Ni^{3+} during the catalytic cycle, accordingly, some of the catalytic intermediate which has Ni^{2+} cannot be detected. In contrast, although FT-IR can detect all the catalytic intermediates, signal assignment is difficult without any information. Therefore, EPR spectra of S77HYB were firstly obtained (Fig. 26).

The EPR spectra of HRED-S77HYB was showed Ni-C signals (g_x=2.189, g_y=2.128 , g_z=2.010). In EPR spectra obtained for HRED-S77HYB under pure N_2, Ni-C signals were increased comparing to those obtained under pure H_2, as well as DvMFSTD (Tai *et al.*, 2014), most probably it reflects the change of redox potential. As well as other [NiFe]-hydrogenases, light irradiation produced the Ni-L state (g_x =2.291, g_y=2.116, g_z=2.047).

In contrast to oxidized DvMFSTD, EPR spectra of AOXI-S77HYB mainly

showed Ni-B signals (g_x=2.311, g_y=2.156, g_z=2.010).

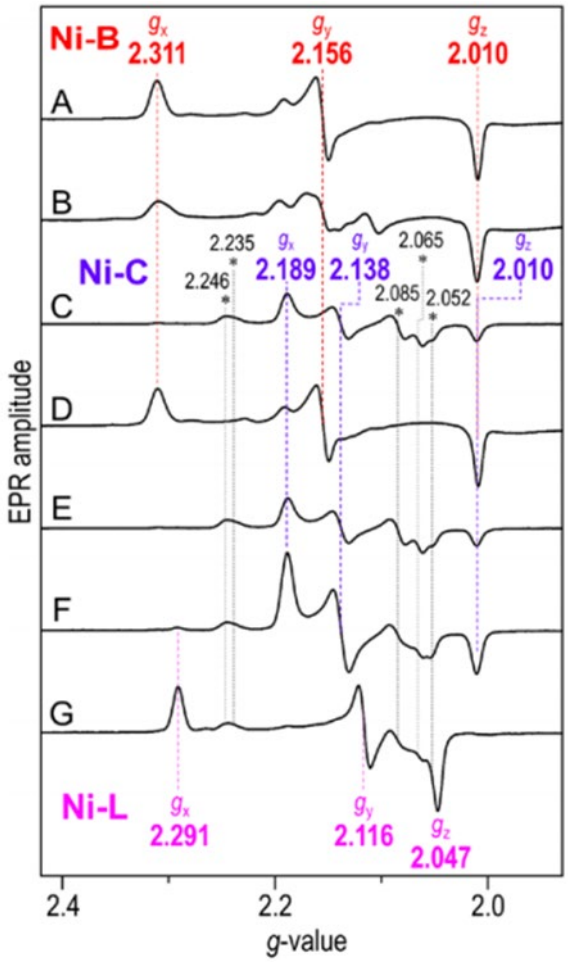

Figure 26. EPR spectra of S77HYB recorded at 77K.

EPR spectra of S77HYB in various conditions: (A)air-oxidized (AOXI), (B)$K_3[Fe(CN)_6]$-oxidized (FOXI), (C)H_2-reduced (HRED), (D)re-AOXI, (E)re-HRED, (F)re-HRED under N_2, (G) light-illuminated on (F). g_x, g_y, g_z of the catalytic intermediates are indicated in the spectra. Asterisk indicates the signals from unknown species, which have not been assigned yet.

EPR spectra were obtained for re-HRED or re-AOXI state in order to investigate the O_2-stability of S77HYB. Intriguingly, the signal intensity was not significantly decreased as in DvMFSTD, hence, the high O_2-stability was strongly supported from the spectroscopic results.

Furthermore, the addition of Na_2S and further air oxidation does not produce Ni-A state as previously reported in DvMFSTD (Ogata *et al*., 2005) (Fig. S13). Therefore, S77HYB might have structural mechanism to avoid the formation of Ni-A state as well as Group 1d O_2-tolerant [NiFe]-hydrogenases (*e.g.* HmMBH, ReMBH). Since EcMBH forms Ni-A state upon oxidation, the correlation between O_2-tolerance and the formation of Ni-A state has still been unclear. In addition, HmMBH is less O_2-stable comparing to S77HYB, even though it preferentially forms Ni-B upon oxidation. Accordingly, the correlation between O_2-stability and the formation of Ni-A has also been unclear. Further investigations and careful comparison among various hydrogenases are required.

3-5-2. FT-IR spectra of S77HYB

To further investigate the detailed catalytic mechanism of S77HYB, FT-IR spectra were recorded at 138 – 198 K. FT-IR spectra of AOXI-S77HYB does not show clear signals from Ni-A state as well as in EPR spectra. FT-IR spectra for HRED-S77HYB (Fig. 27) was similar to those of the standard [NiFe]-hydrogenases (*e.g.* DvMFSTD). In the spectra for HRED-S77HYB, small signal which can be derived from Ni^+ state was observed.

For further investigations on Ni^+ species, FT-IR spectra were recorded with light irradiation. The previous report of FT-IR study on DvMFSTD suggested that Ni-L state is a catalytic intermediate between Ni-C and Ni-SI_a states (Tai *et al*., 2014). As well as in the earlier report, difference FT-IR spectra between with and without light irradiation were obtained at 138-198 K (Fig. 27). Consequently, the Ni-L state was confirmed as an intermediate state between Ni-C and Ni-SI_a states. The Ni^+ species

obtained in HRED-S77HYB was slightly different from Ni-L state.

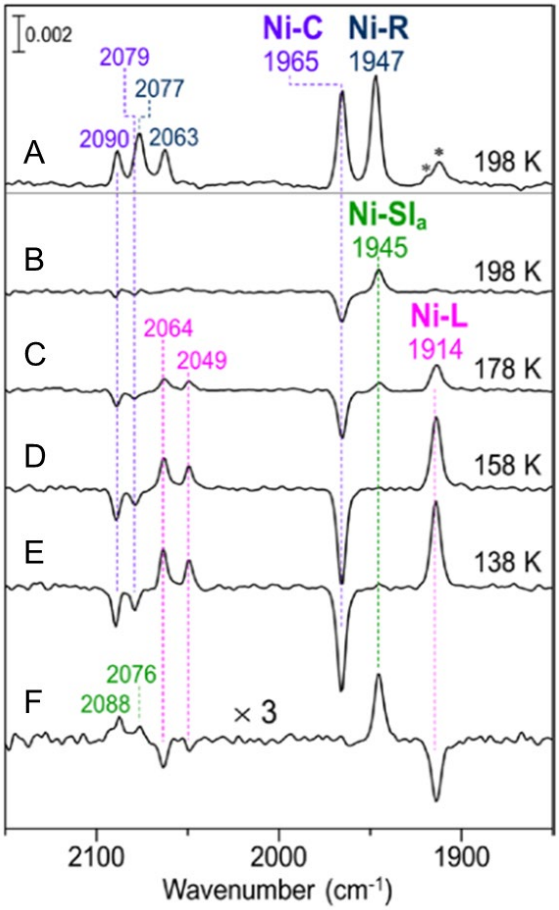

Figure 27. Difference FT-IR spectra of S77HYB between with and without light irradiation recorded at 138-198K.

The difference FT-IR spectra (light irradiated – dark) are illustrated. Normal FT-IR spectra for HRED-S77HYB are shown in top as a reference (A). (B-E) Difference FT-IR spectra between with and without light irradiation recorded at 138-198K. (F)The difference spectra (spectrum B) – 0.32 × (spectrum E), and is magnified by × 3.

3-5-3. EPR spectra of S77HYB and DvMFSTD at extremely low temperature

EPR and FT-IR spectroscopic analyses revealed that S77HYB less forms Ni-A state upon oxidation. However, molecular mechanism of O_2-stability of S77HYB had not still been fully understood from the above described spectroscopic results.

Ni-A state is considered as a result of oxidative inactivated form when the

enzyme has less electrons to reduce molecular oxygen (Evans *et al.*, 2013; Lubitz et al., 2014). As seen in the results from the crystallographic studies, although Ni-Fe active center was similar to other [NiFe]-hydrogenases, the $[4Fe\text{-}4S]_{Prox}$ in S77HYB was different from other enzymes. Therefore, it can be expected that the $[4Fe\text{-}4S]_{Prox}$ in S77HYB has another oxidation state which can contribute to effective O_2 reduction.

In order to investigate the oxidation state of the $[4Fe\text{-}4S]_{Prox}$ in S77HYB, EPR spectra for AOXI- and FOXI-S77HYB were recorded under 4-100 K. At the extremely low temperature (4–20 K), spin-spin interaction between the active site Ni and FeS clusters, especially with the proximal Fe-S cluster, can be observed when both metal complexes are EPR-active (Fig. S13 and Table S12). In the standard [NiFe]-hydrogenase (*e.g.* DvMFSTD), the $[4Fe\text{-}4S]_{Prox}$ has 1+ (reduced) or 2+ (oxidized) state. However, if S77HYB has an additional oxidation state 3+ (superoxidized), the spin-spin interaction can be observed as signal splitting of Ni signals from oxidized state (Ni-B or Ni-A).

In the spectra of AOXI-S77HYB (Fig. 28), signal splitting of Ni-A and Ni-B species were clearly observed. In the spectra of FOXI-S77HYB, although the obvious signal splitting were not observed, signals for Ni-B were broaden most probably due to the interaction between Ni^{3+} and the proximal Fe–S cluster ($[4Fe\text{-}4S]^{+}$ or $[4Fe\text{-}4S]^{3+}$). In addition, some signals were appeared in the range of typical [4Fe-4S] cluster ($[4Fe\text{-}4S]^{+}$ or $[4Fe\text{-}4S]^{3+}$) upon oxidation by $K_3[Fe(CN)_6]$. In this measurement, the samples were well incubated under oxidized conditions (in the presence of air or $K_3[Fe(CN)_6]$) in order to reach equilibration, therefore the proximal Fe–S cluster should not be reduced ($[4Fe\text{-}4S]^{+}$), rather oxidized. The results

strongly suggest that there is an additional oxidation state for the proximal FeS cluster, namely $[4Fe\text{-}4S]^{3+}$, in oxidized S77HYB.

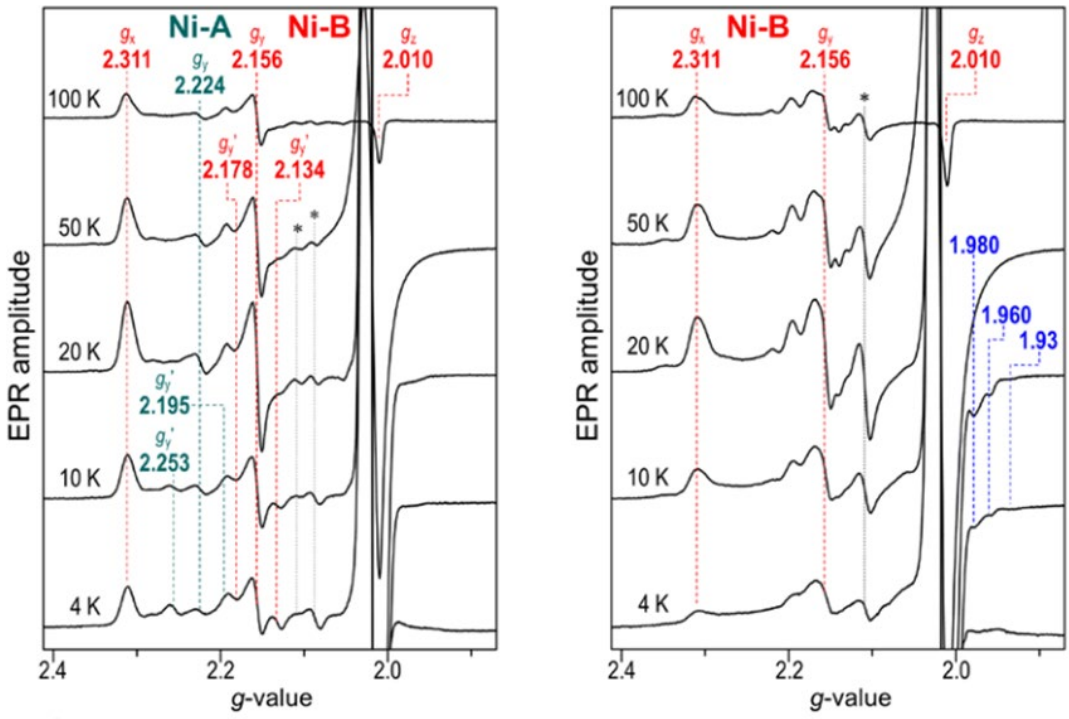

Figure 28. EPR spectra of AOXI- and FOXI-S77HYB recorded at 4–100K.
EPR spectra of S77HYB were recorded at 4 – 100 K. Broken line indicated the signals from observed species. The signals are indicated by different colors; red: Ni-B, green: Ni-A, blue: most probably [4Fe-4S], asterisk: unassigned. Huge signal observed around $g = 2.0$ derives from the oxidized medial Fe-S cluster, $[3Fe\text{-}4S]^{+}$.

For comparison, EPR spectra of AOXI- and FOXI-DvMFSTD were recorded at the same conditions (Fig. 29). However, the obvious signal splitting was not confirmed from the spectra obtained for both AOXI- and FOXI-DvMFSTD. The signal of oxidized medial Fe-S cluster $[3Fe\text{-}4S]^{+}$ was not observed in the EPR spectra of AOXI-DvMFSTD unlike found in the spectra of oxidized S77HYB (Fig. 28). The EPR signal is not sufficiently observed although the EPR spectra for AOXI-DvMFSTD normally has two oxidation state, Ni-A and Ni-B (Ogata *et al.*, 2005). Therefore, the

enzyme sample might have deteriorated.

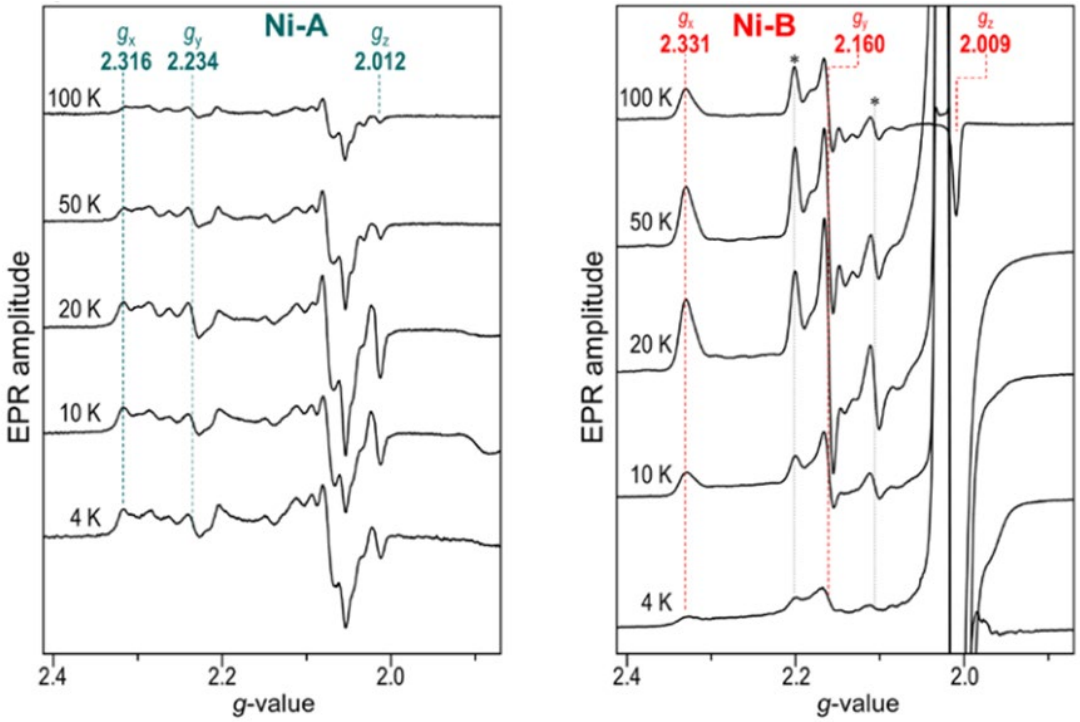

Figure 29. EPR spectra of AOXI- and FOXI-DvMFSTD recorded at 4–100 K.
EPR spectra of DvMFSTD were recorded at 4 – 100 K. Broken line indicated the signals from observed species. The signals are indicated by different colors; red: Ni-B, green: Ni-A, unassigned signals are indicated by asterisk. Huge signal observed around $g = 2.0$ derives from the oxidized medial Fe-S cluster, $[3Fe\text{-}4S]^{+}$.

In EPR spectra of FOXI-DvMFSTD, the signal from medial $[3Fe\text{-}4S]^{+}$ was observed as well as in the spectra for oxidized S77HYB. The enzyme should be oxidized, however, no signal splitting was observed for Ni-B signals even in FOXI-DvMFSTD, suggesting the $[4Fe\text{-}4S]_{Prox}$ in DvMFSTD forms up to $[4Fe\text{-}4S]^{2+}$ state upon oxidation. Accordingly, high O_2-stability of S77HYB should be derived from the electron donation property of $[4Fe\text{-}4S]_{Prox}$ with water relocation system.

3-6. O_2-tolerance and O_2-stability of [NiFe]-hydrogenase

As above described, novel structural changes were identified at the $[4Fe\text{-}4S]_{Prox}$ of S77HYB, and this structural change should contribute to the high O_2-stability of S77HYB. However, this characteristic structural change cannot fully answer why S77HYB has high O_2-stability, because HmMBH does not have such high stability even though it has similar electron donation property with $[4Fe\text{-}3S]_{Prox}$.

Earlier studies revealed a lot of characteristics of hydrogenase relating to the O_2-tolerance and O_2-stability (*e.g.* formation of Ni-A state, CO inhibition, structural change of the proximal FeS cluster). In particular, $[4Fe\text{-}3S]_{Prox}$ has been believed to be an essential structural component for O_2-tolerance. However, as suggested in this study or some of earlier studies, the electron donation property of the proximal FeS cluster cannot fully explain the O_2-tolerance or O_2-stability yet.

Therefore, O_2-tolerance and O_2-stability should be considered as separate and unrelated parameters, at least until the difference of O_2 stability of S77HYB and HmMBH can be clearly explained. Revisited definition of the terms relating to the O_2-tolerance or O_2-stability are suggested in Table 15. This definition will also be convenient to classify hydrogenases for the applicational use.

In further studies on hydrogenases, detailed molecular mechanism of O_2-tolerance and O_2-stability should be elucidated. In addition, appropriate parameters should be defined to compare O_2-tolerance or O_2-stability of hydrogenases. Most probably tolerance or stability against O_2 depends on the experimental conditions (pH, concentration of H_2 or O_2) and characteristics of each hydrogenases. Therefore, for comparing the characteristics of each hydrogenase, appropriate parameters and experimental conditions should be investigated in future work (especially,

electrochemistry will have a key importance).

Table 15. Revisited definition of the terms relating to the O_2-tolerance or O_2-stability of hydrogenases.

Term	Definition (usage)
O_2-tolerant	The enzyme can maintain the catalytic activity in presence of O_2. Usually the enzyme has O_2-reducing ability (oxidase activity). (*e.g.* EcMBH, ReSH)
O_2-insensitive	The enzyme does not interact with O_2, therefore, the enzyme can exhibit the catalytic activity in the presence of O_2 (*e.g.* ReAH)
O_2-sensitive	The enzyme is inactivated by O_2. The enzyme does not have catalytic activity in the presence of O_2. Note that this does not mean the enzyme is irreversibly inactivated by O_2.
O_2-stable	The enzyme may once inactivated by O_2, however, the catalytic activity can be recovered by reduction using H_2 or reducing agents. Generally most of the original activity can be restored, thus the inactivation is reversible. (*e.g.* DvMFSTD, S77HYB)
O_2-unstable	The enzyme is irreversibly inactivated by O_2. (*e.g.* [FeFe]-hydrogenases or [Fe]-hydrogenases)

Chapter 4. CONCLUSION

X-ray structure analysis on S77HYB revealed that the $[4Fe\text{-}4S]_{Prox}$ of S77HYB has a novel structural change (Figs. 17–19) . Combining spectroscopic and theoretical analysis (Figs. 20–22, 26), it is revealed that the structural change was concerted with water relocation system around the $[4Fe\text{-}4S]_{Prox}$, resulting in the structural flexibility and reversibility of $[4Fe\text{-}4S]_{Prox}$.

EPR spectra of S77HYB obtained at extremely low temperature (Fig. 28) indicated that the proximal FeS cluter of oxidized S77HYB has $[4Fe\text{-}4S]^{3+}$ state, which has not so far been identified in the standard [NiFe]-hydrogneases (Table 16). Due to this difference, S77HYB has similar electron donation property as well as [4Fe-3S]-6Cys type cluster in O_2-toelrant Group 1d [NiFe]-hydrogenases.

Table 16. Oxidation level of the proximal FeS cluster in Group 1d O_2-tolerant MBHs, S77HYB and Group 1b standard hydrogenases.

Cluster type	Oxidation states of Fe	Net charge (oxidation level)	
		Inorganic part	With cysteinyl thiolates
		[4Fe-4S]	[4Fe-4S]-4Cys
[4Fe-4S]-4Cys	$1Fe^{3+}$, $3Fe^{2+}$	1+	1-
	$2Fe^{3+}$, $2Fe^{2+}$	2+	2-
		[4Fe-4S]	[4Fe-4S]-4Cys
[4Fe-4S]-4Cys	$1Fe^{3+}$, $3Fe^{2+}$	1+	1-
	$2Fe^{3+}$, $2Fe^{2+}$	2+	2-
	$3Fe^{3+}$, $1Fe^{2+}$	3+	3-
		[4Fe-3S]	[4Fe-3S]-6Cys
[4Fe-3S]-6Cys	$1Fe^{3+}$, $3Fe^{2+}$	3+	1-
	$2Fe^{3+}$, $2Fe^{2+}$	4+	2-
	$3Fe^{3+}$, $1Fe^{2+}$	5+	3-

The standard [NiFe]-hydrogenase without water relocation system can be easily inactivated and forms both Ni-A and Ni-B state. However, S77HYB has similar [4Fe-3S]-6Cys type-like electron donation system, therefore, the enzyme less forms unready Ni-A state as well as Group 1d O_2-tolenrat hydrogenases (Fig. 30).

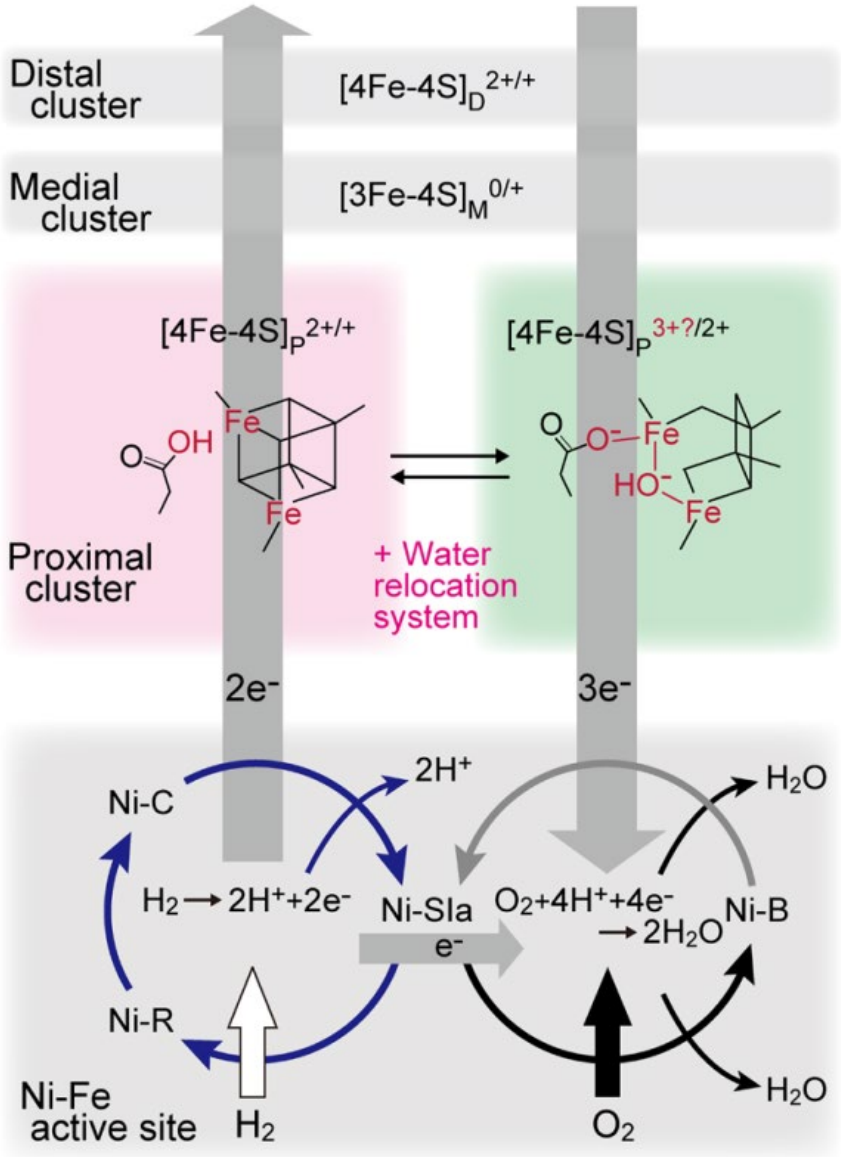

Figure 30. O_2-protecting mechanism in S77HYB.
Protection mechanism against O_2 in S77HYB is depicted. Previously, O_2-tolerance has been considered to be derived only from $[4Fe\text{-}3S]_{Prox}$, however, even with $[4Fe\text{-}4S]_{Prox}$, the enzyme can protect the active site with water relocation system.

Chapter 5 FUTURE PLAN

Novel O_2-protecting mechanism found in S77HYB has been described in earlier chapters, however, the molecular mechanism of O_2-tolerance or O_2-stability has not been fully understood. Here several ideas on future directions are presented.

Determination of the redox potential of FeS clusters

In this study, the novel O_2-protecting mechanism of S77HYB was presented. The mechanism is really similar to hitherto-suggested mechanism of [4Fe-3S]-6Cys system in Group 1d O_2-tolerant hydrogenases.

However, the earlier study for the activity measurement in the presence of O_2 indicated that the level of O_2-tolerance seems to be different (Noor *et al.*, 2016). Efficiency of O_2-reduction may be derived from the redox potential of FeS clusters. Therefore, determination of the redox potential of FeS clusters is of key importance for elucidating the O_2-reducing ability of hydrogenases.

Structural analysis on CO-bound S77HYB

CO is an O_2 analogue and a competitive inhibitor for hydrogenases. Previous studies revealed that O_2-tolerant hydrogenases are less inhibited by CO (Pandelia *et al.*, 2010). While in O_2-sensitive hydrogenases, CO is bound to the active site Ni at high occupancy (Ogata *et al.*, 2002). S77HYB has a different O_2-protecting mechanism, therefore, structural analysis on S77HYB under CO atmosphere is of key importance for further investigations on O_2-tolerance or O_2-stability of [NiFe]-hydrogenases.

Further structural analysis on O_2-tolerant [NiFe]-hydrogenases with [4Fe-4S]$_{Prox}$

In earlier studies, several [NiFe]-hydrogenases have been reported as O_2-tolerant hydrogenase with [4Fe-4S]$_{Prox}$. For example, HtSH is a Group 3d [NiFe]-hydrogenase with [4Fe-4S]$_{Prox}$. However, HtSH has additional FeS clusters because this hydrogenase consists from two different catalytic unit, namely hydrogenase unit and diaphorase unit. In HtSH, additional FeS clusters may contribute to effective O_2 reduction. Moreover, the Ni-Fe active site of HtSH exhibits a novel configuration in its oxidized state (Shomura *et al*., 2017). This may also contribute to the protection of the active site from O_2.

ReAH has been known as "O_2-insensitive" hydrogenase, even though it has [4Fe-4S]$_{Prox}$. Currently only the structure for reduced state has been available, therefore, the protection mechanism against O_2 in ReAH has still been unknown. [4Fe-4S]$_{Prox}$ in ReAH is coordinated by 3 Cys and 1 Asp, not 4 Cys. The impact of this difference for O_2-insensitivity has also been unclear.

Mutagenesis studies on Group 1d O_2-tolerant hydrogenases revealed that these enzymes were still not inhibited by CO even with the O_2-sensitive cluster exchange variants (Goris *et al*., 2011; Lukey *et al*., 2011). The fact may indicate that another structural factor also has important role for O_2-tolerance. Therefore, the proximal FeS cluster does not seem to be only an essential structural component for O_2-tolerance.

Several studies suggested the importance of the gas channel (Dementin *et al*., 2009) or intermolecular electron transfer of hydrogenases (Wulff *et al*., 2016).

Furthermore, the previous structural studies on DfSTD variants indicated the impact of the surrounding residues around the Ni-Fe active site on Ni-A formation (Volbeda *et al*., 2015). Therefore, several structural factors should be related to O_2-tolerance or O_2-stability of [NiFe]-hydrogenases. Structural studies on O_2-tolerant or O_2-stable hydrogenases without $[4Fe\text{-}3S]_{Prox}$ will bring some insights to deeply understand the molecular mechanisms of O_2-tolerance or O_2-stability.

Structural analysis on uncharacterized catalytic intermediates of S77HYB

In spectroscopic measurements, a lot of works applied potential control in order to investigate the transition of catalytic intermediates. Above all, potential control FT-IR spectroscopy, namely spectroelectrochemistry, has been a powerful tool to understand the characteristics of hydrogenases. However, only the local structural change can be monitored by spectroscopic measurement, although X-ray crystallography can reveal overall structure of the enzyme.

Most of the crystallographic studies on hydrogenases have been revealed only reduced active form (most probably Ni-R state) and oxidized inactive form (most probably Ni-A or Ni-B state). Therefore, the overall structures of intermediate states have still been unclear. Spectroelectrochemical studies clearly indicates that hydrogenases change their intermediates depend on the surrounding redox potential. If the potential control is available for crystal sample, the overall structure of unresolved catalytic intermediates will be determined. This may reveal how the structural change of the active site work seamlessly with that of other moiety in the enzyme.

Structural and functional analysis of other subunits in S77HYB

In this study, only the hydrogenase unit of S77HYB has been analyzed. However, S77HYB is considered to be a heterotetramer (HybOABC) in physiological condition. Other subunits are considered to have an important role for electron transfer between the hydrogenase unit and quinone. In earlier studies, functions of HybA and HybB has been studied by molecular biological techniques (Pinske *et al*., 2015; Lubek *et al*., 2019). HybA and HybB subunits has not been isolated not only as a single subunit but also as a complex with the hydrogenase unit (HybOC). HybA and HybB are characteristic subunits in Hyb-type hydrogenase (Group 1c), therefore, it is of key importance to investigate their structures and functions in order to understand the physiological significance of Hyb-type hydrogenase.

REFERENCES

Abou-Hamdan, A., Ceccaldi, P., Lebrette, H., Gutiérrez-Sanz, O., Richaud, P., Cournac, L., Guidliarelli, B., De Lacye, A. L., Léger, C., Volbeda, A., Burlat, B., and Dementin, S. (2015) A threonine stabilized the NiC and NiR catalytic intermediates of [NiFe]-hydrogenase. *J. Biol. Chem.*, 290(13), 8550–8558.

Adam, D., Bösche, L., Castañeda-Losada, L., Winkler, M., Apfel, U.-P., and Happe, T. (2017) Sunlight-dependent hydorgen production by photosensitizer/hydrogenase systems. *Chem. Sus. Chem.*, 10(5), 894–902.

Adams, P. D., Afonine, P. V., Bunkoczi, G., Chen, V. B., Davis, I. W., Echols, N., Headd, J. J., Hung, L.-W., Kapral, G. J., Grosse-Kunstleve, R. W., McCoy, A. J., Moriarty, N. W., Oeffner, R., Read, R. J., Richardson, D. C., Richardson, J. S., Terwilliger, T. C., and Zwart, P. H. (2010) *PHENIX*: a comprehensive Python-based system for macromolecular structure solution. *Acta Crystallogr. Sect. D: Struct. Biol.*, 66, 213–221.

Afonine, P. V., Grosse-Kunstleve, R. W., Echols, N., Headd, J. J., Moriarty, N. W., Mustyakimov, M., Terwilliger, T. C., Urzhumtsev, A, Zwart, P. H., and Adams, P. D. (2012) Towards automated crystallographic structure refinement with *phenix.refine*. *Acta Crystallogr. Sect. D: Struct. Biol.*, 68, 352–367.

Armstrong, F. A. (2013) Copying biology's ways with hydrogen. *Science*, 339(6120), 658–659.

Armstrong, F. A., Evans, R. M., Hexter, S. V., Murphy, B. J., Roessler, M. M., Wulff, P. (2016) Guiding principles of hydrogenase catalysis instigated and clarified by protein film electrochemistry. *Acc. Chem. Res.*, 49, 884–892.

Battye, T. G. G., Kontogiannis, L., Johnson, O., Powell, H. R., and Leslie, A. G. W. (2011)

iMosflm: a new graphical interface for diffraction-image processing with *MOSFLM*. *Acta Crystallogr. Sect. D: Struct. Biol.*, 67, 271–281.

Beaton, S. E., Evans, R. M., Finney, A. J., Lamont, C. M., Armstrong, F. A., Sargent, F., and Carr, S. B. (2018) The structure of hydrogenase-2 from *Escherichia coli*: implications for H_2-driven proton pumping. *Biochem. J.*, 475, 1353–1370.

Becke, A. D. (1993) Density-functional thermochemistry. III. The role of exact exchange. *J. Chem. Phys.*, 98, 5648–5652.

Bleijlevens, B., Faber, B. W., Albracht, S. P. J. (2001) The [NiFe] hydrogenase from *Allochromatium vinosum* studied in EPR-detectable states: H/D exchange experiments that yield new information about the structure of the active site. *J. Biol. Inorg. Chem.*, 6, 763–769

Bleijlevens, B., van Broekhuizen, F. A., De Lacey, A. L., Roseboom, W., Fernandez, V. M., and Albracht, S. P. J. (2004) The activation of the [NiFe]-hydrogenase from *Allochromatium vinosum*. An infrared spectro-electrochemical study. *J. Biol. Inorg. Chem.*, 9, 743–752.

Bowman, L., Flanagan, L., Fyfe, P. K., Parkin, A., Hunter, W. N., and Sargent, F. (2014) How the structure of the large subunit controls function in an oxygen-tolerant [NiFe]-hydrogenase. *Biochem. J.*, 458(3), 449–458.

Brooke, E. J., Evans, R. M., Islam, S. T. A., Roberts, G. M., Wehlin, S. A. M., Carr., S. B., Phillips, S. E. V., and Armstrong, F. A. (2017) Importance of the active site "canopy" residues in an O_2-tolerant [NiFe]-hydrogenase. *J. Am. Chem. Soc.*, 56(1), 132–142.

Burgdorf, T., van der Linden, E., Bernhard, M., Yin, Q. Y., Back, J. W., Hartog, A. F.,

Muijsers, A. O., de Koster, C. G., Albracht, S. P. J., and Friedrich, B. (2005) The soluble NAD^+-reducing [NiFe]-hydrogenase from *Ralstonia eutropha* H16 consists of six subunits and can be specifically activated by NADPH. *J. Bacteriol.*, 187(9), 3122–3132.

Carr, S. B., Evans, R. M., Brooke, E. J., Wehlin, S. A. M., Nomerotskaia, E., Sargent, F., Armstrong, F. A., and Phillips, S. E. V. (2016) Hydrogen activation by [NiFe]-hydrogenases. *Biochem. Soc. Trans.*, 44(3), 863–868.

Case, D. A., Darden, T. A., Cheatham, T. E., III, Simmerling, C. L., Wang, J., Duke, R. E., Luo, R., Walker, R. C., Zhang, W., Merz, K. M., Roberts, B., Hayik, S., Roitberg, A., Seabra, G., Swails, J., Götz, A. W., Kolossváry, I., Wong, K. F., Paesani, F., Vanicek, J., Wolf, R. M., Liu, J., Wu, X., Brozell, S. R., Steinbrecher, T., Gohlke, H., Cai, Q., Ye, X., Wang, J., Hsieh, M.-J., Cui, G., Roe, D. R., Mathews, D. H., Seetin, M. G., Salomon-Ferrer, R., Sagui, C., Babin, V., Luchko, T., Gusarov, S., Kovalenko, A., and Kollman, P. A. (2012) University of California, San Francisco.

Cracknell, J. A., Wait, A. F., Lenz, O., Friedrich, B., and Armstrong, F. A. (2009) A kinetic and thermodynamic understanding of O_2 tolerance in [NiFe]-hydrogenases. *Prot. Natl. Acad. Sci. USA*, 106(49), 20681–20686.

Dance, I. (2015) What is the trigger mechanism for the reversal of electron flow in oxygen-tolerant [NiFe] hydrogenases? *Chem. Sci.*, 6, 1433–1443.

del Barrio, M., Sensi, M., Orain, C., Baffert, C., Dementin, S., Fourmond, V., and Léger, C. (2018) Electrochemical investigations of hydrogenases and other enzymes that produce and use solar fuels. *Acc. C*hem. Res., 51, 769–777.

del Barrio, M., Guendon, C., Kpebe, A., Baffert, C., Fourmond, V., Brugna, M., and Léger,

C. (2019) Valine-to-cysteine mutation further increase the oxygen tolerance of *Escherichia coli* NiFe hydrogenase Hyd-1. *ACS Catal.*, 9, 4084–4088.

Dementin, S., Burlat, B., De Lacey, A. L., Pardo, A., Adryanczyk-Perrier, G., Guigliarelli, B., Fernandez, V. M., and Rousset, M. (2004) A glutamate is the essential proton transfer gate during the catalytic cycle of the [NiFe] hydrogenase. *J. Biol. Chem.*, 279, 10508–10513.

Dementin, S., Leroux, F., Cournac, L., de Lacey, A. L., Volbeda, A., Leger, C., Burlat, B., Martinez, N., Champ, S., Martin, L., Sanganas, O., Haumann, M., Fernandez, V. M., Guigliarelli, B., Fontecilla-Camps, J. C., and Rousset, M. (2009) Introduction of methionines in the gas channel makes [NiFe] hydrogenase aero-tolerant. *J. Am. Chem. Soc.*, 131(29), 10156–10164.

Eguchi, S., Yoon, K.-S., and Ogo, S. (2012) O_2-stable membrane-bound [NiFe]hydrogenase from a newly isolated *Citrobacter* sp. S-77. *J. Biosci. Bioeng.* 114(5), 479–484.

Emsley, P., and Cowtan, K. (2004) Coot: model-building tools for molecular graphics. *Acta Crystallogr. Sect. D: Biol. Crystallogr.*, 60, 2126–2132.

Emsley, P., Lohkamp, B, Scott, W. G., and Cowtan, K. (2010) Features and development of *Coot*. *Acta Crystallogr. Sect. D: Struct. Biol.*, 66, 486–501.

Evans, R. M., Parkin, A., Roessler, M. M., Murphy, B. J., Adamson, H., Lukey, M. J., Sargent, F., Volbeda, A., Fontecilla-Camps, J. C., and Armstrong, F. A. (2013) Principles of sustained enzymatic hydrogen oxidation in the presence of oxygen — the crucial influence of high potential Fe-S clusters in the electron relay of [NiFe]-hydrogenases. J. Am. Chem. Soc., 135(7), 2694–2707. #O2-

tolerant echem measurement

Evans, R. M., Brooke, E. J., Wehlin, S. A., Nomerotskaia, E., Sargent, F., Carr, S. B., Phillips, S. E., and Armstrong, F. A. (2016) Mechanism of hydrogen activation by [NiFe] hydrogenases. *Nat. Chem. Biol.*, 12(1), 46–50.

Evans, R. M., Ash, P. A., Beaton, S. E., Brooke, E. J., Vincent, K. A., Carr, S. B., and Armstrong, F. A. (2018) Mechanistic exploitation of a self-repairing, blocked proton transfer pathway in an O_2-tolerant [NiFe]-hydrogenase. *J. Am. Chem. Soc.*, 140, 10208–10220.

Fernandez, V. M., Hatchikian, E. C., Patil, D. S., and Cammack, R. (1986) ESR-detectable nickel and iron-sulphur centers in relation to the reversible activation of *Desulfovibrio gigas* hydrogenase. *Biochim. Biophys. Acta*, 1986, 145–154.

Fichtner, C., Laurich, C., Bothe, E., and Lubitz, W. (2006) Spectroelectrochemical characterization of the [NiFe] hydrogenase of *Desulfovibrio vulgaris* Miyazaki F. *Biochemistry*, 45(32), 9706–9716.

Fritsch, J., Lenz, O., and Friedrich, B. (2013) Structure, function and biosynthesis of O_2-tolerant hydrogenases. *Nature Rev. Microbiol.*, 11, 106–114.

Flanagan, L. A., and Parkin, A. (2016) Electrochemical insights into the mechanism of NiFe membrane-bound hydrogenases. *Biochem. Soc. Trans.*, 44, 315–328.

Frielingsdorf, S., Fritsch, J., Schmidt, A., Hammer, M., Löwenstein, J., Siebert, E., Pelmenschikov, V., Jaenicke, T., Kalms, J., Rippers, Y., Lendzian, F., Zebger, I., Teutloff, C., Kaupp, M., Bittl, R., Hildebrandt, P., Friedrich, B., Lenz, O., and Scheerer, P.

Frisch, G. M. J., Trucks, W., Schlegel, H. B., Scuseria, G. E., Robb, M. A., Cheeseman, J. R., Scalmani, G., Barone, V., Mennucci, B., Petersson, G. A., Nakatsuji, H., Caricato, M., Li, X., Hratchian, H. P., Izmaylov, A. F., Bloino, J., Zheng, G., and Sonnenberg, J. L., *Inc. Wallingford*, *CT*, 2009.

Fritsch, J., Scheerer, P., Frielingsdorf, S., Kroschinsky, S., Friedrich, B., Lenz, O., and Spahn, C. M. T. (2011) The crystal structure of an oxygen-tolerant hydrogenase uncovers a novel iron-sulphur centre. *Nature*, 479, 249–252.

Galván, I. F., Volbeda, A., Fontecilla-Camps, J. C., and Field, M. J. (2008) A QM/MM study of proton transport pathways in a [NiFe] hydrogenase. *Proteins*, 73, 195–203.

Garcin, E., Vernede, X., Hatchikian, E. C., Volbeda, A., Frey, M., and Fontecilla-Camps, J. C. (1999) The crystal structure of a reduced [NiFeSe] hydrogenase provides an image of the activated catalytic center. *Structure*, 7(5), 557–566. #Db[NiFeSe] 1CC1

Geßner, C., Trofanchuk, O., Kawagoe, K., Higuchi, Y., Yasuoka, N., and Lubitz, W. (1996) Single crystal EPR study of the Ni center of NiFe hydrogenase. *Chem. Phys. Lett.*, 256, 518–524.

Ghosh, D., Bisaillon, A., and Hallenbeck, P. C. (2013) Increasing the metabolic capacity of *Escherichia coli* for hydrogen production through heterologous expression of the *Ralstonia eutropha* SH operon. *Biotechnol. Biofuels*, 6, 122.

Goris, T., Wait, A. F., Saggu, M., Fritsch, J., Heidary, N., Stein, M., Zebger, I., Lendzian, F., Armstrong, F. A., Friedrich, B., and Lenz, O. (2011) A unique iron-sulfur cluster is crucial for oxygen tolerance of a [NiFe]-hydrogenase. *Nat. Chem. Biol.*, 7(5),

310–318. #ReMBH [4Fe-3S] crucial for O2-tolerance.

Greening., C., Biswas, A., Carere, C. R., Jackson, C. J., Taylor, M. C., Stott, M. B., Cook, G. M., and Morales, S. E. (2016) Genomic and metagenomic surveys of hydrogenase distribution indicate H2 is a widely utilised energy source for microbial growth and sruvival. *IMSE J.*, 10, 761–777.

Hamdan, A. A., Liebgott, P.-P., Fourmond, V., Gutiérrez-Sanz, O., De Lacey, A. L., Infossi, P., Rousset, M., Dementin, S., and Léger, C. (2012) Relation between anaerobic inactivation and oxygen tolerance in a large series of NiFe hydrogenase mutants. *Prot. Natl. Acad. Sci. USA*, 109(49), 19916–19921.

Hartmann, S., Frielingsdorf, S., Ciaccafava, A., Lorent, C., Fritsch, J., Siebert, E., Priebe, J., Haumann, M., Zebger, I., and Lenz, O. (2018) O_2-tolerant H_2 activation by an isolated large subunit of a [NiFe] hydrogenase. *Biochemistry*, 57(36), 5339–5349.

Hedderich, R. (2004) Energy-converting [NiFe] hydrogenase from archaea and extremophiles: ancestors of complex I. *J. Bioenergetics Biomembranes*, 36(1), 65–75.

Higuchi, Y., Yagi, T. and Yasuoka, N. (1997) Unusual ligand structure in Ni-Fe active center and an additional Mg site in hydrogenase revealed by high resolution X-ray structure analysis.

Higuchi, Y., Ogata, H., Miki, K., Yasuoka, N., and Yagi, T. (1999) Removal of the bridging ligand atom at the Ni–Fe active site of [NiFe] hydrogenase upon reduction with H2, as revealed by X-ray structure analysis at 1.4 Å resolution. *Structure*, 7(5), 549–556.

Horch, M., Lauterbach, L., Mroginski, M. A., Hildebrandt, P., Lenz, O., and Zebger, I. (2015) Reversible active site sulfoxygenation can explain the oxygen tolerance of a NAD^+-reducing [NiFe] hydrogenase and its unusual infrared spectroscopic properties. *J. Am. Chem. Soc.*, 137, 2555–2564.

Ilina, Y., Lorent, C., Katz, S., Jeoung, J.-H., Shima, S., Horch, M., Zebger, I., and Dobbek, H. (2019) X-ray crystallography and vibrational spectroscopy reveal the key determinants of biocatalytic dihydrogen cycling by [NiFe] hydrogenases. *Angew. Chem. Int. Ed.*, 58, 2–7.

Kabsch, W. (2010) XDS. *Acta Crystallogr. Sect. D: Biol. Crystallogr.*, 66, 125–132. #XDS citation

Kalms, J., Schmidt, A., Frielingsdorf, S., van der Linden, P., von Stetten, D, Lenz, O., Carpentier, P., and Scheerer, P. (2016) Krypton derivatization of an O_2-tolerant membrane-bound [NiFe] hydrogenase reveals a hydrophobic tunnel network for gas transport. *Angew. Chem. Int. Ed.*, 55(18), 5586–5590.

Kalms, J., Schmidt, A., Frielingsdorf, S., Utesch, T., Gotthard, G., von Stetten, D., van der Linden, P., Royant, A., Mroginski, M. A., Carpentier, P., Lenz, O, and Scheerer, P. (2018) Tracking the route of molecular oxygen in O_2-tolerant membrane-bound [NiFe] hydrogenase. *Prot. Natl. Acad. Sci. USA*, 115(10), E2229–E2237.

Karstens, K., Wahlefeld, S., Horch, M., Grunzel, M., Lauterbach, L, Lendzian, F., Zebger, I. and Lenz, O. (2015) Impact of the iron–sulfur cluster proximal to the active site on the catalytic function of an O_2-tolerant NAD^+-reducing [NiFe]-hydrogenase. *Biochemistry*, 54, 389–403.

Kawahara-Nakagawa, Y., Nishikawa, K., Nakashima, S., Inoue, S., Ohta, T., Ogura, T.,

Shigeta, Y., Fukutani, K., Yagi, T., and Higuchi, Y. (2019) New assay method based on Raman spectroscopy for enzymes reacting with gaseous substrates. *Prot. Sci.*, 28, 663–670.

Kellers, P., Pandelia, M.-E., Currell, L. J., Görner, H., and Lubitz, W. (2009) FTIR study on the light sensitivity of the [NiFe] hydrogenase from *Desulfovibrio vulgaris* Miyazaki F: Ni-C to Ni-L photoconversion, kinetics of proton rebinding and H/D isotope effect. *Phys. Chem. Chem. Phys.*, 11, 8680–8683.

Kessler, E. (1973) Effect of anaerobiosis on photosynthetic reactions and nitrogen metabolism of algae with and without hydrogenase. *Arch. Mikrobiol.*, 93(2), 91-100.

Kim, J., Kang, J., Nishigami, H., Kino, H, and Tateno, M. (2018) Ab initio electronic structure calculation of [4Fe-3S] cluster of hydrogenase as dihydrogen dissociation/production catalyst. *J. Phys. Soc. Jpn.*, 87, 034804.

Kleihues, L., Lenz, O., Bernhard, M., Buhrke, T., and Friedrich, B. (2000) The H_2 sensor of *Ralstonia eutropha* is a member of the subclass of regulatory [NiFe] hydrogenases. *J. Bacteriol.*, 182 (10), 2716–2724.

Koo, J., and Swartz, J. R. (2018) Improved [FeFe] hydrogenase O_2 tolerance suggests feasibility for photosynthetic H_2 production. *Metabolic Engineering*, 49, 21–27.

Lacasse, M. J., and Zamble, D. B. (2016) [NiFe]-hydrogenase maturation. *Biochemistry*, 55, 1689–1701.

Lamle, S. E., Albracht, S. P. J., and Armstrong, F. A. (2004) Electrochemical potential-step investigations of the aerobic interconversions of [NiFe]-hydrogenase from *Allochromatium vinosum*: insights into the puzzling difference between

unready and ready oxidized inactive state. *J. Am. Chem. Soc.*, 126(45), 14899–14909.

Larkin, M. A., Blackshields, G., Brown, N. P., Chenna, R., McGettigan, P. A., McWilliam, H., Valentin, F., Wallace, I. M., Wilm, A., Lopez, R., Thompson, J. D., Gibson, T. J., and Higgins, D. G. (2007) Clustal W and Clustal X version 2.0. *Bioinformatics*, 23(21), 2947–2948.

Lauterbach, L., Liu, J., Horch, M., Hummel, P., Schwarze, A., Haumann, M., Vincent, K. A., Lenz, O., and Zebger, I. (2011) The hydrogenase subcomplex of the NAD^+-reducing [NiFe] hydrogenase from *Ralstonia e*utropha — insights into catalysis and redox interconversions. *Eur. J. Inorg. Chem.*, 7, 1067–1079.

Lauterbach, L., and Lenz, O. (2013) Catalytic production of hydrogen peroxide and water by oxygen-tolerant [NiFe]-hydrogenase during H_2 cycling in the presence of O_2. *J. Am. Chem. Soc.*, 135, 17897–17905.

Lee, C., Yang, W., and Parr, R. G. (1988) Development of the Colle-Salvetti correlation-energy formula into a functional of the electron density. *Phys. Rev. B*, 37, 785–789.

Leger, C., Jones, A. K., Roseboom, W., Albracht, S. P. J., and Armstrong, F. A. (2002) Enzyme electrokinetics: hydrogen evolution and oxidation by *Allochromatium vinosum* [NiFe]-hydrogenase. *Biochemistry*, 41(52), 15736–15746.

Leroux, F., Dementin, S., Burlat, B., Cournac, L., Volbeda, A., Champ, S., Martin, L., Guigliarelli, B., Bertrand, P., Fontecilla-Camps, J., Rousset, M., and Leger, C. (2008) Experimental approaches to kinetics of gas diffusion in hydrogenase. *Prot. Natl. Acad. Sci. USA*, 105(32), 11188–11193.

Liebgott, P.-P., de Lacey, A. L., Burlat, B., Cournac, L., Richaud, P., Brugna, M., Fernandez, V. M., Guigliarelli, B., Rousset, M., Leger, C., and Dementin, S. (2011) Original design of an oxygen-tolerant [NiFe] hydrogenase: major effect of a valine-to-cysteine mutation near the active site. *J. Am. Chem. Soc.*, 133, 986–997.

Lu, Y., and Koo, J. (2019) O_2 sensitivity and H_2 production activity of hydrogenases—a review. *Biothechnol. Bioeng.*, 116(11), 3124–3135.

Lubek, D., Simon, A. H., and Pinske, C. (2019) Amino acid variants of the HybB membrane subunit of *Escherichia coli* [NiFe]-hydrogenase-2 support a role in proton transfer. FEBS Lett., 593(16), 2194–2203.

Lubitz, W., Reijerse, E., and van Gastel, M. (2007) [NiFe] and [FeFe] hydrogenases studied by advanced magnetic resonance techniques. *Chem. Rev.*, 107, 4331–4365.

Lubitz, W., Ogata, H., Rüdiger, O., and Reijerse, E. (2014) Hydrogenases. *Chem. Rev.*, 114, 4081–4148.

Ludwig, M. (2008) The oxygen-tolerant, membrane-bound hydrogenase of *Ralstonia* species: Variations in the active site structure the Fe-S cluster composition and maturation. Ph.D. Dissertation, Humboldt-Universität zu Berlin.

Lukey, M. J., Parkin, A., Roessler, M. M., Murphy, B. J., Harmer, J., Palmer, T., Sargent, F., and Armstrong, F. A. (2010) How *Escherichia coli* is equipped to oxidize hydrogen under different redox conditions. *J. Biol. Chem.*, 285, 3928–3938.

Maier, J. A. H., Ragozin, S., and Jeltsch, A. (2015) Identification, cloning and heterologous expression of active [NiFe]-hydrogenase 2 from *Citrobacter* sp.

SG in *Escherichia coli*, *J. Biotechnol.*, 199, 1–8.

Marques, M. C., Coelho, R., De Lacye, A. L., Pereira, I. A. C., and Matias, P. M. (2010) The three-dimensional structure of [NiFeSe] hydrogenase from *Desulfovibrio vulgaris* Hildenborough: a hydrogenase without a bridging ligand in the active site in its oxidised, "as-isolated" state. *J. Mol. Biol.*, 396, 893–907.

Marques, M. C., Coelho, R., Pereira, I. A. C., and Patias, P. M. (2013) Redox state-dependent changes in the crystal structure of [NiFeSe] hydrogenase from *Desulfovibrio vulgaris* Hildenborough. *Int. J. Hydrogen Energy*, 38, 8664–8682.

Marques, M. C., Tapia, C., Gutierrez-Sanz, O., Ramos, A. R., Keller, K. L., Wall, J. D., De Lacey, A. L., Matias, P. M., and Pereira, I. A. C. (2017) The direct role of selenocysteine in [NiFeSe] hydrogenase maturation and catalysis. *Nat. Chem. Biol.*, 13(5), 544–550.

Matias, P. M., Soares, C. M., Saraiva, L. M., Coelho, R., Morais, J., Gall, J. L., and Carrondo, M. A. (2001) [NiFe] hydrogenase from *Desulfovibrio desulfuricans* ATCC 27774: gene sequencing, three-dimensional structure determination and refinement at 1.8 Å and modelling studies of its interaction with the tetrahaem cytochrome c_3. *J. Biol. Inorg. Chem.*, 6, 63–81.

Matsumoto, T., Eguchi, S., Nakai, H., Hibino, T., Yoon, K.-S., and Ogo, S. (2014) [NiFe]hydrogenase from *Citrobacter* sp. S-77 surpasses platinum as an electrode for H_2 oxidation reaction. *Angew. Chem. Int. Ed.*, 53, 1–5.

McCoy, A. J., Grosse-Kunstleve, R. W., Adams, P. D., Winn, M. D., Storoni, L. C., and Read, R. J. (2007) Phaser crystallographic software. *J. Appl.* Cryst., 40, 658–674.

Mitchell, P., and Moyle, J. (1967) Chemiosmotic hypothesis of oxidative

phosphorylation. *Nature*, 213, 137–139.

Mitchell, P. (2011) Chemiosmotic coupling in oxidative and photosynthetic phosphorylation. *Biochim. Biophys. Acta*, 1807, 1507–1538.

Murphy, B. J., Sargent, F., and Armstrong, F. A. (2014) Transforming an oxygen-tolerant NiFe uptake hydrogenase into a proficient, reversible hydrogen producer. *Energy Environ. Sci.*, 7(4), 1426–1433.

Murphy, B. J., Hidalgo, R., Roessler, M. M., Evans, R. M., Ash, P. A., Myers, W. K., Vincent, K. A., and Armstrong, F. A. (2015) Discovery of dark pH-dependent H+ migration in a [NiFe]-hydrogenase and its mechanistic relevance: mobilizing the hydrido ligand of the Ni-C intermediate. *J. Am. Chem. Soc.*, 137(26), 8484–8489.

Murshudov, G. N., Skubak, P., Lebedev, A. A., Pannu, N. S., Steiner, R. A., Nicholls, R. A., Winn, M. D., Long, F., and Vagin, A. A. (2011) *REFMAC5* for the refinement of macromolecular crystal structures. *Acta Crystallogr. Sect. D: Biol. Crystallogr.*, 67, 355–367.

Natale, P., Bruser, T., and Driessen, A. J. M. (2008) Sec- and Tat-mediated protein secretion across the bacterial cytoplasmic membrane—Distinct translocases and mechanisms. Biochim. Biophys. Acta, 1778, 1735–1756.

Nishikawa, K., Mochida, S., Hiromoto, T., Shibata, N., and Higuchi, Y. (2017) Ni-elimination from the active site of the standard [NiFe]-hydrogenase upon oxidation by O_2. *J. Inorg. Biochem.*, 177, 435–437.

Nishikawa, K., Ogata, H., and Higuchi, Y. (2020) Structural basis of the function of [NiFe]-hydrogenases. *Chem. Lett.*, 49(2), 164–173.

Noodleman, L., and Case, D. A. (1992) Density-functional theory of spin polarization and spin coupling in iron-sulfur clusters. *Adv. Inorg. Chem.*, 38, 423–470.

Noor, N. D. M., Nishikawa, K., Nishihara, H., Yoon, K.-S., Ogo, S., and Higuchi, Y. (2016a) Improved purification, crystallization and crystallographic study of Hyd-2-type [NiFe]-hydrogenase from *Citrobacter* sp. S-77. *Acta Crystallogr.*, *Sect. F: Struct. Biol. Commun.*, 72, 53–58.

Noor, N. D. M. (2016b) Biochemical and crystallographic study of Hyd-2 type [NiFe]-hydrogenase from *Citrobacter* sp. S-77. Ph.D. Dissertation, University of Hyogo.

Ogata, H., Mizoguchi, Y., Mizuno, N., Miki, K., Adachi, S., Yasuoka, N., Yagi, T., Yamauchi, O., Hirota, S., and Higuchi, Y. (2002) Structural studies of the carbon monoxide complex of [NiFe]hydrogenase from *Desulfovibrio vulgaris* Miyazaki F: suggestion for the initial activation site for dihydrogen. *J. Am. Chem. Soc.*, 124, 11628–11635.

Ogata, H., Hirota, S., Nakahara, A., Komori, H., Shibata, N., Kato, T., Kano, K., and Higuchi, Y. (2005) Activation process of [NiFe] hydrogenase elucidated by high-resolution X-ray analyses: conversion of the ready to the unready state. *Structure*, 13, 1635–1642.

Ogata, H., Lubitz, W., and Higuchi, Y. (2009) [NiFe] hydrogenases: structural and spectroscopic studies of the reaction mechanism. *Dalton Trans.*, 7577–7587.

Ogata, H., Kellers, P., and Lubitz, W. (2010) The crystal structure of the [NiFe] hydrogenase from the photosynthetic bacterium *Allchromatium vinosum*: characterization of the oxidized enzyme (Ni-A state). *J. Mol. Biol.*, 402(2), 428–444.

Ogata, H., Nishikawa, K., and Lubitz, W. (2015) Hydrogens detected by subatomic resolution protein crystallography in a [NiFe] hydrogenase. *Nature*, 520, 571–574.

Ohki, Y., and Tasumi, K. (2011) Thiolate-bridged iron-nickel models for the active site of [NiFe] hydrogenase. *Eur. J. Inorg. C*hem., 973–985.

Osuka, H., Shomura, Y., Komori, H., Shibata, N., Nagao, S., Higuchi, Y., and Hirota, S. (2013) Photosensitivity of the Ni-A state of [NiFe] hydrogenase from *Desulfovibrio vulgaris* Miyazaki F with visible light. *Biochem. Biophys. Res. Commun.*, 430, 284–288.

Otwinowski, Z., and Minor, W. (1997) Processing of X-ray diffraction data collected in oscillation mode. *Methods Enzymol.*, 276, 307–326.

Owen, R. L., Rudiño-Piñera, E., and Farman, E. F. (2006) Experimental determination of the radiation dose limit for cryocooled protein crystals. *Prot. Natl. Acad. Sci. USA*, 103(13), 4912–4917.

Pandelia, M.-E., Ogata, H., Currell, L. J., Flores, M., and Lubitz, W. (2009) Probing intermediates in the activation cycle of [NiFe] hydrogenase by infrared spectroscopy: the Ni-SI_r state and its light sensitivity. *J. Biol. Inorg. Chem.*, 14, 1227–1241.

Pandelia, M.-E., Fourmond, V., Tron-Infossi, P., Lojou, E., Bertrand, P., Léger, C., Giudici-Orticoni, M.-T., and Lubitz, W. (2010) Membrane-bound hydrogenase I from the hyperthermophilic bacterium *Aquifex aeolicus*: enzyme activation, redox intermediates and oxygen tolerance. *J. Am. Chem. Soc.*, 132, 6991–7004.

Pandelia, M.-E., Ogata, H., Currell, L. J., Flores, M., and Lubitz, W. (2010) Inhibition of

the [NiFe] hydrogenase from *Desulfovibrio vulgaris* Miyazaki F by carbon monoxide: An FTIR and EPR spectroscopic study. *Biochim. Biophys. Acta*, 1797, 304–313.

Pandelia, M.-E., Infossi, P., Giudici-Orticoni, M. T., and Lubitz, W. (2010) The oxygen-tolerant hydrogenase I from *Aquifiex aeolicus* weakly interacts with carbon monoxide: an electrochemical and time-resolved FTIR study. *Biochemistry*, 49(41), 8873–8881.

Pandelia, M.-E. (2010) [NiFe] hydrogenases from *Desulfovibrio vulgaris* Miyazaki F and *Aquifex aeolicus* studied by FTIR, EPR and electrochemical techniques: Redox intermediates, O2/CO sensitivity and light-induced effects, PhD dissertation, Technische Universität Berlin.

Pandelia, M.-E., Nitschke, W., Infossi, P., Guidici-Orticoni, M.-T., Bill, E., and Lubitz, W. (2011) Characterization of a unique [FeS] cluster in the electron transfer chain of the oxygen tolerant [NiFe] hydrogenase from *Aquifex aeolicus*. *Prot. Natl. Acad. Sci. USA*, 108(15), 6097–6102.

Pandelia, M.-E., Bykov, D., Izsak, R., Infossi, P., Giudici-Orticoni, M.-T., Bill, E., Neese, F., and Lubitz, W. (2013) Electronic structure of the unique [4Fe-3S] cluster in O_2-tolerant hydrogenases characterized by ^{57}Fe Mössbauer and EPR spectroscopy. *Prot. Natl. Acad. Sci. USA*, 110(2), 483–488.

Pelmenschikov, V., and Kaupp, M. (2013) Redox-dependent structural transformations of the [4Fe-3S] proximal cluster in O2-tolerant membrane-bound [NiFe]-hydrogenase: a DFT study. *J. Am. Chem. Soc.*, 135(32), 11809–11823.

Peters., J. W., Schut, G. J., Boyd, E. S., Mulder, D. W., Shepard, E. M., Broderick, J. B., King, P. W., and Adams, M. W. W. (2015) [FeFe]- and [NiFe]-hydrogenase diversity, mechanism, and maturation. *Biochim. Biophys. Acta*, 1853, 1350–1369.

Pfirrmann, T., Lokapally, A., Andreasson, C., Ljungdahl, P., and Hollemann, T. (2013) SOMA: a single oligonucleotide mutagenesis and cloning approach. *PLoS ONE*, 8(6), e64870.

Pinske, C., Jaroschinsky, M., Linek, S., Kelly, C. L., Sargent, F., and Sawers, R. G. (2015) Physiology and bioenergetics of [NiFe]-hydrogenase 2-catalyzed H_2-consuming and H_2-producing reactions in *Escherichia coli*. *J. Bacteriol.*, 197, 296–306.

Plumeré, N., Rüdiger, O., Oughli, A. A., Williams, R., Vivekananthan, J., Pöller, S., Schuhmann, W., and Lubitz, W. (2014) A redox hydrogel protects hydrogenase from high-potential deactivation and oxygen damage. *Nat. Chem. Biol.*, 6, 822–827.

Potterton, E., Briggs, P., Turkenburg, M, and Dodson, E. (2003) A graphical user interface to the CCP4 program suite. *Acta Crystallogr. Sect. D: Biol. Crystallogr.*, 59, 1131–1137.

Preissler, J., Wahlefeld, S., Lorent, C., Teutloff, C., Horch, M., Lauterbach, L., Cramer, S. P., Zebger, I., and Lenz, O. (2018) Enzymatic and spectroscopic properties of a thermostable [NiFe]-hydrogenase performing H_2-driven NAD^+-reduction in the presence of O_2. *Biochim. Biophys. Acta Bioenerg.*, 1859(1), 8–18.

Roessler, M. M., Evans, R. M., Davies, R. A., Harmer, J., and Armstrong, F. A. (2012) EPR spectroscopic studies of the Fe–S clusters in the O_2-tolerant [NiFe]-

hydrogenase Hyd-1 from *Escherichia coli* and characterization of the unique [4Fe–3S] cluster by HYSCORE. *J. Am. Chem. Soc.*, 134(37), 15581–15594.

Rousset M., Montet, Y., Guigliarelli, B., Forget, N., Asso, M., Bertrand, P., Fontecilla-Camps, J. C., and Hatchikian, E. C. (1998) [3Fe-4S] to [4Fe-4S] cluster conversion in *Desulfovibrio fructosovorans* [NiFe] hydrogenase by site-directed mutagenesis. *Proc. Natl. Acad. Sci. USA*, 95, 11625–11630.

Ruff, A., Szczesny, J., Markovic, N., Conzuelo, F., Zacarias, S., Pereira, I. A. C., Lubitz, W., and Schuhmann, W. (2018) A fully protected hydrogenase/polymer-based bioanode for high-performance hydrogen/glucose biofuel cells. *Nature Communications*, 9, 3675.

Saggu, M., Zebger, I., Ludwig, M., Lenz, O., Friedrich, B., Hildebrandt, P., and Lendzian, F. (2009) Spectroscopic insights into oxygen-tolerant membrane-associated [NiFe] hydrogenase of *Ralstonia eutropha* H16. *J. Biol. Chem.*, 284(24), 16264–16276.

Sargent, F. (2016) The model [NiFe]-hydrogenases of *Escherichia coli*. *Adv. Microb. Physiol.*, 68, 433–507.

Shafaat, H. S., Rudiger, O., Ogata, H., and Lubitz, W. (2013) [NiFe] hydrogenases: a common active site for hydrogen metabolism under diverse conditions. *Biochim. Biophys. Acta*, 1827(8-9), 986–1002.

Schäfer, A., Horn, H., and Ahlrichs, R. (1992) Fully optimized contracted Gaussian basis sets for atoms Li to Kr. *J. Chem. Phys.*, 97, 2571–2577.

Schäfer, C., Friedrich, B., and Lenz, O. (2013) Novel, oxygen-insensitive group 5 [NiFe]-hydrogenase in *Ralstonia eutropha*. *Appl. Environ. Microbiol.*, 79(17),

5137–5145.

Schäfer, C., Bommer, M., Hennig, S. E., Jeoung, J.-H., Dobbek, H., and Lenz, O. (2016) Structure of an Actinobacterial-type [NiFe]-hydrogenase reveals insight into O_2-tolerant H_2 oxidation. *Structure*, 24, 285–292.

Schilter, D., Camara, J. M., Huynh, M. T., Hammes-Schiffer, S., and Rauchfuss, T. B. (2016) Hydrogenase enzymes and their synthetic models: the role of metal hydrides. *Chem. Rev.*, 116, 8693–8749.

Schoelmerich, M. C., and Müller, V. (2019) Energy conservation by a hydrogenase-dependent chemiosmotic mechanism in an ancient metabolic pathway. *Prot. Natl. Acad. Sci. USA*, 116(13), 6329–6334.

Schröder, V. (2002) Explosionsgrenzen von Wasserstoff und Wasserstoff/Methan-Gemischen., *Forschungsberichit, 253,* Bundesanstalt für Materialforschung und -prüfung.

Schrödinger, LLC. The PyMOL Molecular Graphics System, Version 2.0

Shomura, Y., Yoon, K.-S., Nishihara, H., and Higuchi, Y. (2011) Structural basis for [4Fe-3S] cluster in the oxygen-tolerant membrane-bound [NiFe]-hydrogenase. *Nature*, 479, 253–256.

Shomura, Y., and Higuchi, Y. (2013) Structural aspects of [NiFe]-hydrogenases. *Rev. Inorg. Chem.*, 33(4), 173–192.

Shomura, Y., Taketa, M., Nakashima, H., Tai, H., Nakagawa, H., Ikeda, Y., Ishii, M., Igarashi, Y., Nishihara, H., Yoon, K.-S., Ogo, S., Hirota, S., and Higuchi, Y. (2017) Structural basis of the redox switches in the NAD^+-reducing soluble [NiFe]-hydrogenase. *Science*, 357, 928–932.

Simon, R., Priefer, U., and Pühler, A. (1983) A broad host range mobilization system for in vivo genetic engineering: transposon mutagenesis in gram negative bacteria. *Nat. Biotechnol.*, 1, 784–791.

Stephenson, M., and Stickland, L. H. (1931a) Hydrogenase: A bacterial enzyme activating molecular hydrogen: the properties of the enzyme. *Biochem. J.*, 25(1), 205–214.

Stephenson, M., and Stickland, L. H. (1931b) Hydrogenase: the reduction of sulphate to sulphide by molecular hydrogen. *Biochem. J.*, 25(1), 215–220.

Stephenson, M., and Stickland, L. H. (1932) Hydrogenlyases: bacterial enzymes liberating molecular hydrogen. *Biochem. J.*, 26(3), 712–724.

Stiebritz, M., and Reiher, M. (2013) Hydrogenases and oxygen. *Chem. Sci.*, 3, 1739–1751

Szczesny, J., Markovic, N., Conzuelo, F., Zacarias, S., Pereira, I. A. C., Lubitz, W., Plumere, N., Schuhmann, W., and Ruff A. (2018) A gas breathing hydrogen/air biofuel cell comprising a redox polymer/hydrogenase-based bioanode. *Nature Commun.*, 9, 4715.

Søndergaard, D., Pedersen, C. N. S., and Greening, S. (2016) HydDB: a web tool for hydrogenase classification and analysis. *Sci. Rep.* 6, 34212

Tabrizi, S. G., Pelmenschikov, V., Noodleman, L., and Kaupp, M. (2016) The Mossbauer parameters of the proximal cluster of membrane-bound hydrogenase revisited: a density functional theory study. *J. Chem. Theory Comput.*, 12(1), 174–187.

Tai, H., Nishikawa, K., Suzuki, M., Higuchi, Y., and Hirota, S. (2014) Control of the

transition between Ni-C and Ni-SI_a states by the redox state of the proximal Fe-S cluster in the catalytic cycle of [NiFe] hydrogenase. *Angew. Chem. Int. Ed.*, 53(50), 13817–13820.

Tai, H., Nishikawa, K., Inoue, S., Higuchi, Y., and Hirota, S. (2015) FT-IR characterization of the light-induced Ni-L2 and Ni-L3 states of [NiFe] hydrogenase from *Desulfovibrio vulgaris* Miyazaki F. *J. Phys. Chem. B*, 119(43), 13668–13674.

Tai, H., Xu, L., Inoue, S., Nishikawa, K., Higuchi, Y., and Hirota, S. (2016) Photoactivation of the Ni-Sir state in [NiFe] hydrogenase: FT-IR study on the light reactivity of the ready Ni-Sir state and as-isolated enzyme revisited. *Phys. Chem. Chem. Phys.*, 18, 22025–22030.

Tai, H., Xu, L, Nishikawa, K., Higuchi, Y. and Hirota, S. (2017) Equilibrium between inactive ready Ni-SI_r and active Ni-SI_a states of [NiFe] hydrogenase studied by utilizing Ni-SI_r-to-Ni-SI_a photoactivation. *Chem. Commun.*, 53, 10444–10447.

Tai, H., Higuchi, Y., and Hirota, S. (2018) Comprehensive reaction mechanisms at and near the Ni-Fe active sites of [NiFe] hydrogenases. *Dalton Trans.*, 47(13), 4408–4423.

Taketa, M., Nakagawa, H., Habukawa, M., Osuka, H., Kihira, K., Komori, H., Shibata, N., Ishii, M., Igarashi, Y., Nishihara, H., Yoon, K.-S., Ogo, S., Shomura, Y., and Higuchi, Y. (2015) Crystallization and preliminary X-ray analysis of the NAD^+-reducing [NiFe] hydrogenase from *Hydrogenophilus thermoluteolus* TH-1. *Acta Crystallogr. Sect. F: Struct. Biol. Commun.*, 71, 96–99.

Vignais, P. M., Billoud, B., and Meyer, J. (2001) Classification and phylogeny of

hyrogenases. *FEMS Microbiol. Rev.*, 25, 455–501.

Vignais, P. M., and Colbeau, A. (2004) Molecular biology of microbial hydrogenases. *Curr. Issues Mol. Biol.*, 6, 159–188.

Vignais, P. M., and Billoud, B. (2007) Occurrence, classification, and biological function of hydrogenases: an overview. *Chem. Rev.*, 107, 4206–4272.

Vincent, K. A., Parkin, A., and Armstrong, F. A. (2007) Investigating and exploiting the electrocatalytic properties of hydrogenases. *Chem. Rev.*, 107, 4366–4413.

Volbeda, A., Charon, M. H., Piras, C., Hatchikian, E. C., Frey, M., and Fontecilla-Camps, J. C. (1995) Crystal structure of the nickel-iron hydrogenase from *Desulfovibrio gigas*. *Nature*, 373, 580–587.

Volbeda, A., Garcin, E., Piras, C., de Lacey, A. L., Fernandez, V. M., Hatchikian, E. C., Frey, M., and Fontecilla-Camps, J. C. (1996) Structure of the [NiFe] hydrogenase active site: evidence for biologically uncommon Fe ligands. *J. Am. Chem. Soc.*, 118(51), 12989–12996.

Volbeda, A., Martin, L., Cavazza, C., Matho, M., Faber, B. W., Roseboom, W., Albracht, S. P. J., Garcin, E., Rousset, M., and Fontecilla-Camps, J. C. (2005) Structural differences between the ready and unready oxidized states of [NiFe] hydrogenases. *J. Biol. Inorg. Chem.*, 10, 239–249.

Volbeda, A., Amara, P., Darnault, C., Mouesca, J.-M., Parkin, A., Roessler, M. M., Armstrong, F. A., and Fontecilla-Camps, J. C. (2012) X-ray crystallographic and computational studies of the O_2-tolerant [NiFe]-hydrogenase 1 from *Escherichia coli*. *Prot. Natl. Acad. Sci. USA.*, 109(14), 5305–5310.

Volbeda, A., Darnault, C., Parkin, A., Sargent, F., Armstrong, F. A. and Fontecilla-Camps,

J. C. (2013a) Crystal structure of the O_2-tolerant membrane-bound hydrogenase 1 from *Escherichia coli* in complex with its cognate cytochrome *b*. *Structure*, 21, 184–190.

Volbeda, A., Amara, P., Iannello, M., De Lacey, A. L., Cavazza, C., and Fontecilla-Camps, J. C. (2013b) Structural foundations for the O_2 resistance of *Desulfomicrobium baculatum* [NiFeSe]-hydrogenase. *Chem. Commun.*, 49, 7061–7063.

Volbeda, A., Martin, L., Barbier, E., Gutiérrez-Sanz, O., De Lacey, A. L., Liebgott, P.-P., Dementin, S., Rousset, M., and Fontecilla-Camps, J. C. (2015a) Crystallographic studies of [NiFe]-hydrogenase mutants: towards consensus structures for the elusive unready oxidized states. *J. Biol. Inorg. Chem.*, 20, 11–22.

Volbeda, A., Martin, L., Liebgott, P.-P., De Lacey, A. L., and Fontecilla-Camps, J. C. (2015b) [NiFe]-hydrogenases revisited: nickel-carboxamido bond formation in a variant with accrued O_2-tolerance and a tentative re-interpretation of Ni-SI states. *Metallomics*, 7, 710–718.

Volbeda, A., Mouesca, J. M., Darnault, C., Roessler, M. M., Parkin, A., Armstrong, F. A., and Fontecilla-Camps, J. C. (2018) X-ray structural, functional and computational studies of the O_2-sensitive *E. coli* hydrogenase-1 C19G variant reveal an unusual [4Fe-4S] cluster. *Chem. Commun.*, 54, 7175–7178.

Winn, M. D., Ballard, C. C., Cowtan, K. D., Dodson, E. J., Emsley, P., Evans, P. R., Keegan, R. M., Krissinel, E. B., Leslie, A. G. W., McCoy, A., McNicholas, S. J., Murshudov, G. N., Pannu, N. S., Potterton, E. A., Powell, H. R., Read, R. J., Vagin, A., and Wilson, K. S. (2011) Overview of the *CCP4* suite and current developments. *Acta Crystallogr. Sect. D: Struct. Biol.*, 67, 235–242.

Wombwell, C., Caputo, C. A., and Reisner, E. (2015) [NiFeSe]-hydrogenase chemistry. *Acc. Chem. Res.*, 48, 2858–2865.

Wu, L. F., and Mandrand, M. A. (1993) Microbial hydrogenases: primary structure, classification, signatures and phylogeny. *FEMS Microbiol. Rev.*, 10, 243–269.

Wulff, P., Day, C. C., Sargent, F., and Armstrong, F. A. (2014) How oxygen reacts with oxygen-tolerant respiratory [NiFe]-hydrogenases. *Prot. Natl. Acad. Sci. USA*, 111(18), 6606–6611.

Wulff, P., Thomas, C., Sargent, F., and Armstrong, F. A. (2016) How the oxygen tolerance of a [NiFe]-hydrogenase depends on quaternary structure. *J. Biol. Inorg. Chem.*, 21, 121–134.

Yagi, T., and Higuchi, Y. (2013) Studies on hydrogenase. *Proc. Jpn. Acad., Ser. B*, 89, 16–33.

Yates, N. D. J., Fascione, M. A., and Parkin, A. (2018) Methodologies for "Wiring" redox proteins/enzymes to electrode surfaces. *Chem. Eur. J.*, 24, 12164–12182.

Yu, H., Wu, C.-H., Schut, G. J., Haja, D. K., Zhao, G., Peters, J. W., Adams, M. W. W., and Li, H. (2018) Structure of an ancient respiratory system. *Cell*, 173, 1–14.

Zeldin, O. B., Gerstel, M., and Garman, E. F. (2013) *RADDOSE-3D*: time- and space-resolved modelling of dose in macromolecular crystallography. *J. Appl. Crystallogr.*, 46, 1225–1230.

Zhang, L., Beaton, S. E., Carr, S. B., and Armstrong, F. A. (2018) Direct visible light activation of a surface cysteine-engineered [NiFe]-hydrogenase by silver nanoclusters. *Energy Environ. Sci.*, 11, 3342.

Zorin, N., Zabelin, A. A., Shkuropatov, A. Y., and Tsygankov, A. A. (2017) Interaction of

HydSL hydrogenase from *Thiocapsa roseopersicina* with cyanide leads to destruction of iron-sulfur clusters. *J. Inorg. Biochem.*, 177, 190–197.

ACKNOWLEDGEMENT

Firstly, I express my sincere appreciation to Prof. Dr. Yoshiki Higuchi for giving me a lot of opportunities to work on challenging projects on hydrogenases with a lot of colleagues and researchers in the world. These experiences must be important for my future career as a researcher. I also thank to his kind and informative advice and fruitful discussions. I had a lot of experiences and spend fruitful time.

I also deeply appreciate to Dr. Koji Nishikawa for his kind and helpful advices during my PhD research. I learned really a lot from him *e.g.* the basic experimental skills and analytical skills of X-ray crystallography. His scientific viewpoints or critical comments always stimulate my research work.

I acknowledge to Prof. Dr. Tsunehiro Mizushima, Prof. Dr. Hiderou Yoshida (University of Hyogo), Dr. Seigo Shima (Max Planck Institute for Terrestrial Microbiology, Germany) and Dr. Hideaki Ogata (Institute for Low Temperature Science, Hokkaido University) for their kind and helpful discussions during the evaluation and defense for my PhD research. Especially, Dr. Shima and Dr. Ogata have a lot of experiences on [Fe]-hydrogeanses and [FeFe]-hydrogeanses, therefore, I could always have a different viewpoint from their interesting research papers or informative comments in discussions.

I appreciate to Dr. Hulin Tai (currently Sun Yat-Sen University, China) and Prof. Dr. Shun Hirota from Nara Institute of Science and Technology (NAIST) for their kind support for measuring EPR and FT-IR spectroscopy. Most of the spectroscopic data in this study were obtained by Dr. Hulin Tai.

I also thank to Dr. Yuki Kitazumi and Prof. Dr. Kenji Kano from Kyoto

University, Prof. Dr. Taiki Adachi, Prof. Dr. Tohru Yamasaki, Dr. Masato Suzuki, Prof. Dr. Tomoyuki Yasukawa from Univerisity of Hyogo, and Dr. Shintaro Kubota from Tateho Chemical Industries Co., Ltd. for their kind support and fruitful discussions on electrochemical measurements of hydrogenases.

I acknowledge to Dr. Jiyoung Kang (currently Yonsei University, Korea) and Prof. Dr. Masaru Tateno (University of Hyogo) for performing the theoretical analysis on S77HYB and DvMFSTD, and also having fruitful discussions.

I also would like to express my appreciation to the continuous supports from Dr. Oliver Lenz, Dr. Lars Lauterbach (Technische Universität Berlin) to construct the expression system of S77HYB in *Ralstonia eutropha*. It was an invaluable experience to have spent half year in Berlin. I learned a lot of molecular biological techniques in Berlin. I also appreciate Dr. Stefan Frielingsdorf and Dr. Giorgio Caserta (Technische Universität Berlin) for fruitful discussions on structural and molecular biological analysis on hydrogenases.

Prof. Dr. Hironobu Hojo (Institute for Protein Research, Osaka University) kindly performed amino acid analysis of S77HYB. Thanks to his kindness, the molar extinction coefficient of S77HYB was estimated.

Dr. Naoki Shibata, Dr. Takeshi Hiromoto (currently National Institutes for Quantum and Radiological Science and Technology), and Dr. Midori Taketa in Higuchi laboratory helped me a lot in various situations in the laboratory. I also acknowledge to Ms. Kiriko Hataguchi and Ms. Kayoko Matsumoto their kind support for bacterial culture of *Desulfovibrio vulgaris* Miyazaki F (DvMF) and *Citrobacter* sp. S-77. I also thank to all the members in Higuchi laboratory for their kindness.

Early stage of the crystallographic studies on S77HYB was conducted by Dr. Noor Dina Muhd Noor (currently a senior lecturer in Universiti Putra Malaysia, Malaysia). Molecular mechanism of O_2-protecting mechanism in S77HYB cannot be elucidated without her numerous efforts on establishing the crystallization conditions. It seems like only yesterday that we work together and have a fruitful discussion.

Finally, I would like to express my biggest gratitude and appreciation to my family, especially my parents who never stopped supporting and encouraging me over the years. And thanks too, to all my friends for kind support for all these years.

SUPPORTING INFORMATION

SI Materials and Methods

I. Spectroscopic analysis on S77HYB

Purified S77HYB (with trypsin treatment) was concentrated to 0.5–2.0 mM for electron paramagnetic resonance (EPR) and Fourier-transform infrared (FT-IR) spectroscopic measurements.

EPR measurement for S77HYB

30 μL of anaerobically purified hydrogenase solution was transferred into the 4 mm ϕ EPR tubes, and EPR tubes were closed with septum rubber cap. The EPR tubes were repeatedly degassed and purged 1 bar of H_2. S77HYB was incubated at 30°C for 3 hours to obtain H_2-reduced (HRED) sample. HRED-S77HYB spectra was recorded under 100% H_2 or 100% N_2. For the EPR spectra of HRED-S77HYB under 100% N_2, HRED sample solution was degassed with a vacuum line, and purged with 1 bar of N_2.

To obtain air-oxidized (AOXI) S77HYB, HRED sample solution was degassed with a vacuum line, and purged with air. The sample was placed at 30°C for 3 hours for oxidation. Before recording the EPR spectra of AOXI-S77HYB, the sample solution was degassed with a vacuum line, and purged with 1 bar of N_2.

Ferricyanide-oxidized (FOXI) S77HYB was prepared by anaerobically adding 10 equivalents of $K_3[Fe(CN)_6]$ to HRED-S77HYB inside the glove box filled with 100% N_2.

Furthermore, EPR-spectra of S77HYB with light irradiation was recorded

using Ar^+ laser (λ = 514.5 nm). The laser power for the light irradiation was adjusted to 500 mW/cm^2 at the sample point.

The EPR spectra was recorded at 77K with an CW-EPR spectrometer JESFA100N (JEOL, Tokyo, Japan) installed in NAIST and at 4–100 K with an CW-EPR spectrometer E-500 (Bruker, Billerica, USA) installed in the Institute for Molecular Science, National Institute of Natural Sciences (Aichi, Japan). All the spectra were averaged over five scans.

FT-IR measurement for S77HYB

50 μL of hydrogenase solution (~1.2 mM) was anaerobically transferred into an FT-IR cell. Hydrogenase solution was exposed to air and placed at 30°C for 3 hours to obtain AOXI-S77HYB. HRED-S77HYB was obtained by placing the purified hydrogenase solution under 100% H_2 atmosphere in the glass vial. FOXI-S77HYB sample was obtained by anaerobic addition of 10 equivalents of $K_3[Fe(CN)_6]$ for HRED-S77HYB. Furthermore, FT-IR spectra of S77HYB with light irradiation was recorded as well as in EPR, using Ar^+ laser (λ = 514.5 nm). The laser power for the light irradiation was adjusted to 500 mW/cm^2 at the sample point as in EPR measurement.

FT-IR spectra was recorded at 138-198 K with a FT-IR spectrometer FT-IR 6100V (JASCO, Tokyo, Japan) equipped with an MCT detector. A cryostat system CoolSpeK IR USP-203IR-A (Unisoku, Osaka, Japan) was used to control the temperature of the FT-IR cell. All the spectra were collected at a 2 cm^{-1} resolution and averaged over 1024 scans. The spectra from the buffer solution as a reference were subtracted from

the spectra from samples.

II. Computational method

Ab initio quantum mechanics (QM) calculations.

To explore the molecular species and the spin states of the crystallographically unassigned atomic species (U_A and U_B in Fig. S6), *ab initio* electronic structure calculations, the deformed $[4Fe\text{-}4S]_{Prox}$ moiety in the FOXI-S77HYB was extracted from the atomic coordinates, which included four cysteine residues (Cys 22, Cys25, Cys120, and Cys154), Asp81, W2, and a crystallographically unassigned atomic species (U_A and U_B). The amino acid residues were truncated by replacing the Ca atoms with methyl groups, and the peptide bonds of Glu21-Cys22, Cys22-Thr23, Thr23-Gly24, Gly24-Cys25, Asp81-Gly82, Ile117-Gly118, and Cys120-Ala121 were included in the structural models. To identify the species of the unassigned atoms together with the precise positions, H_2O, HO^-, O_2^-, O^-, HS^-, or S_2^- were assigned to U_A, and H_2O or HO^- was assigned to U_B in the models. Thus, totally 12 structural models were examined by employing the geometry optimization (Table S16).

For $[4Fe\text{-}4S]_{Prox}$ in the crystal structure, each of the Fe ions forms the tetrahedral structure with the coordinated atoms, and the charge and spin states of each Fe ion would be Fe^{2+} or Fe^{3+}, and 4/2 or 5/2, respectively (Pelmenschikov & Kaupp, 2013; Tabrizi *et al*., 2016). The FOXI state would further restrict the possible combinations of Fe^{2+} and Fe^{3+}. Here, we can also refer to the optimum charge and spin states that were elucidated in previous studies of the proximal clusters of O_2-

tolerant MBHs (Pandelia *et al.*, 2011; Pandelia *et al*., 2013) , which also exhibit O_2-tolerance. Thereby, we assume that the appropriate charge and spin states of the [4Fe-4S] core in the FOXI state are +3 and 1/2, respectively, and thus infer that the [4Fe-4S] core consisits of 1 Fe^{2+} and 3 Fe^{3+}. The total charge and spin states of the present models are shown in Table S16.

Owing to the tetrahedral structure of the Fe ions in $[4Fe\text{-}4S]_{Prox}$, all Fe ions are assumed to exhibit high spin states (Pelmenschikov & Kaupp, 2013; Tabrizi *et al*., 2016), and thus the combinations of the spin states of the four Fe ions are restricted; that is, two Fe ions are +5/2 and the others are -4/2 and -5/2. This condition is imposed to determine the spin states, as follows. To assign the spin states of the [4Fe-4S] core, the nomenclature BSij is used. BS is an acronym for the broken symmetry state (Noodleman & Case, 1992), and i and j indicate the numbers of Fe ions where -4/2 and -5/2 are assigned, respectively (Pelmenschikov & Kaupp, 2013; Tabrizi *et al*, 2016). For example, BS12 indicates that the spin states that the spin states of Fe1 and Fe2 are -4/2 and -5/2, respectively (accordingly, those of Fe3 and Fe4 are both +5/2), and thus the total spin is 1/2. For quantum mechanical calculations, six spin assignments (BS12, BS13, BS14, BS23, BS234, and BS34) were imposed with respect to each of the 12 models (Table S16).

All *ab initio* calculations were performed employing Gaussian09 (Frisch *et al*., 2009), and all-electron hybrid spin-unrestricted Hartree-Fock/density functional theory calculations used the B3LYP functional (Lee *et al*., 1988; Becke, 1993). The triple-ζ valence polarized basis set (Schäfer *et al*., 1992) was applied to the Fe ions, the atoms that directly coordinate to the Fe ions, and the species relevant

to UA and UB. For the remaining atoms, the 6-311G** basis set was adopted. As mentioned, for each of 12 models, six spin states were examined in the following calculations (in total, 72 calculations were performed), as mentioned above. For geometry optimization, the following species including U_A and U_B atoms were movable, and then Fe and S ions were also movable together with the U_A and U_B species, where the other atoms in the models were fixed.

MD simulations on water molecule distribution around the [4Fe-4S]$_{Prox}$ of S77HYB and DvMFSTD.

MD simulations of the fully solvated modeled structures were performed to theoretically investigate the distributions of the water molecules around the [4Fe-4S]$_{Prox}$ of S77HYB and DvMFSTD. The crystal structure for ReMBH (PDB ID: 4IUD) was employed as the initial structure for modelling of the fully solvated systems of S77HYB and DvMFSTD, and the hydrogen atoms were attached by employing the LEAP module in the amber12 program package (Case *et al*., 2012). Then, box water with a solvent distance of 12 A from the enzyme was set. The force field parm99SB was adopted to evaluate the energy function, and all MD calculations were performed using the sander module in the amber12 suite. To relax the configuration of solvent water molecules, energy minimizations and MD simulations were performed by employing the following three step procedure. First, the configurations of the hydrogen atoms of the box water were optimized by performing i) 1000-step energy minimization, ii) 10 ps MD simulation at 300 K, and finally iii) 1000-step energy minimization. Second, this type of three-step procedure

was adopted to optimize the configurations of the hydrogen atoms of the box water together with those of the crystal water. Finally, all hydrogen atoms in the system were optimized by 1000-step energy minimization. In all of these relaxation procedures, the other moieties (*e.g.* the heavy atoms of the enzyme) were restrained by a harmonic potential with a 100 kcal/mol·Å^2 force constant. Then, to relax the configuration of the solvent water molecules, a 10 ps MD simulation was performed, where a harmonic constraint was applied to all heavy atoms of the enzyme with a force constant of 100 kcal/mol·Å^2. The force constant was then reduced to 50, 25, 10, 5, 4, and 1 kcal/mol·Å^2 in six MD simulations, and the time of each simulation was 5 ps. Employing the resultant system, the fully solvated S77HYB and DvMFSTD structures were built by replacing the atomic coordinates of the corresponding regions. A water molecule postulated to be generated in the reduction of the [4Fe-4S]$_{Prox}$ was added to a site close to Fe2. The structures were carefully relaxed by multistep combined energy minimization and MD simulations. Then, for each of the fully solvated S77HYB and DvMFSTD structures, the 5 ns MD simulations were conducted for structural relaxation. Then, for each of the distinct 32 replicas of each system, 5 ns productive MD simulations were performed using different set of initial velocities to generate a structural ensemble. In total 160 ns MD simulations were performed for each system.

SI Figures and Tables

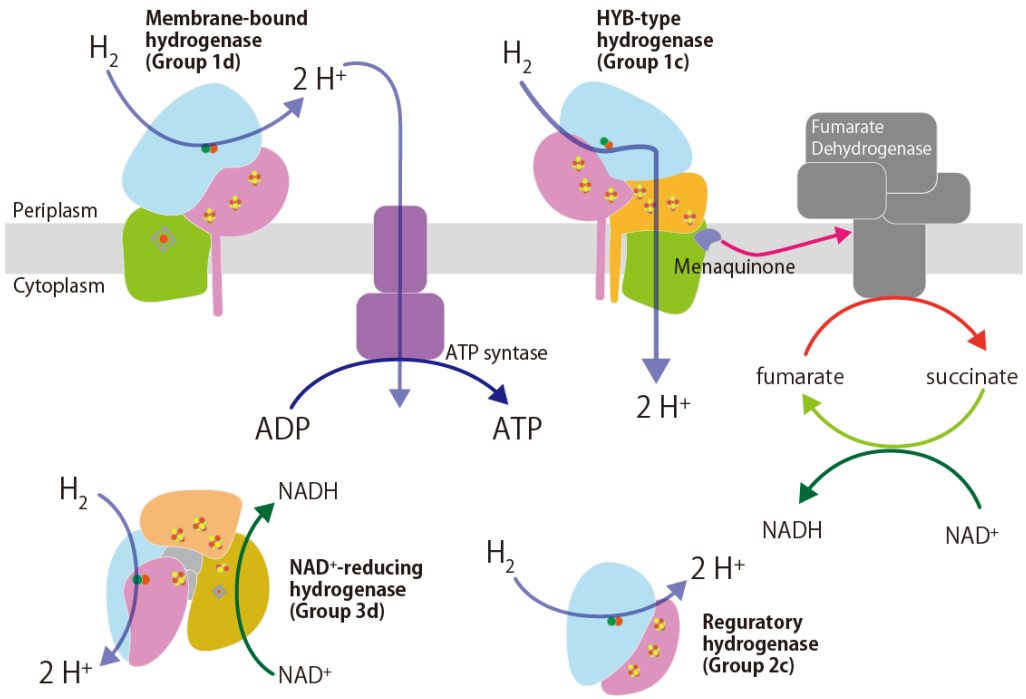

Figure S1. Localization and functions of various [NiFe]-hydrogenases.
There are several kinds of hydrogenases in the cell. Those hydrogenases commonly have H_2 converting activity at the Ni-Fe active site, while some of them have another function with additional subunits.

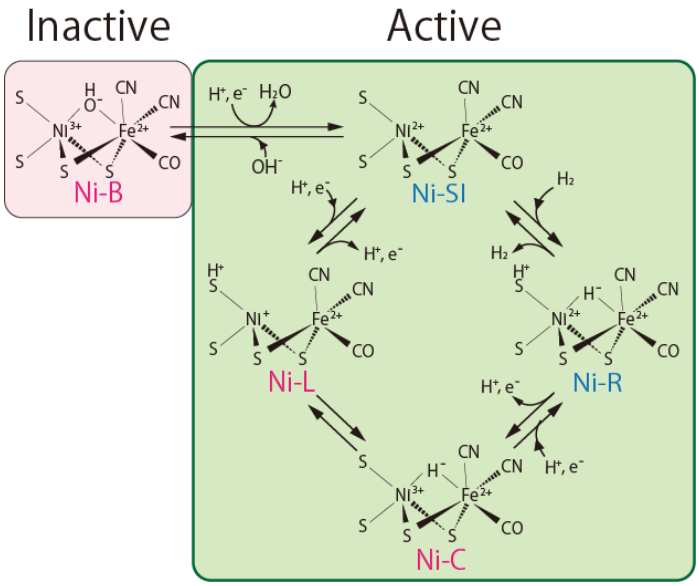

Figure S2. Catalytic intermediates of O_2-tolerant Group 1d [NiFe]-hydrogenases. As indicated in this figure, O_2-tolerant Group 1d [NiFe]-hydrogenases less form Ni-A state unlike standard [NiFe]-hydrogenases. In addition, there is no Ni-SI_a or Ni-SI_r states. The structure of Ni-SI state corresponds to Ni-SI_a state in the standard hydrogenases. No catalytic intermediate corresponding to the Ni-SI_r state in the standard hydrogenase has so far been identified in Group 1d O_2-tolerant hydrogenases.

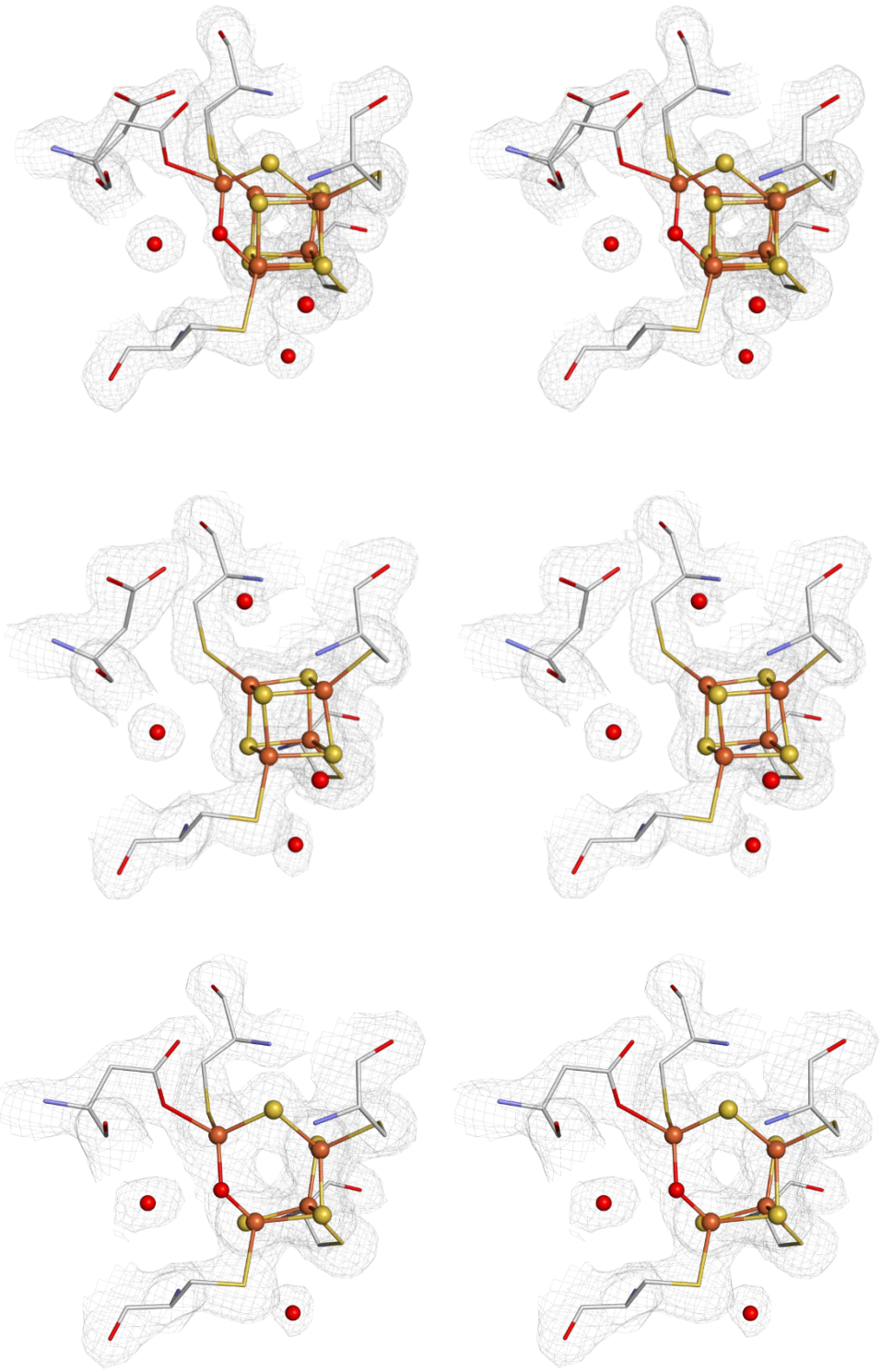

Figure S3. Stereo-view of the [4Fe-4S]$_{Prox}$ for AOXI-, HRED- and FOXI-S77HYB. Stereo-view of the [4Fe-4S]$_{Prox}$ of AOXI-, HRED-, and FOXI-S77HYB are illustrated with 2Fo-Fc map contoured at 1.0 σ.

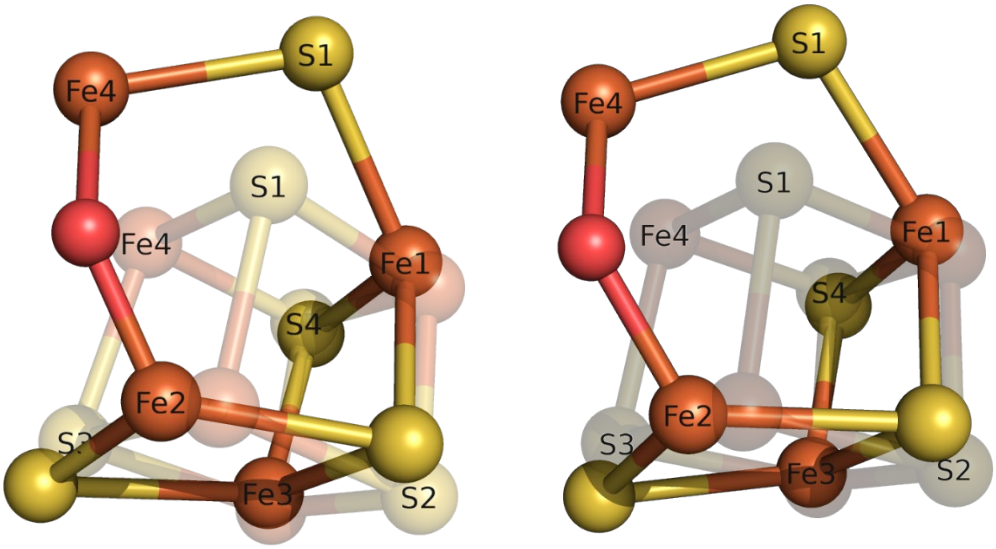

Figure S4. Structural change of the [4Fe-4S]$_{Prox}$ in S77HYB (HRED vs. FOXI).
Structural changes of the [4Fe-4S]$_{Prox}$ in S77HYB (left) Molecule 1, (right) Molecule 2 are illustrated. The structure of the [4Fe-4S]$_{Prox}$ in HRED state is illustrated transparent ball-and-stick representation.

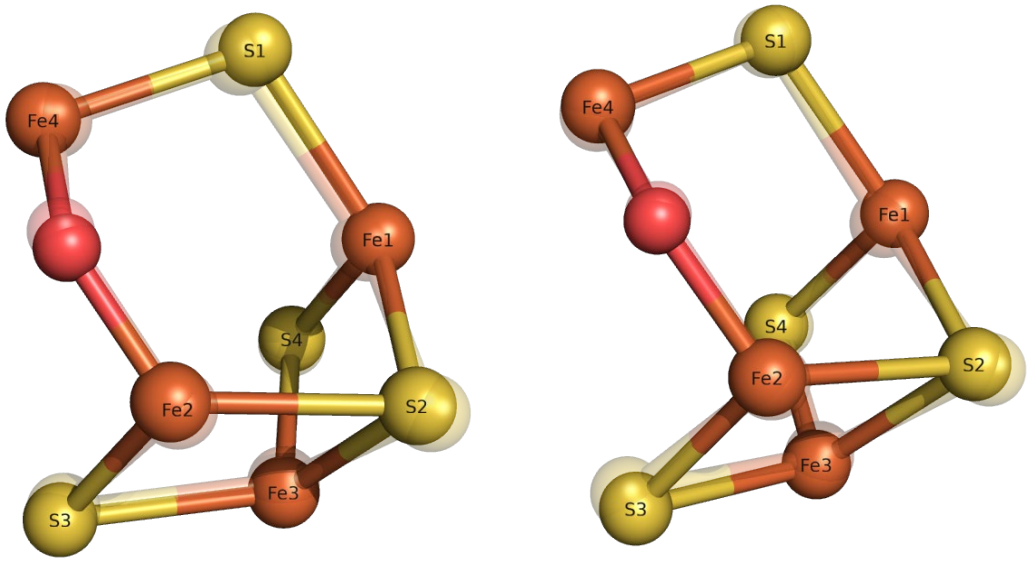

Figure S5. Structural change of the [4Fe-4S]$_{Prox}$ in S77HYB (AOXI vs. FOXI).
Structural changes of the [4Fe-4S]$_{Prox}$ in S77HYB (left) Molecule 1, (right) Molecule 2 are illustrated. Only distorted conformation of [4Fe-4S]$_{Prox}$ is illustrated for AOXI state. The structure for AOXI state is depicted by transparent ball-and-stick representation.

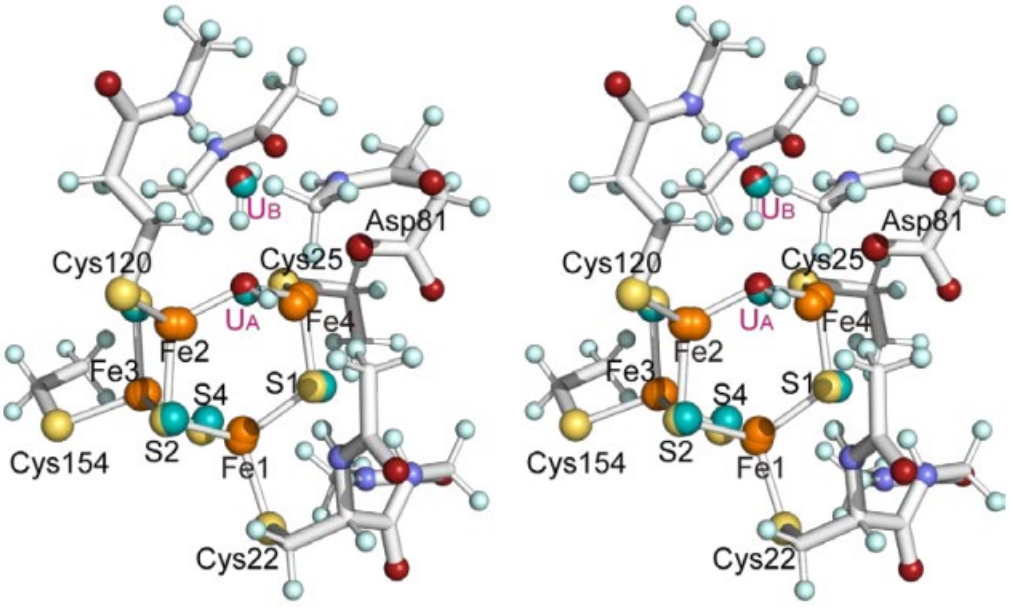

Figure S6. Stereo view of the most energetically favorable structure obtained by geometry optimization.

To confirm the atomic species between Fe4 and Fe2, most energetically favorable structure was estimated by theoretical calculation. U_A and U_B are crystallographically unassignable atomic species, which predicted by geometry optimization.

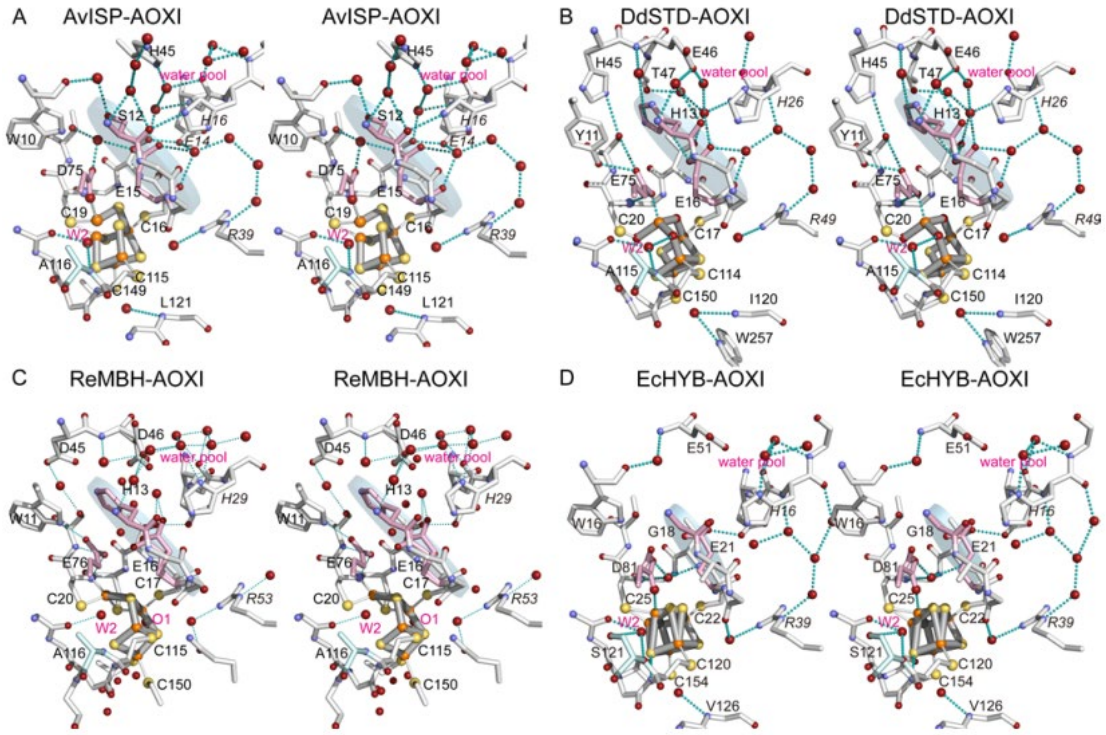

Figure S7. Proximal FeS cluster and surrounding water molecule network in various [NiFe]-hydrogenases.

The proximal iron-sulfur clusters and surrounding water molecule networks for (a) AvISP (Group 1e), (b) DdSTD (Group 1b), (c) ReMBH (Group 1d), (d) EcHYB (Group 1c) are illustrated as ball and stick representation. Blocking water "wall" is located in the center of each figure (gray disk is depicted). Water molecules are represented by small red spheres, and hydrogen bonding networks are indicated by dashes. The figures are illustrated for stereo-viewing.

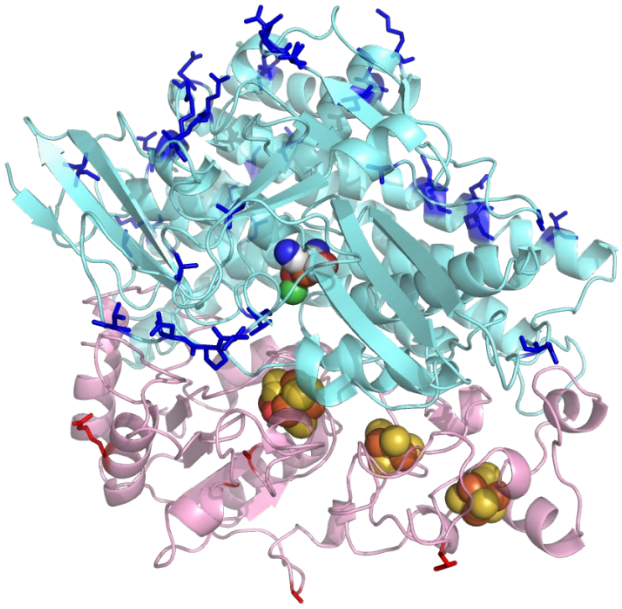

Figure S8. Amino acid difference between S77HYB and EcHYB.
Difference of amino acid residues between S77HYB and EcHYB is mapped on the structure of AOXI-S77HYB. Whole structure is represented by cartoon model. Ni–Fe active center and Fe–S clusters are illustrated as spheres. The position of the difference are depicted by colored sticks; blue (in large subunit) and red (in small subunit).

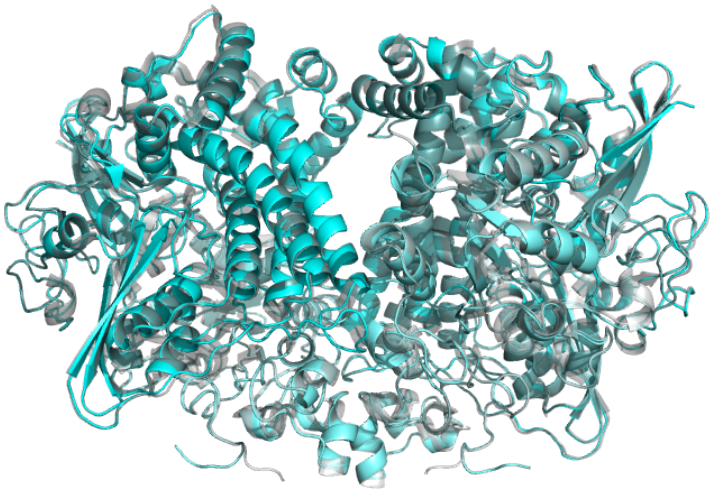

Figure S9. Comparison of the overall structure of AOXI-S77HYB and as-isolated EcHYB.
Overall structures of AOXI-S77HYB (cyan) and as-isolated EcHYB (PDB ID: 6EHQ; gray) are illustrated in cartoon representation. No significant structural difference in overall folding was observed.

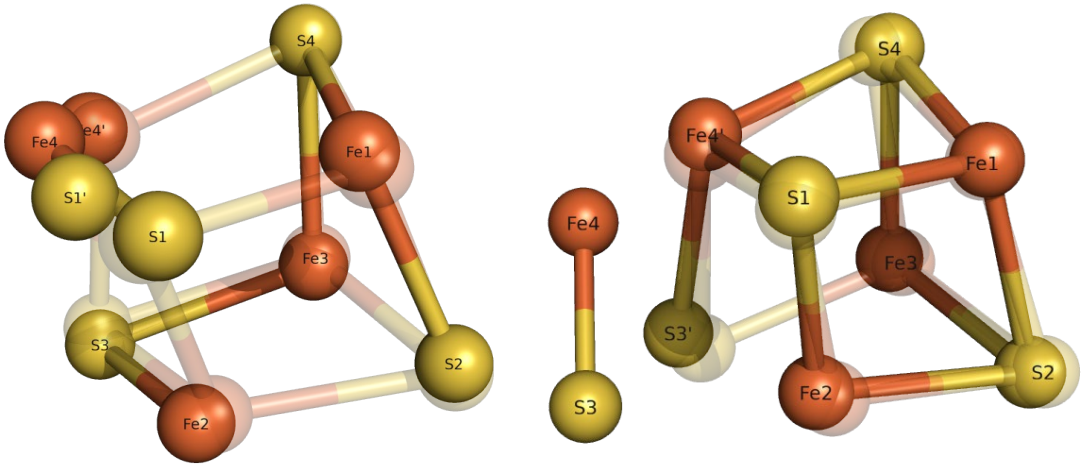

Fig. S10 Structural change of the [4Fe-4S]$_{Prox}$ in EcHYB (as-isotated vs. HRED).
Structures of the [4Fe-4S]$_{Prox}$ in EcHYB for (left) Molecule 1 and (right) Molecule 2 are illustrated by ball-and-stick representation. The structure for HRED state is depicted as transparent cubane-like conformation.

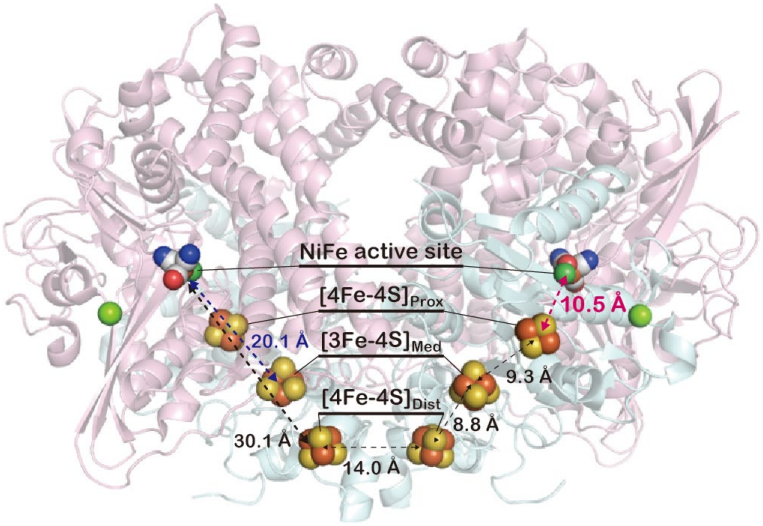

Figure S11. Distances between metal clusters in S77HYB.
Distances between metal clusters are presented on the structural model of AOXI-S77HYB. The distances are also summarized in Table S12.

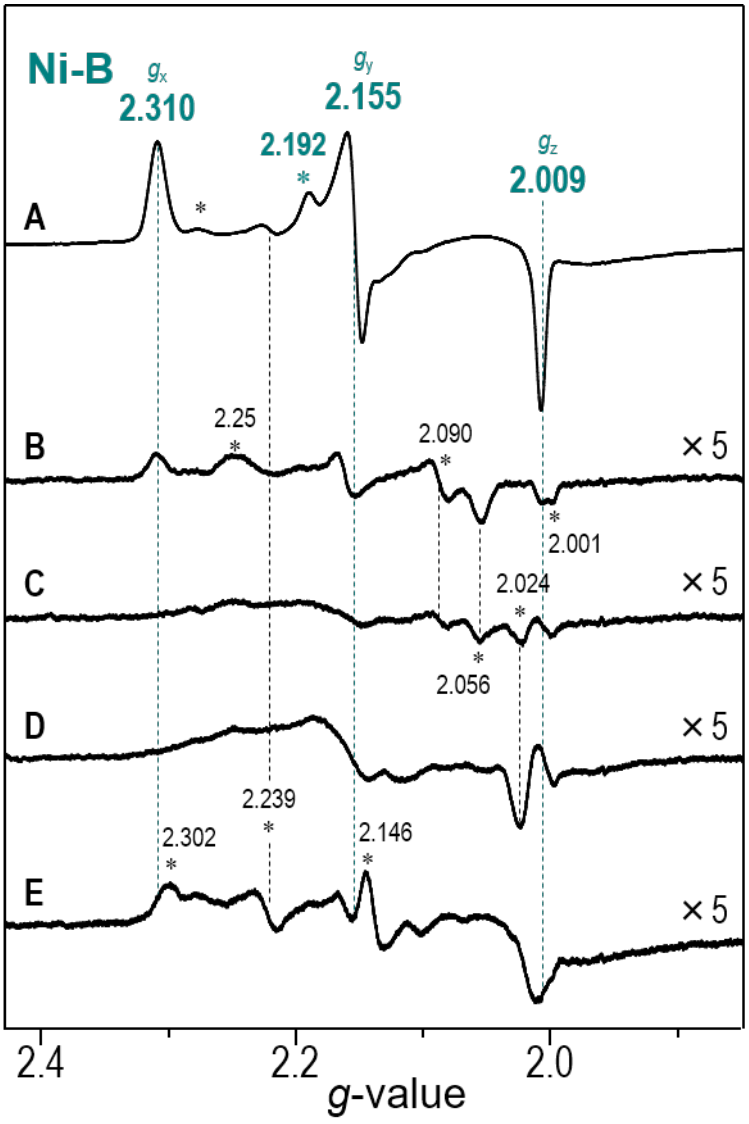

Figure S12. EPR spectra of S77HYB with Na_2S treatment.

EPR spectra of S77HYB recorded at 77K. (A) AOXI-S77HYB, (B) after anaerobic addition of Na_2S (final concentration: 80 mM), and incubation for 30 minutes, (C) 3 hours incubated after Na_2S treatment, (D) air exposed S77HYB after Na_2S treatment, (E) Na2S removed from (D). Ni-B was not converted to Ni-A by Na_2S and O_2 as reported previously on DvMFSTD (Ogata *et al.*, 2005).

Table S1. List of the composition of buffers used in this study.

Buffer	Composition
Disruption	10 mM MOPS-KOH pH 7.0, 1 mM DTT
Solubilization	10 mM MOPS-KOH pH 7.0, 1 % *w/v* Triton X-100, 1 mM DTT
1A	10 mM MOPS-KOH pH 7.0, 0.03% *w/v* Triton X-100, 0.5 mM DTT
1B	10 mM MOPS-KOH pH 7.0, 0.03% *w/v* Triton X-100, 1 M NaCl, 0.5 mM DTT
2A	10 mM MOPS-KOH pH 7.0, 0.5 mM DTT
2B	10 mM MOPS-KOH pH 7.0, 1 M NaCl, 0.5 mM DTT
3A’	10 mM MOPS-KOH pH 7.0, 0.4 M Ammonium sulfate, 0.5 mM DTT
3A	10 mM MOPS-KOH pH 7.0, 0.2 M Ammonium sulfate, 0.5 mM DTT
3B	10 mM MOPS-KOH pH 7.0, 0.5 mM DTT
Dialysis	10 mM MOPS-KOH pH 7.0, 0.2 M NaCl
Active staining	20 mM MOPS-KOH pH 7.0, 1 mM BV, 1 mM TTC

Table S2. List of the composition of culture media used in this study.

Media	Reagent	Amount
S77	Yeast extract	3 g
(liquid)	Polypeptone	3 g
1 L	$(NH_4)_2SO_4$	3 g
	$MgSO_4 \cdot 7H_2O$	0.5 g
	K_2HPO_4	2 g
	KH_2PO_4	1 g
	$Na_2S_2O_3 \cdot 5H_2O$	2 g
	Ammonium ferric citrate	0.2 g
	$CaCl_2$	0.1 g
	water	up to 1 L

Table S3. Classification of [NiFe]-hydrogenases (whole group 1-4) (Greening *et al.*, 2016) and hitherto structurally characterized [NiFe]-hydrogenases.

Group	Proposed function	Structure and reference
1a Ancestral	Liberates electrons for sulfate, metal, organohalide and methanogenic heterodisulfide respiration. Includes [NiFeSe] hydrogenase.	DvH[NiFeSe] (Matias *et al.*, 2001?) Db[NiFeSe] (Volbeda *et al.*, 2013?)
1b Prototypical	Liberates electrons for sulfate, fumarate and nitrate respiration.	DvMFSTD (Higuchi *et al.*, 1997), DgSTD (Volbeda *et al.*, 1995) DfSTD (Rousset *et al.*, 1998) DdSTD (Matias *et al.*, 2001)
1c Hyb-type	Liberates electrons primarily for fumarate respiration. Possibly bidirectional.	EcHYB (Beaton *et al.*, 2018), S77HYB
1d O_2-tolerant	Electron input for aerobic respiration and O_2-tolerant anaerobic respiration.	HmMBH (Shomura *et al.*, 2011), ReMBH (Fritsch *et al.*, 2011), EcMBH (Volbeda *et al.*, 2012) SeMBH (Bowman *et al.*, 2014)
1e Isp-type	Liberates electrons primarily for sulfur respiration. Possibly bidirectional.	AvISP (Ogata *et al.*, 2010)
1f O_2-protecting	Unresolved. May liberate electrons to reduce reactive oxygen species.	*N.D.*
1g Crenarchaeota-type	Unresolved. May liberate electrons primarily for sulfur respiration.	*N.D.*
1h (5) Actinobacteria-type	Scavenges electrons from tropospheric H_2 to sustain aerobic respiration during starvation.	ReAH (Schafer *et al.*, 2015?)
1i Coriobacteria-type (putative)	Unconfirmed role. Likely to mediate hydrogenotrophic respiration using unresolved electron acceptor. Enzyme may transfer H_2-liberated electrons through cyt *b* and quinone to unresolved terminal reductase.	*N.D.*
1j	Hydrogenotrophic respiration using sulfate, iron, or nitrate as terminal electron acceptors. Enzyme transfers	*N.D.*

	H2-liberated electrons through cyt *b* and quinone to terminal reductase.	
1k	Hydrogenotrophic respiration using heterodisulfide as a terminal electron acceptor. Enzyme transfers H_2-liberated electrons through cyt *b* and methanophenazine to heterodisulfide reductase.	*N.D.*
2a Cyanobacteria-type	Electron input for aerobic respiration and recycling H_2 produced by cellular processes (*e.g.* nitrogenase, fermentation).	*N.D.*
2b Histidine kinase-linked	Senses H_2 and activates two-component cascade controlling hydrogenase expression.	*N.D.*
2c Diguanylate cyclase-linked (putative)	Unknown. Predicted to sense H_2 and induce cyclic di-GMP production.	*N.D.*
2d Aquificae-type	Unknown. May generate reductant for carbon fixation or have a regulatory role.	*N.D.*
2e Metallosphaera-type (putative)	Undetermined role. Likely to mediate hydrogenotrophic respiration using O_2 as a terminal electron acceptor. Route of electron transfer unresolved.	*N.D.*
3a F_{420} coupled	Directly couples oxidation of H_2 to reduction of F_{420} during methanogenesis. Reverse reaction may also occur. Includes [NiFeSe] variants.	MbFRH (Ilina *et al.*, 2019)
3b NADP coupled	Directly couples oxidation of NADPH to evolution of H_2. May be reversible. Some complexes are proposed to have sulfhydrogenase activity.	*N.D.*
3c Heterodisulfide reductase-linked	Bifurcates electrons from H_2 to heterodisulfide and ferredoxin in methanogens without cytochromes.	*N.D.*
3d NAD-coupled	Directly interconverts electrons between H_2 and NAD depending on redox state.	HtSH (Shomura *et al.*, 2017)
4a Formate hydrogenlyases	Couples oxidation of formate to fermentative evolution of H_2. Hyf-type complexes may translocate protons via antiporter modules.	*N.D.*

4b Formate-respiring	Forms respiratory supercomplex that couples oxidation of low-potential carbon compounds to reduction of H^+ concomitant with Na^+ translocation. Electron-input modules include formate dehydrogenases, carbon monoxide dehydrogenases, and potentially glutamate synthases. Electrons flow through hydrogenase resulting in H^+ reduction to H_2. The energy released is used to translocate Na^+ ions through Mrp-like antiporter subunits to generate a sodium-motive force.	*N.D.*
4c CO-respiring	Forms complex with carbon monoxide dehydrogenase to anaerobically respire CO using protons as terminal electron acceptors.	*N.D.*
4d Ferredoxin-coupled, Mrp-linked	Forms respiratory supercomplex that couples oxidation of $ferredoxin_{red}$ to reduction of H^+ to H_2. The energy released is used to translocate Na^+ ions through Mrp-like antiporter subunits to generate a sodium-motive force.	PfMBH (Yu *et al.*, 2018?)
4e Ferredoxin-coupled, Ech-type	Forms respiratory complex that couples oxidation of $ferredoxin_{red}$ to reduction of H^+ to H_2 in acetoclastic methanogenesis. This process appears to be coupled to sodium or H^+ translocation through the transmembrane modules. The complex can also act in the reverse direction during hydrogenotrophic methanogenesis.	*N.D.*
4f Formate-coupled (Putative)	Unconfirmed role. May form respiratory complex that couples oxidation of formate to H^+ reduction. The energy generated is likely to be used to translocate H^+ through the antiporter-like subunits.	*N.D.*
4g Ferredoxin-coupled (Putative)	Unconfirmed role. May form respiratory complex that couples $ferredoxin_{red}$ oxidation to H^+ reduction. The energy generated is likely to be used to translocate sodium or H^+.	*N.D.*

4h Ferredoxin-coupled, Eha-type	Forms supercomplex that couples H_2 oxidation to ferredoxin reduction by utilizing the sodium-motive force. The reduced ferredoxin generated can be used anaplerotically to replenish the Wolfe cycle of methanogenesis. While the reverse direction is energetically favorable, it is unclear whether it occurs physiologically.	*N.D.*
4i Ferredoxin-coupled, Ehb-type	Forms supercomplex that couples H_2 oxidation to ferredoxin reduction by utilizing the sodium-motive force. The reduced ferredoxin generated can be used anabolically to sustain biosynthetic reactions. While the reverse direction is energetically favorable, it is unclear whether it occurs physiologically.	*N.D.*

Table S4. List of the structurally characterized [NiFe]-hydrogenases.

Group	Species	Resolution[Å]	PDB ID	Reference
1a	Db	2.15	1CC1	Garcin *et al.*, 1999
		1.4	4KN9	Volbeda *et al.*, 2013
		1.55	4KO1	
		1.6	4KO2	
		1.7	4KO3	
		2	4KO4	
		1.52	4KL8	
	DvH	2.04	2WPN	Marques *et al.*, 2010
		1.82	3ZEA	Marques *et al.*, 2013
		1.95	3ZE7	
		1.8	3ZE8	
		1.33	3ZE9	
		1.5	3ZE6	
		1.3	5JSH	Marques *et al.*, 2017
		1.04	5JSY	
		1.35	5JT1	
		0.95	5JSK	
		1.4	5JSU	
1b	DvMF	1.4	1H2R	Higuchi *et al.*, 1997
		1.8	1H2A	Higuchi *et al.*, 1999
		1.35	1UBH	Ogata *et al.*, 2002
		1.35	1UBJ	

		1.18	1UBK	
		1.2	1UBL	
		1.4	1UBM	
		1.35	1UBO	
		1.34	1UBR	
		1.34	1UBT	
		1.35	1UBU	
		1.24	1WUH	Ogata *et al.*, 2005
		1.04	1WUI	
		1.1	1WUK	
		1.5	1WUL	
		0.89	4U9H	Ogata *et al.*, 2015
		1.06	4U9I	
		1.69	5Y4N	Nishikawa *et al.*, 2017
		1.69	5XLE	
		1.71	5XLF	
		1.64	5XLG	
		1.93	5XLH	
	Df	2.7	1FRF	Rousset *et al.*, 1998
		2.1	1YRQ	Volbeda *et al.*, 2005
		2.35	4FRF	
		1.44	4URH	
		1.83	1YQW	
		2.2	3CUS	Leroux *et al.*, 2008
		2.4	3CUR	
		2.7	3H3X	Dementin *et al.*, 2009
		1.42	4UQP	Volbeda *et al.*, 2015
		1.22	4UQL	
		1.52	4UPV	
		1.8	4UPE	
		2.3	4UD2	
		2.12	4UD6	
		2.02	4UE2	
		2.3	4UE6	
		1.7	4UEQ	
		2.08	4UEW	
		2.6	4UCQ	Abou-Hamdan *et al.*, 2015
		2.3	4UCW	
		1.95	4UCX	
	Dg	2.85	1FRV	Volbeda *et al.*, 1995
		2.54	2FRV	Volbeda *et al.*, 1996
		2.35	1YQ9	Volbeda *et al.*, 2005
	Dd	1.8	1E3D	Matias *et al.*, 2001
1c	Ec	2.2	6EHQ	Beaton *et al.*, 2018

		1.5	6EHS	
		1.5	6EN9	
		1.4	6GAM	Evans *et al.*, 2018
		1.6	6GAN	
	CS77	1.84	5XVB	this study (Noor *et al.*, 2018)
		2.05	5XVC	
		1.57	5XVD	
1d	Hm	1.84	3AYX	Shomura *et al.*, 2011
		1.22	3AYZ	
		1.32	5Y34	Noor *et al*, 2018
			(3AYY)	(Shomura *et al.*, 2011)
	Re	1.5	3RGW	Fritsch *et al.*, 2011
		1.61	4IUB	Frielingsdorf *et al.*, 2014
		1.45	4IUC	
		1.45	4IUD	
		1.47	5D51	Kalms *et al*, 2016
		1.48	5MDJ	Kalms *et al*, 2018
		1.5	5MDK	
		1.41	5MDL	
		1.72	4TTT	
	Ec	1.47	3UQY	Volbeda *et al.*, 2012
		2	3USC	
		1.67	3USE	
		3.3	4GD3	Volbeda *et al.*, 2013
		1.25	5A4F	Evans *et al.*, 2016
		1.23	5A4I	
		1.7	5A4M	
		1.1	5ADU	
		1.4	4UE3	
		1.2	5JRD	Brooke *et al.*, 2017
		2.5	6G94	Volbeda *et al.*, 2018
		1.05	6FPO	Evans *et al.*, 2018
		1.35	6FPW	
		1.2	6G7R	
		1.25	6GAL	
1d	Se	3.2	4C3O	Bowman *et al.*, 2014
1e	Av	2.1	3MYR	Ogata *et al.*, 2010
1h	Re	2.497	5AA5	Schäfer *et al.*, 2016
3a	Mb	1.839	6QGR	Illina *et al.*, 2019
		1.988	6QGT	
		2.28	6QII	
3d	Ht	2.7	5XFA	Shomura *et al.*, 2017
		2.58	5XF9	
4d	Pf	3.7	6CFW	Yu *et al.*, 2018

Abbreviations for the name of bacterial species are following: Db: *Desulfomicrobium baculatum*, DvH: *Desulfovibrio vulgaris* Hildenborough, DvMF: *Desulfovibrio vulgaris* Miyazaki F, Df: *Desulfovibrio fructosovorans*, Dg: *Desulfovibrio gigas*, Dd: *Desulfovibrio desulfricans*, Ec: *Escherichia coli*, CS77: *Citrobacter* sp. S-77, Hm: *Hydrogenovibrio marinus*, Re: *Ralstonia eutropha*, Se: *Salmonella enterica*, Av: *Allochromatium vinosum*, Mb: *Methanosarcina barkeri*, Ht: *Hydrogenophilus thermoluteolus* TH-1, Pf: *Pyrococcus furiosus*.

Table S5. *g* values of catalytic intermediates for S77HYB (this study).

state	g_x	g_y	g_z
Ni-A	2.31?	2.22	2.01
Ni-B	2.31	2.16	2.01
Ni-C	2.20	2.14	2.01
Ni-L	2.30	2.12	2.05

Table S6. *g* values of catalytic intermediates for DvMFSTD (Ogata *et al.*, 2005; Tai *et al.*, 2014).

state	g_x	g_y	g_z
Ni-A	2.31?	2.22	2.01
Ni-B	2.31	2.16	2.01
Ni-C	2.20	2.14	2.01
Ni-L	2.30	2.12	2.05
Ni-CO	2.13	2.08	2.02

Table S7. *g* values of catalytic intermediates for AvISP. (Kellers *et al.*, 2010)

state	g_x	g_y	g_z
Ni-A	2.32	2.24	2.01
Ni-B	2.33	2.16	2.01
Ni-C	2.21	2.15	2.01
Ni-L	2.28	2.11	2.05
Ni-CO	2.13	2.08	2.02

Table S8. *g* values of catalytic intermediates for AaMBH (Pandelia *et al.*, 2010?).

state	g_x	g_y	g_z
Ni-B	2.30	2.17	2.01
Ni-C	2.21	2.15	2.01
Ni-L	2.28	2.12	2.05
Ni-CO	*N.D.*	*N.D.*	*N.D.*

Table S9. FT-IR stretching vibrations corresponding to the CO and CN ligands of the S77HYB.

state	CO	CN_{asym}	CN_{sym}
Ni-B	1957	2081	2091
Ni-SI_r	*N.A.*	*N.A.*	*N.A.*
Ni-A	*N.A.*	*N.A.*	*N.A.*
Ni-SU	*N.A.*	*N.A.*	*N.A.*
Ni-SI_a	1945	2076	2088
Ni-C	1965	2079	2090
Ni-R	1947	2063	2077
Ni-L	1914	2049	2064

Table S10. FT-IR stretching vibrations corresponding to the CO and CN ligands of the DvMFSTD (Fichtner *et al.*, 2006, Pandelia *et al.*, 2010).

state	CO	CN_{asym}	CN_{sym}
Ni-B	1955	2081	2090
Ni-SI_r	1922	2056	2070
Ni-A	1956	2084	2094
Ni-SU	1946	2075	2086
Ni-SI_a	1943	2075	2086
Ni-C	1961	2074	2085
Ni-R	1948	2061	2074
Ni-L	1911	2048	2062
Ni-CO	1939	2070	2083
Ni-SCO	1941	2071	2084

Table S11. FT-IR stretching vibrations corresponding to the CO and CN ligands of the AaMBH (Pandelia *et al.*, 2010).

state	CO	CN_{asym}	CN_{sym}
Ni-B	1939	2081	2092
Ni-SI	1927	2077	2086
Ni-C	1949	2078	2088
Ni-R	1910	2047	2066
Ni-L	-	-	-
Ni-SCO	1925	2072	2082

Table S12. Distance between metal centers (Ni-Fe active site and FeS clusters).

	Molecule 1	Molecule 2
[NiFe]–[4Fe–4S]$_{Prox}$	10.5	10.5
[4Fe-4S]$_{Prox}$–[3Fe-4S]$_{Med}$	9.3	9.3
[3Fe-4S]$_{Med}$–[4Fe-4S]$_{Dist}$	8.7	8.8
[NiFe]–[3Fe–4S]$_{Med}$	20.1	20.1
[NiFe]–[4Fe–4S]$_{Dist}$	30.1	30.1
[4Fe-4S]$_{Dist,Mol1}$–[4Fe-4S]$_{Dist,Mol2}$	14.0	

Table S13. Structural difference of each atom in [4Fe-4S]$_{Prox}$ of S77HYB upon oxidation (HRED vs. FOXI).

	Difference in Molecule 1 [Å]	Difference in Molecule 2 [Å]
Fe1	0.4	0.4
Fe2	0.5	0.5
Fe3	0.2	0.2
Fe4	1.9	1.8
S1	1.7	1.7
S2	0.6	0.6
S3	0.5	0.6
S4	0.3	0.4

Table S14. Structural difference of each atom in [4Fe-4S]$_{Prox}$ of S77HYB (AOXI vs. FOXI).

	Difference in Molecule 1 [Å]	Difference in Molecule 2 [Å]
Fe1	0.1	0.2
Fe2	0.1	0.1
Fe3	0.1	0.1
Fe4	0.1	0.1
S1	0.2	0.1
S2	0.2	0.2
S3	0.1	0.2
S4	0.1	0.1
O	0.2	0.1

Table S15. Structural difference of each atom in [4Fe-4S]$_{Prox}$ of EcHYB (as-isolated vs. HRED).

	Difference in Molecule 1 [Å]	Difference in Molecule 2 [Å]
Fe1	0.2	0.1
Fe2	0.2	0.2
Fe3	0.1	0.2
Fe4/Fe4'	1.1/0.3	1.9/0.2
S1(S1')	0.5/0.7	0.1
S2	0.3	0.2
S3(/S3')	0.2	1.6/0.3
S4	0.1	0.2

Table S16A. Structural models and the resultant geometries obtained by geometry optimization.

Initial species given to U_B		U_A	H_2O_A		HO_A^-		O_A^{2-}	
	H_2O_B	Structural model (charge, spin)	Model 1 (-2, 1/2)		Model 2 (-3, 1/2)		Model 3 (-4, 1/2)	
		Most stable spin state	BS34		BS34		BS34	
		Distances [Å]	$HO_BH...H—O_AH$		$HO_B—H...O_AH$		$HO_B—H...O_A$	
			$HO_BH...H$	$H—O_AH$	$HO_B—H$	$H...O_AH$	$HO_B—H$	$H...O_A$
			1.50	1.03	1.13	1.63	1.05	1.44
		Deviation of U_A and U_B [Å]	0.71	0.53	0.12	0.12	0.16	0.33
	HO_B^-	Structural model (charge, spin)	Model 7 (-3, 1/2)		Model 8 (-4, 1/2)		Model 9 (-5, 1/2)	
		Most stable spin state	BS34		BS23		BS23	
		Distances [Å]	$HO_B—H...O_AH$		$HO_B—H...O_A$		$HO_B—H_N...O_A$	
			$HO_B—H$	$H...O_AH$	$HO_B—H$	$H...O_A$	$HO_B—H_N$	$H_N...O_A$
			0.99	1.61	1.03	1.48	1.02	3.40
		Deviation of U_A and U_B [Å]	0.12	0.15	0.16	0.55	0.47	0.65

Table S16B. Structural models and the resultant geometries obtained by geometry optimization.

Initial species given to U_B		U_A	O_A^-		HS_A^-		S_A^{2-}	
	H_2O_B	Structural model (charge, spin)	Model 4 (-3, 1)		Model 5 (-3, 1/2)		Model 6 (-4, 1/2)	
		Most stable spin state	BS23		BS34		BS12	
		Distances [Å]	$HO_BH—H...O_A$		$HO_B—H...S_AH$		$HO_B—H...S_A$	
			$HO_BH—H$	$H...O_A$	$HO_B—H$	$H...S_AH$	$HO_B—H$	$H...S_A$
			1.01	1.55	0.98	1.99	0.99	2.12
		Deviation of U_A and U_B [Å]	0.13	0.64	0.34	0.11	1.05	0.30
	HO_B^-	Structural model (charge, spin)	Model 10 (-4, 1)		Model 11 (-4, 1/2)		Model 12 (-5, 1/2)	
		Most stable spin state	BS34		BS23		BS23	
		Distances [Å]	$HO_B—H_N...O_A$		$HO_B—H_N...S_AH$		$HO_B—H_N...S_A$	
			$HO_B—H_N$	$H_N...O_A$	$HO_B—H_N$	$H_N...S_AH$	$HO_B—H_N$	$H_N...S_A$
			1.05	3.70	1.03	3.65	1.03	3.40
		Deviation of U_A and U_B [Å]	0.46	0.72	1.60	0.73	1.47	0.71

LIST OF FIGURES

LIST OF TABLES